SPACECRAFT FORMATION FLIGHT: ANALYSIS OF THE PERTURBED J_2-MODIFIED HILL-CLOHESSY-WILTSHIRE EQUATIONS

by

JEFFERY SCOTT GINN

Presented to the Faculty of the Graduate School of

The University of Texas at Arlington in Partial Fulfillment

of the Requirements

for the Degree of

MASTER OF SCIENCE IN AEROSPACE ENGINEERING

THE UNIVERSITY OF TEXAS AT ARLINGTON

August 2006

ACKNOWLEDGEMENTS

"I can do all things through Christ who strengthens me."
- Philippians 4:13

Behind every personal achievement lies strong convictions and wonderful support. I would first like to thank my wife, Megan, for her love and patience during these past two years. To my parents and sister for their constant love and guidance through life's trials and tribulations.

I would also like to extend deep gratitude to Dr. Subbarao, whose love of teaching, and research in broad areas allows his graduate students to explore their passions while also broadening their horizons. To Dr. Wilson, who made the transition from the Midwest to North Texas possible. To Dr. Dogan, whose research interests in aircraft formation flight dynamics and control brought inspiration when I first joined the graduate school in fall, 2004. Finally, to my friends in the ASL who made these past two years enjoyable.

July 15, 2006

ABSTRACT

SPACECRAFT FORMATION FLIGHT: ANALYSIS OF THE PERTURBED J_2-MODIFIED HILL-CLOHESSY-WILTSHIRE EQUATIONS

Publication No. _____

Jeffery S. Ginn, M.S.

The University of Texas at Arlington, 2006

Supervising Professor: Kamesh Subbarao

With the recent technological gains made in satellite design and manufacturing, there has been great interest in utilizing a cluster of satellites to perform the same tasks performed by larger satellites. Historically, this has been done utilizing the *Clohessy-Wiltshire* equations, or the *Hill's* equations, as a benchmark for understanding the physics of the relative motion between two spacecraft.

A variety of different models have been derived and implemented to study the relative motion dynamics since the *Hill-Clohessy-Wiltshire* (*HCW*) equations. Some of these models, like the *HCW* equations, are linearized and have analytical solutions.

These models make the underlying physics due to higher order perturbations more easily understood, as well as more computationally efficient in solving. Perturbations to the relative dynamics are of necessary importance in order to obtain a model of high fidelity.

The research presented in this thesis will explore an approximation of the relative motion under the disturbance of relative second-order differential gravity and the effects of the linearized second-order zonal harmonics (J_2), which may be described analytically. This problem is the compilation of two previous models which each focused on solutions to one of these perturbations. The new solution will be used to obtain appropriate initial conditions for the nonlinear second-order differential gravity model that will provide periodic solutions. These solutions will be compared to those obtained by these models, as well as the *HCW* equations. This will determine the overall fidelity of each model in describing the true relative dynamics between two spacecraft.

TABLE OF CONTENTS

LIST OF ILLUSTRATIONS

LIST OF TABLES

Table Page

CHAPTER 1

INTRODUCTION

1.1 Background

Over the past decade, spacecraft formation flight has become a topic of great interest. With the advent of micro-satellite technology, it is possible for more economically viable satellites to fly in formation and accomplish the same task as larger, more costly satellites. These satellite clusters may be put to use as space-based radars, telescopes, ground imaging, and interferometers, navigation and communications.[1] With the onset of NASA's New Millennium Program (NMP) and the Air Force Research Laboratory's (AFRL) TechSat 21 (Technology Satellite of the 21st Century) program, satellites are expected to be an order of magnitude smaller and lighter than current versions of satellites.

Describing the relative motion dynamics is of great importance in designing any mission involving spacecraft in autonomous formation. It is important to understand what governs a spacecraft's motion about an attracting body, and how that motion affects the relative motion with respect to another spacecraft. "Spacecraft formation flight" can be a misnomer, as, for the most part, spacecraft do not "fly," they orbit.[2] The literature review will discuss various techniques explored and used to describe the relative motion dynamics between spacecraft.

Autonomous spacecraft formation flight is already a reality. The first NMP program, Earth Observing (EO-1), and was put into formation with the Landsat 7 satellite with the purpose of validating new technology that reduces the cost of land-imaging missions.[3, 4]

1.2 Landmark: The Gemini Program

The desire to distribute the various tasks of large satellites amongst smaller satellites flying in precise formation has led to the need for high fidelity modeling of the motion within the satellite cluster. The concept of spacecraft formation is not a new one. The *Hill-Clohessy-Wiltshire (HCW)* equations, the most basic equations which describe the relative motion dynamics between spacecraft, were originally developed for the Gemini Program. This eventually culminated into the first docking of two spacecraft in March, 1966 with Gemini VIII.[5, 6]

The Gemini missions were designed for rendezvous and docking – short period motion where spacecraft are in relatively close proximity (0 - 100 meters). For this type of formation the *HCW* equations are a valid approximation. Because the relative distance is small, the perturbations ignored by the *HCW* equations do not affect the formation on such small time scales and distances.

The *HCW* equations are derived for a deputy or pursuer spacecraft, with respect to a chief or target spacecraft. The chief spacecraft is assumed to be in a circular orbit, which is used as the reference orbit for the relative motion. Any deviation from these assumptions causes the *HCW* equations to no longer admit periodic solutions. As such, the description of motion between spacecraft in eccentric orbits, and at greater relative

distance needs the added perturbations to more accurately describe the relative motion dynamics.

1.3 Perturbations

Perturbations are all relative to a specific problem. In this thesis, a perturbation is ultimately described as any effect that disturbs the relative motion as defined by the *HCW* equations. The two main perturbations which cause a formation in Earth orbit described by the *HCW* equations to lose periodicity are nonlinear differential gravity and J_2 disturbances.

It is possible to develop a set of linearized, constant-coefficient differential equations that describe the linearized, periodic nature of the J_2 disturbance, and these equations are referred to as the J_2*-Modified Hill-Clohessy-Wiltshire (MHCW)* equations.[7,8] It will be shown that the introduction of the linearized J_2 acceleration to the *HCW* equations will improve the relative out-of-plane motion dynamics, as it accounts for the frequency difference in the out-of-plane motion from the in-plane motion. The nonlinear differential gravity terms may be added to the *HCW* equations by using the method of perturbations.[9] This allows the dynamics associated with this perturbation to be solved for using the linear, time-varying, state transition matrix calculated from the solution to the *HCW* equations. The addition of nonlinear differential gravity to the *HCW* equations results in an improved description on the relative in-plane equations of motion.

1.4 Organization of the Thesis

In this thesis, these two improvements to the Hill's equations will be combined to produce a higher fidelity model, which includes the effects of second-order differential gravity, as well as the linearized effects of the J_2 disturbance as described above. The perturbations due to second-order differential gravity are added to the *MHCW* equations utilizing the state transition matrix calculated from the *MHCW* equations. The addition of these perturbations to the *HCW* equations produces a better description of both the in-plane and out-of-plane dynamics. The analytical solution gives good insight and description of the effects these two perturbations have on the system. This allows for a more robust controller to be implemented in real-world applications.

Chapter 2 will present the recent research contributions to the problem of spacecraft formation flight. Linear and nonlinear equations of motion will be discussed. Chapter 3 will define the inertial and rotating reference frames, as well as the rotation matrices used to transform the inertial to local relative coordinate system and vice versa. The chapter will conclude with derivations of the relative equations of motion and the full nonlinear truth model. Chapters 4-5 will derive the various dynamical models, and simulated results will be presented after each model is derived. Chapter 6 compares the simulations to determine what is gained from the new linearized equations of motion, and describes some interesting properties of the perturbed *MHCW* equations.

CHAPTER 2

PREVIOUS WORK

2.1 Motivation

Recent studies on the relative motion dynamics and control of spacecraft in formation began in the early 1990's with interest in using multiple spacecraft for interferometery, space-based communications, and missions to study the magnetosphere.[10] This topic has required research in formation dynamics and control. Specific insight on formation geometry is needed for mission planning and reconfiguration, which would not be possible without accurate description of the dynamics and optimal control methods.

As with any three-dimensional dynamical system, three second-order scalar differential equations are required to describe the motion of a spacecraft orbiting about a central body. The n-body problem admits 10 integrals of motion; six come from the *Conservation of Total Linear Momentum* (producing two vector constants of integration), three from the *Conservation of Total Angular Momentum* (one vector constant of integration), and one from the *Conservation of Total Energy* (one scalar constant of integration).[11] Therefore, when one is considering even the absolute motion of two-bodies, a closed-form solution does not exist.

The relative motion between two bodies, however, does admit closed-form solutions in the form of conic sections. This is expressed most notably in terms of the

six orbital elements of a spacecraft in relative motion about a central body. However, it is also possible to describe the motion in terms of relative position and velocity, as is done when using the two-body form of Newton's Second Law of Motion (also known as Keplerian Motion). In this form, the only acceleration is that of the gravitational attraction between the orbiting body and the central body, which is assumed to be spherical in nature.

2.2 Hill-Clohessy-Wiltshire-Equations

In order to specify a satellite formation, certain constraints must be considered which allow the spacecraft to follow the governing dynamics. Ideally, a formation will be force-free, as the more control input needed to keep a cluster in formation, the more expensive the mission will become. As such, the governing equations for the dynamics and control system must be as physically accurate as possible, minimizing the amount of fuel needed to keep the cluster in formation. In a paper by Yeh and Sparks[2], the Hill's equations are used to define "legal formations," – closed paths of relative motion traced out by a spacecraft under force-free motion.

The physical laws governing spacecraft flight differ greatly than land and air vehicle formations. For a chief/deputy system, where the chief defines the reference for relative motion of the deputy, the spacecraft will not remain in a constant relative position from one another unless they are both in the same circular orbit. While not all missions require such a formation (for example, sparse aperture radar), it is necessary to define other legal formations.

Yeh and Sparks examine the linearized, force-free *HCW* equations from a geometrical standpoint to define these legal formations. A legal formation which satisfies the *HCW* equations must lie on the intersection of a plane and an elliptic cylinder with an eccentricity of $\sqrt{3}/2$ in a moving coordinate system fixed to the leader (LVLH frame). The plane can be at any slope that is not perpendicular to the orbit plane of the chief satellite, as the elliptical cylinder lies normal to the orbit plane. This would not yield a legal formation as the relative motion would not be closed.[2]

2.3 Describing J_2 Perturbations

An aspherical body may be modeled using spherical harmonics, which break down into three types – zonal, sectorial, and tesseral harmonics. The derivation of these harmonics will be presented in §3.4 and Appendix A. The J_2 zonal harmonic, which captures the equatorial bulge of the Earth, is the largest coefficient when describing the Earth's shape. There is about a 21*km* difference in equatorial and polar radii due mainly to this bulge.[12]

In 1997, Kechihian presented a paper that derives the full set of second-order nonlinear differential equations for the relative motion between two spacecraft subject to the full effects of the J_2 perturbation and atmospheric drag.[13] By using the osculating elements, mapping to and from mean elements is avoided. The in-plane and out-of-plane relative motion is shown to be coupled, unlike the linearized solution of these relative equations.[14] The fact that these equations are exact leaves no room for

error in calculating specific changes in velocity needed for rendezvous, station keeping, and formation keeping, unlike the linearized analytical solutions.

Linearizing the gravitational terms in the presence of J_2 for the deputy satellite with respect to the chief's reference orbit, analytical solutions similar to that of the *HCW* equations are obtained.[7] These J_2-*Modified Hill's Equations* describe the mean motion changes in both the in-plane and out-of-plane motion considerably well. Much like the *HCW* equations, it is necessary to understand the physical geometry of the legal formations of these new relative equations of motion. One way to define legal formations under the presence of a linearized J_2 field is by mean orbit elements.[6]

If one averages the perturbing potential due to J_2 on the motion of a satellite over one orbit, and uses this averaged potential in Lagrange's planetary equations, the mean orbit element rates due to J_2 may be calculated. This shows that three of the six orbit elements show a secular drift (longitude of ascending node, right ascension of the ascending node, and mean anomaly). It is shown that it is these secular drifts that need to be avoided for the relative orbit between two spacecraft to be J_2-invariant. The conditions for J_2-invariance imply that specific values should be chosen for the semi-major axis, eccentricity, and inclination of the deputy spacecraft in order to avoid drifting of the deputy and chief satellites.[15] Trying to match these conditions between all spacecraft in the cluster compounds the problem even more. Other changes to the orbit elements besides secular drift include short-period and long-period oscillations. These

are not required to describe bounded relative motion, but do add to the fidelity of the describing dynamics.

Vadali obtains an analytical solution to the relative equations of motion using the geometric method.[16] These equations provide accurate results for orbits of low eccentricity in the presence of the secular effects of J_2 (mean orbit elements). Further work done by Sengupta has derived an analytical method to propagate the relative motion between two spacecraft in highly elliptic orbits.[17] In his Master's thesis, Sengupta presents the modified unit sphere model, including the secular effects of J_2.

Another description of the J_2 perturbation that has recently received new interest is the exploration of using non-osculating elements. In a series of papers by Efroimsky, he correlates gauge invariance in electrodynamics to the ability to freely choose the submanifold in which the orbit resides. This connection was lost due to Lagrange's choice of the three extra constraints, which needed to be imposed on the system to solve the six functions. The Lagrange constraint is an artificially imposed condition on the underdetermined dynamics that fixes the velocity of the perturbed solution equal to the velocity of the unperturbed solution. [18, 19]

The use of non-osculating elements has already been utilized in describing J_2 perturbed motion. In Ref. 20, Gurfil utilizes gauge freedom to describe the dynamics using non-osculating elements. The paper derives an orbit representation in which the mean non-osculating periapsis is stable under the oblateness perturbation, thus

nullifying four planetary equations instead of three through the use of mean osculating elements.

2.4 Nonlinear Differential Gravity

The addition of nonlinear differential gravity effects to the *HCW* equations causes even the bounded solutions of the *Hill's* equations to drift. Relative drift is seen in formation dynamics when the period-matching constraint is not applied. This constraint is prevalent in all descriptions of the relative formation dynamics, including the *HCW* equations. The period-matching constraint is the first to be looked at when defining legal formations. Spacecraft which follow Keplerian orbits cannot have unbounded separation. In terms of the short-period dynamics, as is the case for the *HCW* equations, if the orbits do not commensurate then the relative motion will appear unbounded. In Ref. 21, Gurfil defines the energy-matching condition needed for orbit commensurability using the full nonlinear equations of motion derived from the force-free, two-body Keplerian motion (i.e., nonlinear differential gravity perturbations are included). A similar condition may be derived for the relative motion including the oblateness effects (J_2), and will be explored in this thesis.

Vaddi et al accommodate nonlinear differential gravity up to second-order as described in the introduction and repeated here.[9] The nonlinear differential gravity terms may be added to the *HCW* equations by using the method of perturbations, which allow the dynamics associated with this perturbation to be solved for using the linear, time-varying, state transition matrix calculated from the solution to the *HCW* equations.

The addition of nonlinear differential gravity to the *HCW* equations applies an improved description on the relative in-plane equations of motion.

Sengupta and Vadali in Ref. 22 use the *Tschauner-Hempel* (*TH*) equations (eccentric form of the *HCW* equations) to determine initial conditions for periodic relative motion for an arbitrary eccentric reference orbit and under the disturbance of second-order differential gravity. These solutions may be obtained analytically by evaluating numerous integrals using the eccentric anomaly.

All of these methods greatly improve the describing dynamics associated with the *HCW* equations. However there is a need to strike a balance between the fidelity and computational efficiency of these models.

CHAPTER 3

SATELLITE RELATIVE MOTION DYNAMICS

3.1 Frames of Reference

In this chapter various reference frames that are used to describe the motion of a satellite in orbit around the Earth are illustrated and defined. This includes the geometry used to describe the potential due to J_2.[11, 12] Fig. 3.1 displays the respective frames.

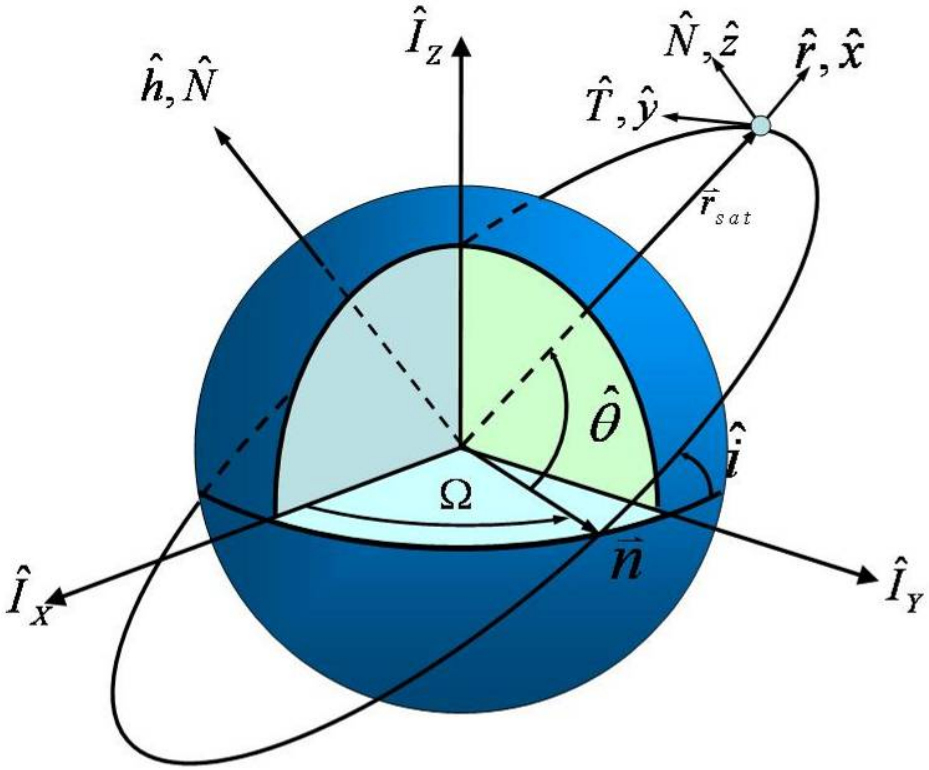

Fig. 3.1 ECI, LVLH and RTN reference frames

3.1.1. Earth-Centered Inertial

The first frame considered is the Earth-Centered Inertial (ECI) frame. The frame is defined by the Earth's equatorial plane and axis of rotation. The fundamental plane coincides with the equatorial plane, and the X-axis points toward the vernal equinox (principal direction) at a specific epoch, which is actually arbitrary for our describing functions. The Y-axis lies in the in the equatorial plane and points in a direction 90^o to the east of the vernal equinox. The Z-axis passes through the North Pole. This system originates at the center of the Earth, and is therefore geocentric.

3.1.2 Local-Vertical Local Horizontal

The local-vertical local-horizontal (LVLH) coordinate system is defined by the radial (in-track), transverse (along-track), and normal (cross-track) directions $(R-T-N)$. The LVLH coordinate system is orbit-fixed, with an origin at the center of the satellite as it moves about its orbit. The radial (and principal) direction points in the direction of the satellite radius vector. The along-track direction completes the triad. Eqn. (3.1) lists the unit vectors of the LVLH coordinate system in terms of the ECI system.

$$\begin{aligned} \hat{e}_R &\equiv \frac{\vec{r}}{r} \\ \hat{e}_T &\equiv \hat{e}_h \times \hat{e}_r \\ \hat{e}_N &\equiv \frac{\vec{r} \times \dot{\vec{r}}}{r\dot{r}} \end{aligned} \tag{3.1}$$

It is noted that, in general, the transverse direction does not always coincide with the velocity vector. This vector is tangent only for circular orbits, and eccentric orbits at apogee and perigee.

3.1.3 Satellite-Centered Nodal Coordinate System

The satellite-centered nodal coordinate system ($r-\theta-i$) is defined in essence by the Earth-Centered nodal coordinate system. It is satellite-based, with the fundamental plane being the satellite orbit. Its origin is at the center of the satellite, but the principal axis points in the direction of the satellite's radial position. The inclination angle i is defined as the angle between the equatorial plane and the orbit plane. It is measured from the line of nodes, which is the direction of the longitude of ascending node. This is the location in which the satellite's orbit crosses the equator into the northern hemisphere, or equivalently from the ECI normal to the orbit normal axis. The co-latitude gives the third direction, or more commonly the argument of latitude, and is the angle between the ascending node and the satellite radius vector at any given time, also shown in Fig. 3.1.

3.1.3 The (x - y - z) Coordinate System

The equations of motion derived in this paper are relative equations, describing the motion of a deputy satellite around that of a chief satellite, both in orbit around the same central body, in this case the Earth. The *x*, *y*, and *z* directions will be used to denote the relative distance of the deputy from the chief. As such, this system is satellite-centered, and is the same as the satellite-centered nodal coordinate system and very similar to the rectangular LVLH coordinate system.

3.2 Coordinate Transformations

We define the subscript $\mathcal{N}$ to denote a vector in the ECI frame, and a subscript $\mathcal{O}$ to denote a vector in the satellite-centered frame.

The $(r-\theta-i)$ coordinate system is used in describing the J_2 disturbance in the local (x-y-z) coordinate system. The presence of r and the two Euler angles, θ and i, complete the geometry of the associated transform from the ECI frame to the $(r-\theta-i)$ frame, utilizing the direction cosine matrix formed by the 3-1-3 Euler angle sets Ω, i and θ. This is shown in Fig. 3.1 and defined as the longitude of ascending node, the argument of latitude, and the inclination angle, respectively.

$$[ON] = \begin{bmatrix} \cos\Omega\cos\theta - \sin\Omega\sin\theta\cos i & \sin\Omega\cos\theta + \cos\Omega\sin\theta\cos i & \sin\theta\sin i \\ -\cos\Omega\sin\theta - \sin\Omega\cos\theta\cos i & -\sin\Omega\sin\theta + \cos\Omega\cos\theta\cos i & \cos\theta\sin i \\ \sin\Omega\sin i & -\cos\Omega\sin i & \cos i \end{bmatrix} \quad (3.2)$$

A similar direction cosine matrix (DCM) is written in terms of the LVLH coordinate frame as described in the ECI frame, which is a direct rotation from ECI coordinates into the satellite-centered frame. As such, these two rotations are equivalent.

$$[ON] = \begin{bmatrix} e_{rX} & e_{rY} & e_{rZ} \\ e_{\theta X} & e_{\theta Y} & e_{\theta Z} \\ e_{hX} & e_{hY} & e_{hZ} \end{bmatrix} \quad (3.3)$$

3.3 Equations of Relative Motion

Consider the two-body motion between a satellite and the orbited body. If the orbited body, such as the Earth, is assumed to be a uniform sphere, there exists a

potential function Φ that imparts a relative acceleration between the satellite and the orbited body. For a point mass or uniformly distributed sphere, the gravitational potential is

$$\Phi = \frac{\mu}{r_s} \tag{3.4}$$

where μ is the gravitational parameter and $r_s = \|\vec{r}_s\|$, is the distance between the center of the satellite and central body. This relative motion is free of any perturbations. The equations of motion between the orbiting satellite and the Earth in the ECI frame $\mathcal{N}$ is given as

$$\ddot{\vec{r}}_s = \frac{\partial \Phi}{\partial \vec{r}_s} = -\frac{\mu}{r_s^3}\vec{r} \tag{3.5}$$

Now consider the problem of two spacecraft orbiting a common center body (see Fig. 3.2). One of these spacecraft flies on a given reference orbit and is called the chief satellite. The other will be designated as the deputy satellite. The inertial equations of motion for the chief and deputy satellite about a central body in the absence of any perturbation and control forces are then given as

$$\ddot{\vec{r}}_c = -\frac{\mu}{r_c^3}\vec{r}_c \tag{3.6}$$

$$\ddot{\vec{r}}_d = -\frac{\mu}{r_d^3}\vec{r}_d \tag{3.7}$$

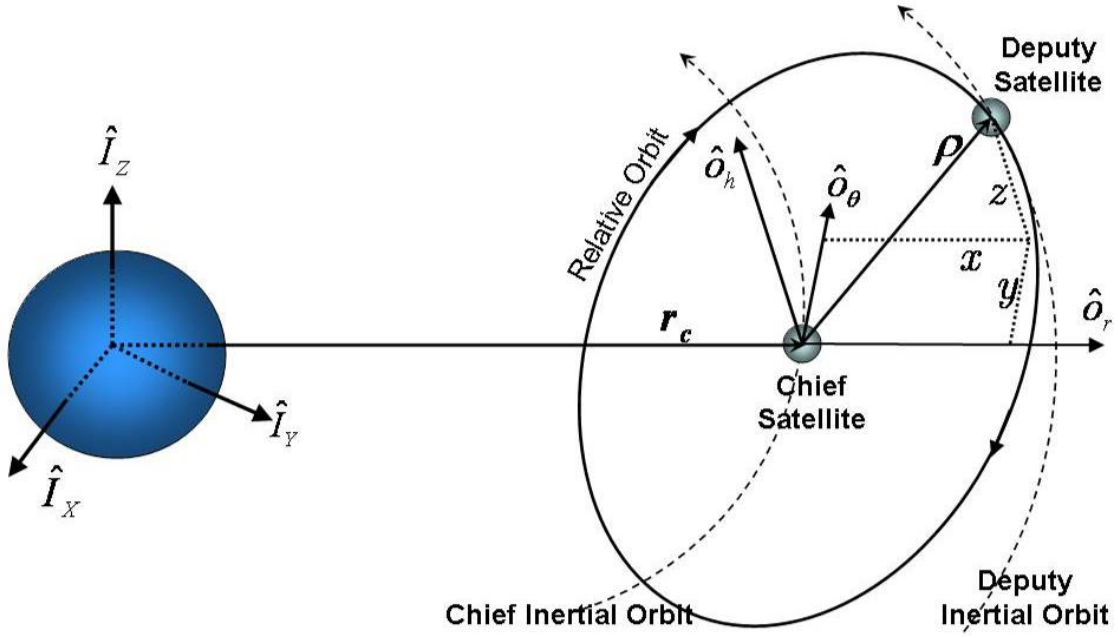

Fig. 3.2 Relative motion of a deputy satellite from a chief (reference) satellite

We now wish to determine the relative equations of motion between the chief and deputy satellite. The relative inertial vector as measured from the deputy satellite to the chief is

$$\left[\vec{\rho}\right]_{\mathcal{N}} = \vec{r}_d - \vec{r}_c \tag{3.8}$$

For assumed two-body Keplerian motion, the relative inertial acceleration is then

$$\left[\ddot{\vec{\rho}}\right]_{\mathcal{N}} = -\frac{\mu}{r_d^3}\vec{r}_d + \frac{\mu}{r_c^3}\vec{r}_c \tag{3.9}$$

In order to express the relative motion between the chief and deputy satellite in the rotating reference frame $\mathcal{O}$, we need to express the relative motion in the inertial frame in terms of the Hill frame. From the *transport theorem*[6]

$$\left[\dot{\vec{\rho}}\right]_{\mathcal{N}} = \left[\dot{\vec{\rho}}\right]_{\mathcal{O}} + \vec{\omega}_{\mathcal{O}/\mathcal{N}} \times \left[\vec{\rho}\right]_{\mathcal{O}} \tag{3.10}$$

$$\left[\ddot{\vec{\rho}}\right]_{\mathcal{N}} = \left[\ddot{\vec{\rho}}\right]_{\mathcal{O}} + 2\vec{\omega}_{\mathcal{O}/\mathcal{N}} \times \left[\dot{\vec{\rho}}\right]_{\mathcal{O}} + \dot{\vec{\omega}}_{\mathcal{O}/\mathcal{N}} \times \left[\dot{\vec{\rho}}\right]_{\mathcal{O}} + \vec{\omega}_{\mathcal{O}/\mathcal{N}} \times \left(\vec{\omega}_{\mathcal{O}/\mathcal{N}} \times \left[\vec{\rho}\right]_{\mathcal{O}}\right) \tag{3.11}$$

Where $\left[\vec{\rho}\right]_{\mathcal{O}} = [x, y, z]^T$ is the position vector of the deputy satellite relative to the chief satellite in the rotating Hill frame $\mathcal{O}$ and

$$\vec{\omega}_{\mathcal{O}/\mathcal{N}} = \left[0, 0, \dot{\theta}_c\right]^T \tag{3.12}$$

is the angular velocity vector of the rotation Hill frame relative to the inertial frame in the orbit frame components. $\vec{\omega}_{\mathcal{O}/\mathcal{N}}$ is equivalent to the angular velocity vector of the chief at each instant. Unless otherwise noted, $\vec{\rho} = \left[\vec{\rho}\right]_{\mathcal{O}}$ throughout the remainder of this thesis. The chief position is expressed in the Hill frame as $\vec{r}_c = \left(r_c, 0, 0\right)^T$. Therefore, the position of the deputy satellite may be defined using the Hill coordinates $\left(x - y - z\right)$ as

$$\vec{r}_d = [(r_c + x), y, z]^T \tag{3.13}$$

Substituting Eqns. (3.9) and (3.12-13) into (3.11), the relative motion in the chief LVLH frame is then given as

$$\begin{aligned}
\ddot{x} - 2\dot{\theta}_c\dot{y} - \ddot{\theta}_c y - \dot{\theta}_c^2 x &= -\frac{\mu\left(r_c + x\right)}{\left(\left(r_c + x\right)^2 + y^2 + z^2\right)^{\frac{3}{2}}} + \frac{\mu}{r_c^2} \\
\ddot{y} + 2\dot{\theta}_c\dot{x} + \ddot{\theta}_c x - \dot{\theta}_c^2 y &= -\frac{\mu y}{\left(\left(r_c + x\right)^2 + y^2 + z^2\right)^{\frac{3}{2}}} \\
\ddot{z} &= -\frac{\mu z}{\left(\left(r_c + x\right)^2 + y^2 + z^2\right)^{\frac{3}{2}}}
\end{aligned} \tag{3.14}$$

The chief inertial orbit radial and angular accelerations are shown to be

$$\begin{aligned} \ddot{r}_c &= r_c\dot{\theta}_c^2 - \frac{\mu}{r_c^2} \\ \ddot{\theta}_c &= -\frac{2\dot{r}_c\dot{\theta}_c}{r_c} \end{aligned} \tag{3.15}$$

We will refer to Eqns. (3.14-15) as the nonlinear *HCW* equations.

3.4 Adding the J_2 Perturbation

The previous section assumed the central body was a sphere of uniform density. This allows the two-body equations of motion to be written in a more simplified form. However, the Earth is not a perfect sphere with uniform density. Therefore, we would like to determine the gravitational potential due to an aspherical central body. The geometry describing the aspherical gravitational potential is shown in Fig. 3.3.

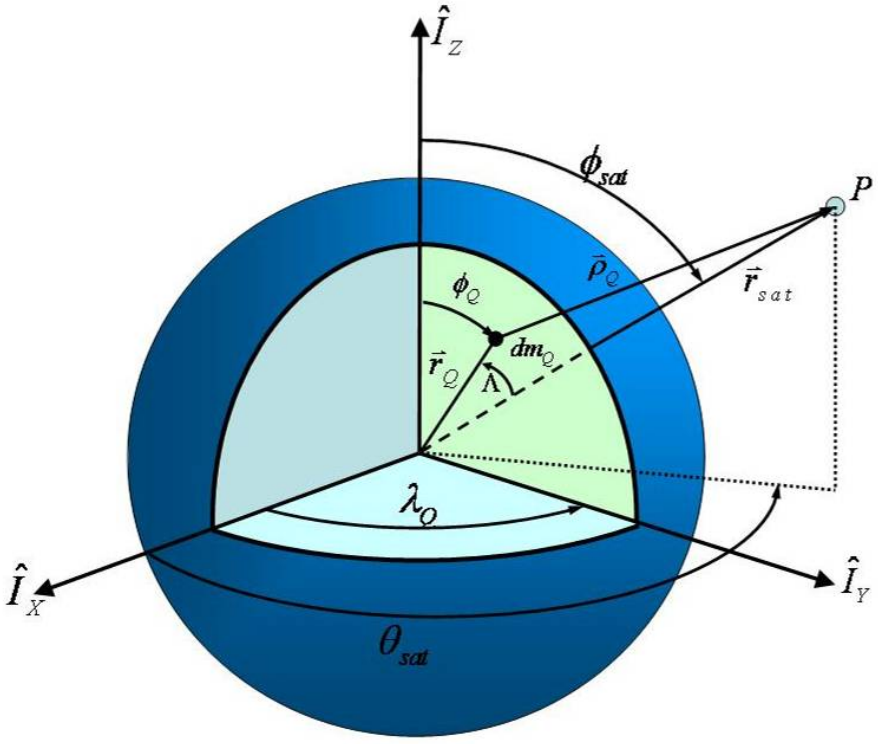

Fig. 3.3 Geometry used to derive the gravitational potential

In order to determine the gravitational potential at point *P*, each point in the Earth, m_Q must be taken into account. The angles ϕ_{sat} and ϕ_Q are the respective co-latitudes, λ_Q and θ_{sat} are the longitudinal arguments, and Λ is the angle between the vectors $\vec{r}_Q$ and $\vec{r}_{sat}$, also known as the ground range or total range angle. All the above angle measurements are geocentric.

The potential that describes an aspherical central body is then given as

$$U = \frac{\mu}{r}\left[\begin{array}{l} 1-\sum_{\ell=2}^{\infty} J_\ell \left(\frac{R_\oplus}{r}\right)^\ell P_\ell\left[\cos\left(\phi_{gc_{sat}}\right)\right] \\ +\sum_{\ell=2}^{\infty}\sum_{m=1}^{\ell}\left(\frac{R_\oplus}{r}\right)^\ell P_{\ell,m}\left[\cos\left(\phi_{gc_{sat}}\right)\right]\left\{C_{\ell,m}\cos\left(m\lambda_{sat}\right)+S_{\ell,m}\sin\left(m\lambda_{sat}\right)\right\} \end{array}\right] \tag{3.16}$$

where $J_\ell, C_{\ell,m}$, and $S_{\ell,m}$ are gravitational coefficients (refer to Appendix A for derivation of Eqn. (3.16)) and $R_\oplus$ is the equatorial radius of the Earth. The first term is the two-body potential, whereas the second term is the potential due to zonal harmonics (J_ℓ terms, where *m*=0, and represent bands of latitude). An aspherical body which only deviates from a perfect sphere due to zonal harmonics is axially symmetric about the Z-axis. The third term represents two other harmonics. The sectorial harmonics, where $\ell = m$, represent bands of longitude, and tesseral harmonics, where $\ell \neq m \neq 0$, represent tile-like regions of the Earth (see Fig. 3.4).

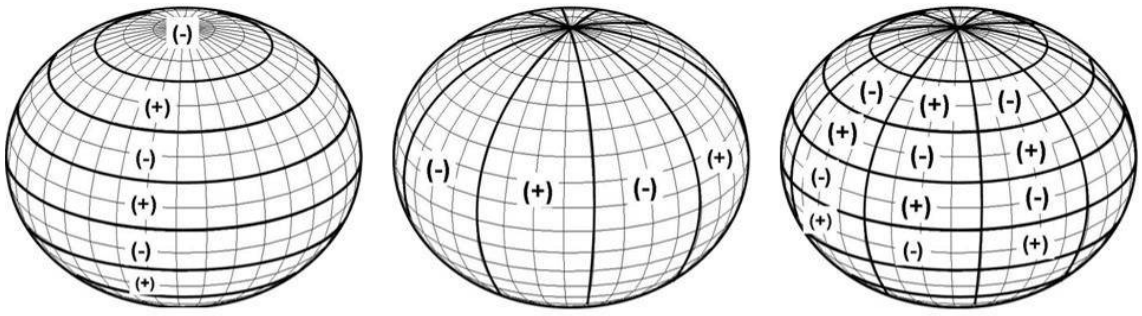

(a) (b) (c)

Fig. 3.4 Representation of spherical harmonics which are broken down into (a) zonal, (b) sectorial, and (c) tesseral. The zonal harmonics account for the Earth's oblateness, the sectorial harmonics account for mass distribution in longitudinal regions, and tesseral harmonics model tiled regions of the Earth's mass distribution.

There are ℓ bands of latitude in which the *Legendre polynomial* $P_\ell\left[\cos\left(\phi_{gc_{sat}}\right)\right]$ is zero, thus dividing the earth into ℓ +1 zones, in which the function is alternately increasing and decreasing in signs. The two trigonometric terms associated with the sectorial harmonics are zero for 2ℓ different values of λ_{sat}, and hence divide the sphere into 2ℓ slices of alternately increasing and decreasing functions, associated with meridians of longitude. The tesseral harmonics are divided up by ($\ell - m$) bands of latitude and $2m$ meridians of longitude.

The J_2 coefficient is about 1000 times larger than the next largest aspherical coefficient, and is therefore very important when describing the motion of a satellite around the Earth. The potential due to the J_2 disturbance is described from (3.16) as

$$U_{zonal} = -\frac{\mu}{r} J_2 \left(\frac{R_\oplus}{r}\right)^2 P_2\left[\cos\left(\phi_{gc_{sat}}\right)\right] \tag{3.17}$$

where $P_2\left[\cos\left(\phi_{gc_{sat}}\right)\right]$ is the associated Legendre polynomial of J_2 and the second zonal gravitational coefficient according to the JGM-2 model has been calculated as[12] $J_2 = 1.082626925638815\times10^{-3}$. Using the spherical geometry shown in Fig. 3.3, the co-latitude may be written as

$$\sin^2\phi_{gc_{sat}} = 1-\frac{Z^2}{r^2} \tag{3.18}$$

Therefore the potential due to J_2 is written as

$$\begin{aligned} U_{J_2} &= -\frac{\mu}{r}J_2\left(\frac{R_\oplus}{r}\right)^2 P_2\left[\cos\phi_{gc_{sat}}\right] \\ &= -\frac{\mu R_\oplus^{\ 2}}{r^3}J_2\left[\frac{1}{2}\left(2-3\sin^2\phi_{gc_{sat}}\right)\right] \\ &= -\frac{\mu R_\oplus^{\ 2}}{r^3}J_2\left[\frac{1}{2}\left(\frac{3Z^2}{r^2}-1\right)\right] \end{aligned} \tag{3.19}$$

The acceleration due to J_2 in the ECI frame is then calculated as the gradient of the potential

$$\nabla U_{J_2} = \vec{J}_2 = \begin{bmatrix} \frac{\partial U_{J_2}}{\partial X} \\ \frac{\partial U_{J_2}}{\partial Y} \\ \frac{\partial U_{J_2}}{\partial Z} \end{bmatrix} = -\frac{3\mu J_2 R_\oplus^2}{2r^5}\begin{bmatrix} X\left(1-\frac{5Z^2}{r^2}\right) \\ Y\left(1-\frac{5Z^2}{r^2}\right) \\ Z\left(3-\frac{5Z^2}{r^2}\right) \end{bmatrix} \tag{3.20}$$

We rewrite the chief and deputy equations of motion in the inertial frame as

$$\ddot{\vec{r}}_c = -\frac{\mu}{r_c^3}\vec{r}_c + \vec{J}_{2_c} \tag{3.21}$$

$$\ddot{\vec{r}}_d = -\frac{\mu}{r_d^3}\vec{r}_d + \vec{J}_{2_d} \tag{3.22}$$

The acceleration due to J_2 in the LVLH frame may be calculated from the gradient in the *r* and *Z* directions:

$$\begin{aligned} \nabla U_{J_2} &= \frac{\partial U}{\partial r}\hat{e}_r + \frac{\partial U}{\partial z}\hat{e}_z \\ &= -\mu J_2 R_\oplus^2 \left[\left(\frac{3}{2r^4} - \frac{15z^2}{2r^6} \right)\hat{e}_r + \frac{3z}{r^5}\hat{e}_z \right] \end{aligned} \tag{3.23}$$

where the *Z* component may be expressed in the LVLH frame as

$$\hat{e}_z = \sin i \sin\theta\, \hat{e}_r + \sin i \cos\theta\, \hat{e}_T + \cos i\, \hat{e}_N \tag{3.24}$$

$$z = r\cos\phi = r\sin i \sin\theta \tag{3.25}$$

Substituting this back into (3.23) yields the acceleration to be

$$\nabla U_{J_2} = \vec{J}_2 = -\frac{3\mu J_2 R_\oplus^2}{r^4} \begin{bmatrix} \left(\frac{1}{2} - \frac{3\sin^2 i \sin^2\theta}{2} \right) \\ \sin^2 i \sin\theta\cos\theta \\ \sin i \cos i \sin\theta \end{bmatrix} \tag{3.26}$$

Adding the full effects of the J_2 perturbation to the relative equations of motion can be tricky. The addition of this force adds to the number of differential equations needed to describe the motion, which means longer computational time. The full nonlinear relative model, which includes the full, nonlinear J_2 and differential gravity terms, will be written in terms of the inertial truth model defined in the next section.

3.5 Truth Model

The truth model for the relative motion dynamics may be written based off the relative motion in the ECI frame. In this paper, the truth model is defined as the full nonlinear relative equations of motion, which include the full effects of J_2 and differential gravity. As seen from the derivation of the nonlinear *HCW* equations in §3.3, the differential gravity effects are inherent from the relative Keplerian motion, and in the previous section, it is seen that the effects of J_2 are intrinsically determined from an aspherical central body. We begin by defining the inertial equations of motion for the chief and deputy satellites as

$$\ddot{\vec{r}}_c = -\frac{\mu}{r_c^3}\vec{r}_c + \vec{J}_{2_c} \tag{3.27}$$

$$\ddot{\vec{r}}_d = -\frac{\mu}{r_d^3}\vec{r}_d + \vec{J}_{2_d} \tag{3.28}$$

which are modeled as the two-body Keplerian motion with added J_2 perturbations.

The inertial relative position and velocity is defined as the position and velocity of the deputy relative to the chief.

$$\left[\vec{\rho}\right]_{\mathcal{N}} = \vec{r}_d - \vec{r}_c \tag{3.29}$$

$$\left[\dot{\vec{\rho}}\right]_{\mathcal{N}} = \dot{\vec{r}}_d - \dot{\vec{r}}_c \tag{3.30}$$

The relative position in the LVLH is calculated using the direction cosine matrix, $\left[ON\right]$, defined by Eqn. (3.3) as

$$\left[\vec{\rho}\right]_{\mathcal{O}} = \left[ON\right]\left[\vec{\rho}\right]_{\mathcal{N}} \tag{3.31}$$

The relative velocity in the LVLH frame is defined using the *transport theorem* as

$$\left[\dot{\vec{\rho}}\right]_{\mathcal{O}} = \left[\dot{\vec{\rho}}\right]_{\mathcal{N}} - \vec{\omega}_{\mathcal{O}/\mathcal{N}} \times \left[\vec{\rho}\right]_{\mathcal{O}} \tag{3.32}$$

where $\vec{\omega}_{\mathcal{O}/\mathcal{N}}$ is the rotation rate of the LVLH frame, which is the angular velocity of the chief orbit as stated before, and is defined as the angular momentum times the magnitude of the position squared:

$$\vec{\omega}_{\mathcal{O}/\mathcal{N}} = \frac{\vec{r}_c \times \dot{\vec{r}}_c}{r_c^2} \tag{3.33}$$

As the relative position and velocity is now fully defined from the exact nonlinear equations of motion in the ECI frame (Eqns. (3.27-33)), we have our **truth model** to be used as a basis for comparison.

Example 1. Full Nonlinear Model Simulation (J_2 and Differential Gravity Included)

Consider a chief satellite in circular orbit about the Earth, with an orbit inclination of 35^o from the Earth equatorial plane, and at a radius $r_c = 8000\,km$. We assume at t_0 the chief is at the line of nodes, which coincides with the X-axis in the ECI frame. The initial conditions are chosen to match those imposed by Vaddi et al, which removes secular growth terms for the *HCW* solution derived in §4.3 to allow for comparison of results.[9] The initial conditions for the chief in inertial coordinates are given as:

$$\begin{aligned} R_{c,0} &= \begin{bmatrix} r_c & 0 & 0 \end{bmatrix}^T \; km \\ \dot{R}_{c,0} &= \begin{bmatrix} 0 & 5.7821430 & 4.04870010 \end{bmatrix}^T \; km/sec \end{aligned} \tag{3.34}$$

The chief orbit initial conditions are the same for all example simulations performed.

Now consider two deputy satellites. The first has an initial relative displacement that places it 5 *km* out from the chief in the radial direction, and 10 *km* above the chief in the cross-track (*z*) direction The relative initial conditions are based off *HCW* initial conditions for a bounded formation, derived in §4.3.

$$\begin{aligned} R_{d1,0} &= \begin{bmatrix} r_c + 5 & -5.7357644 \times 10^{-3} & 8.1915204 \times 10^{-3} \end{bmatrix}^T \; km \\ \dot{R}_{d1,0} &= \begin{bmatrix} 0 & 5.7785291 & 4.046169666 \end{bmatrix}^T \; km/sec \end{aligned} \tag{3.35}$$

The second deputy satellite has displacement in the along-track (*y*) direction from the chief satellite of $-10\,km$. The initial conditions for this satellite in the inertial frame are given as:

$$R_{d2,0} = \begin{bmatrix} r_c & -8.1915204\times10^{-3} & -5.7357644\times10^{-3} \end{bmatrix}^T \; km$$
$$\dot{R}_{d2,0} = \begin{bmatrix} 4.4116832\times10^{-3} & 5.7872039 & 4.0414724 \end{bmatrix}^T \; km/sec$$

The relative positions in the LVLH frame will be used to compare the accuracy of the various models from the full nonlinear truth model. These will be displayed as errors from the desired relative position in the Hill frame (the *HCW* equations in Chapter 4, and the J_2*-Modified HCW* equations in Chapter 5). For now, we plot the full relative nonlinear dynamical system governed by Eqns. (3.27-28) and transformed into the relative Hill frame using Eqn. (3.31). It is noted that the governing equations for the plots shown will be listed in the figure title for reference.

The initial conditions imposed, when applied to the truth model, still causes a drift in the *y* direction, but the drift is small, as can be seen from both cases in Fig. 3.5 and 3.6. These plots display actual relative positions of the deputy satellites from the chief with full nonlinearities of J_2 and differential gravity. The drift from a bounded periodic motion of 10 *km* for deputy satellite 1, which displays the largest drift in the along-track direction, is around 155*m* per orbit. This is because the initial conditions used were obtained using a linearized solution, which does not capture the full energy-matching constraint required for bounded relative motion.

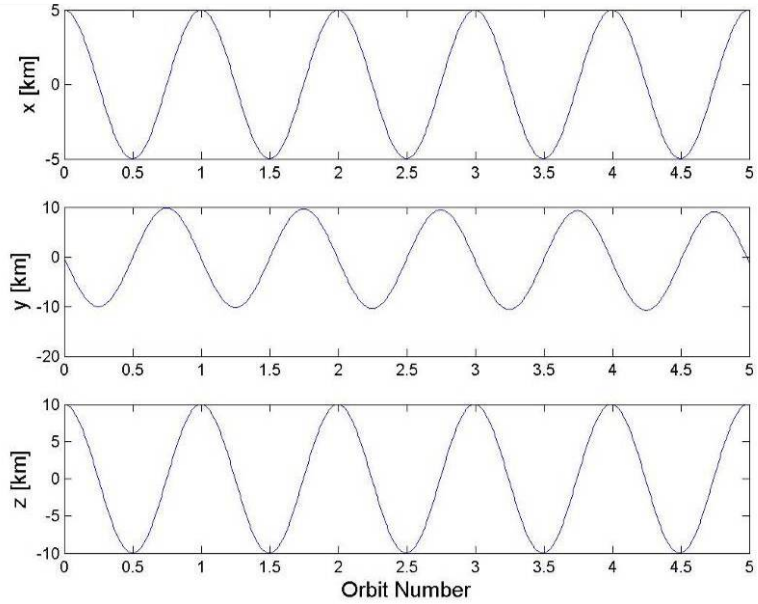

Fig. 3.5 Relative Hill truth positions for deputy satellite 1 using Eqns. (3.27-33)

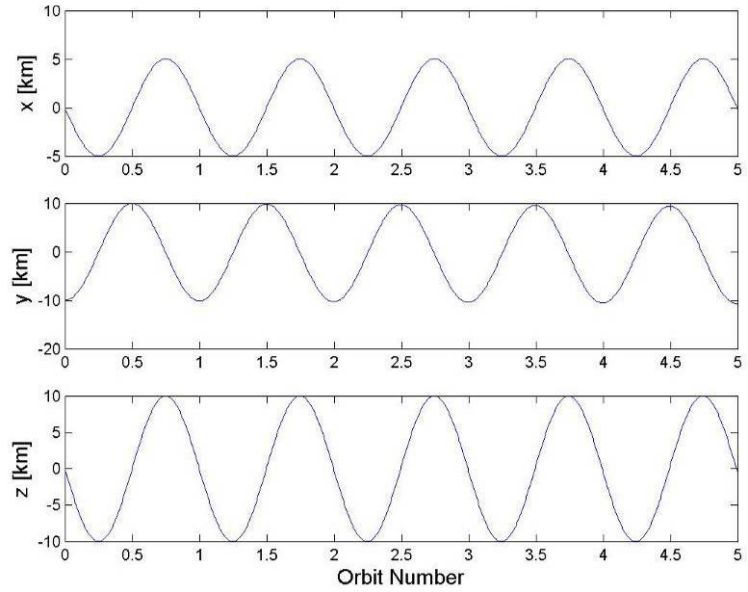

Fig. 3.6 Relative Hill truth positions for deputy satellite 2 using Eqns. (3.27-28, 31)

Example 2. Ignoring J_2 Effects: the Nonlinear HCW Equations

What if we ignore the effects of the oblateness of the Earth, as governed by the nonlinear *HCW* equations defined in Eqns. (3.14-15)? The error between the truth model governed by Eqns. (3.27-28, 31) and the nonlinear *HCW* equations are seen in Fig. 3.7 and 3.8. The absence of the J_2 perturbation causes a significant drift over 5 orbits in the along-track direction, and as such the effects of J_2 should not be neglected for models of high fidelity.

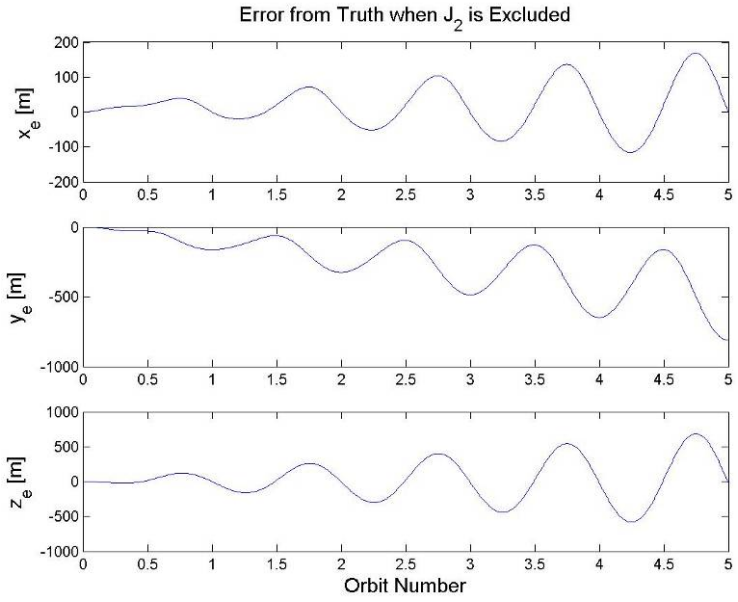

Fig. 3.7 Error of nonlinear *HCW* governed by (3.14-3.15) from truth governed by (3.27-28, 31) for deputy satellite 1

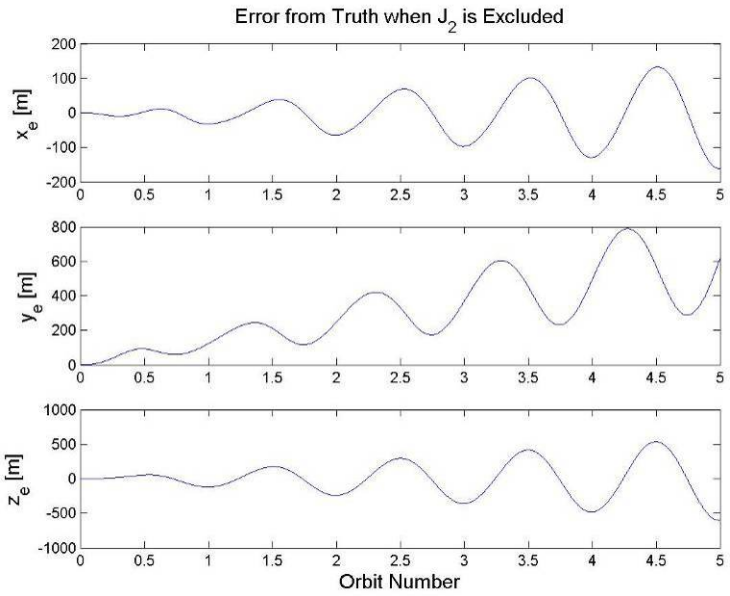

Fig. 3.8 Error of nonlinear *HCW* governed by (3.14-3.15) from truth governed by (3.27-28, 31) for deputy satellite 2

The truth model has been derived for the system and the simulated results of two deputy satellites about the same chief satellite have been presented. The nonlinear *HCW* equations have also been compared to the truth model. These will become the basis of comparison for the analytical models to be presented.

CHAPTER 4

DIFFERENTIAL GRAVITY MODELS

4.1 Hill-Clohessy-Wiltshire Equations

We begin our analysis of various linearized approximations with the most simplified model. Starting with the nonlinear *HCW* equations, which only include the effects of nonlinear differential gravity, we have the 10th order nonlinear system

$$\begin{aligned}
\ddot{x} - 2\dot{\theta}_c\dot{y} - \ddot{\theta}_c y - \dot{\theta}_c^2 x &= -\frac{\mu\left(r_c + x\right)}{\left(\left(r_c + x\right)^2 + y^2 + z^2\right)^{\frac{3}{2}}} + \frac{\mu}{r_c^2} \\
\ddot{y} + 2\dot{\theta}_c^2\dot{x} + \ddot{\theta}_c x - \dot{\theta}_c^2 y &= -\frac{\mu y}{\left(\left(r_c + x\right)^2 + y^2 + z^2\right)^{\frac{3}{2}}} \\
\ddot{z} &= -\frac{\mu z}{\left(\left(r_c + x\right)^2 + y^2 + z^2\right)^{\frac{3}{2}}}
\end{aligned} \tag{4.1}$$

$$\begin{aligned}
\ddot{r}_c &= r_c\dot{\theta}_c^2 - \frac{\mu}{r_c^2} \\
\ddot{\theta}_c &= -\frac{2\dot{r}_c\dot{\theta}_c}{r_c}
\end{aligned} \tag{4.2}$$

which includes effects of eccentricity. If we assume that the chief satellite is in a circular orbit ($e = 0$), then the angular velocity is equal to the mean motion, which is a constant, so the angular acceleration terms vanish.

$$\dot{\theta}_c = \sqrt{\frac{\mu}{r_c^3}} = n_c \tag{4.3}$$

The mean motion of the chief satellite, n_c, will be referred to henceforth as *n*. The new equations of motion are now expressed as

$$\begin{aligned}
\ddot{x} - 2n\dot{y} - n^2 x &= -\frac{\mu\left(r_c + x\right)}{\left(\left(r_c + x\right)^2 + y^2 + z^2\right)^{\frac{3}{2}}} + \frac{\mu}{r_c^2} \\
\ddot{y} + 2n\dot{x} - n^2 y &= -\frac{\mu y}{\left(\left(r_c + x\right)^2 + y^2 + z^2\right)^{\frac{3}{2}}} \\
\ddot{z} &= -\frac{\mu z}{\left(\left(r_c + x\right)^2 + y^2 + z^2\right)^{\frac{3}{2}}}
\end{aligned} \tag{4.4}$$

$$\begin{aligned}
\ddot{r}_c &= r_c n^2 - \frac{\mu}{r_c^2} \\
\ddot{\theta} &= 0
\end{aligned} \tag{4.5}$$

These equations will be referred to as the **circular nonlinear *HCW* equations**.

4.2 Differential Gravity

The gravitational acceleration terms on the RHS due to the deputy satellite may be calculated from the potential function

$$\begin{aligned}
U_d &= -\frac{\mu}{r_d} = -\frac{\mu}{r_c + \rho} = -\frac{\mu}{\sqrt{\left(r_c + x\right)^2 + y^2 + z^2}} \\
&= -\frac{\mu}{r_c\sqrt{1 + 2\frac{\vec{r}_c \cdot \vec{\rho}}{r_c^2} + \left(\frac{\rho}{r_c}\right)^2}}
\end{aligned} \tag{4.6}$$

The irrational term has the form of the generating function

$$g\left(\alpha, \gamma\right) = \left(1 - 2\alpha\gamma + a^2\right)^{-1/2} \tag{4.7}$$

which is expressed as the series expansion,

$$\sum_{\ell=0}^{\infty} \alpha^{\ell} P_{\ell}[\gamma] \tag{4.8}$$

where P_ℓ is the ℓth Legendre polynomial, $\alpha = -\frac{\rho}{r_c}$ and $\gamma = \frac{\vec{r}_c \cdot \vec{\rho}}{r_c \rho}$. This potential is then expressed as the infinite series

$$U_d = -\frac{\mu}{r_c} \sum_{\ell=0}^{\infty} (-1)^{\ell} \left(\frac{\rho}{r_c} \right)^{\ell} P_{\ell} \left(\frac{x}{\rho} \right) \tag{4.9}$$

Using the relations,

$$\frac{d}{dz} P_{\ell}(z) = \frac{\ell}{z^2 - 1} \left[z P_{\ell}(z) - P_{\ell-1}(z) \right] \tag{4.10}$$

$$\frac{\partial x}{\partial \vec{\rho}} = \hat{e}_r \tag{4.11}$$

the differential gravity field may then be calculated as the gradient of the potential,

$$\frac{\partial U_d}{\partial \vec{\rho}} = \frac{\mu}{r_c^3} \sum_{\ell=0}^{\infty} (-1)^{\ell} \left(\frac{\rho}{r_c} \right)^{\ell-2} \frac{\ell}{y^2 + z^2} \left[\rho^2 P_{\ell} \left(\frac{x}{\rho} \right) \hat{e}_1 - \rho P_{\ell-1} \left(\frac{x}{\rho} \right) \hat{e}_2 \right] \tag{4.12}$$

where $\hat{e}_1 = y\hat{e}_\theta + z\hat{e}_h$ and $\hat{e}_2 = \left(y^2 - z^2 \right) \hat{e}_r - xy\hat{e}_\theta - xz\hat{e}_h$. Summing the first three terms (ℓ = 0, 1, 2) gives the linearized differential gravitational acceleration as,

$$\frac{\partial U_d}{\partial \vec{\rho}} = \begin{bmatrix} -\frac{\mu}{r_c^2} + 2\frac{\mu}{r_c^3} x & -\frac{\mu}{r_c^3} y & -\frac{\mu}{r_c^3} z \end{bmatrix}^T \tag{4.13}$$

4.3 Unperturbed HCW Equations

We ignore the nonlinear differential gravity terms presently, and by substituting (4.13) into (4.4) we obtain the equations of motion known as the *Hill-Clohessy-Wiltshire* equations

$$\begin{aligned} \ddot{x} - 2n\dot{y} - 3n^2 x &= 0 \\ \ddot{y} + 2n\dot{x} &= 0 \\ \ddot{z} + n^2 z &= 0 \end{aligned} \tag{4.14}$$

Notice that this linearized form of (4.4) has decoupled the in-plane (*x*-*y*) motion from the out-of-plane (z) motion. The out-of-plane motion is modeled as a harmonic oscillator, where the in-plane motion is described as coupled harmonic oscillators. These second-order differential equations have the general solutions

$$\begin{aligned} x(t) &= A\cos(nt+\alpha) + x_{off} \\ y(t) &= -2A\sin(nt+\alpha) - \frac{3}{2}nx_{off}t + y_{off} \\ z(t) &= B\cos(nt+\beta) \end{aligned} \tag{4.15}$$

where $A, \alpha, x_{off}, y_{off}, B,$ and β are the six integral constants. The velocities are found as the time derivatives of (4.15). In order to produce bounded relative motion, the radial offset term must be equal to zero to eliminate the secular growth present in the along-track direction. We also set the in-track offset term to zero, so that the bounded equations now have the form

$$\begin{aligned} x(t) &= A\cos(nt+\alpha) \\ y(t) &= -2A\sin(nt+\alpha) \\ z(t) &= B\cos(nt+\beta) \end{aligned}$$

Example 3. HCW Model Simulation

Consider the same initial conditions for the chief and two deputy satellites as given in *Example 1*. These initial conditions also impose a circular projection in the *y-z* plane, which imposes two more conditions to (4.15)

$$B = 2A$$
$$\beta = \alpha$$

We may solve for the remaining four integral constants by evaluating the three position and three velocity equations at $t = t_0$. The constants of integration for both satellites are given in Table 4.1.

Table 4.1. IC values for both cases

	Deputy 1	Deputy 2
A	5 km	5 km
α	0 rad	$\pi/2$ km
x_{off}	0 km	0 km
y_{off}	0 km	0 km

The relative positions at each instant are Eqns. (4.15) evaluated at each time *t*. When comparing the *HCW* solution for both satellites to the nonlinear system defined by Eqns. (4.4) and (4.5), the error from the linearized equations can be seen mainly as a secular growth in the along-track direction for both models (see Fig. 4.1 and 4.2). The *HCW* solution is the desired relative orbit when other perturbations are ignored. It will be used as comparison to the truth models calculated by nonlinear simulations.

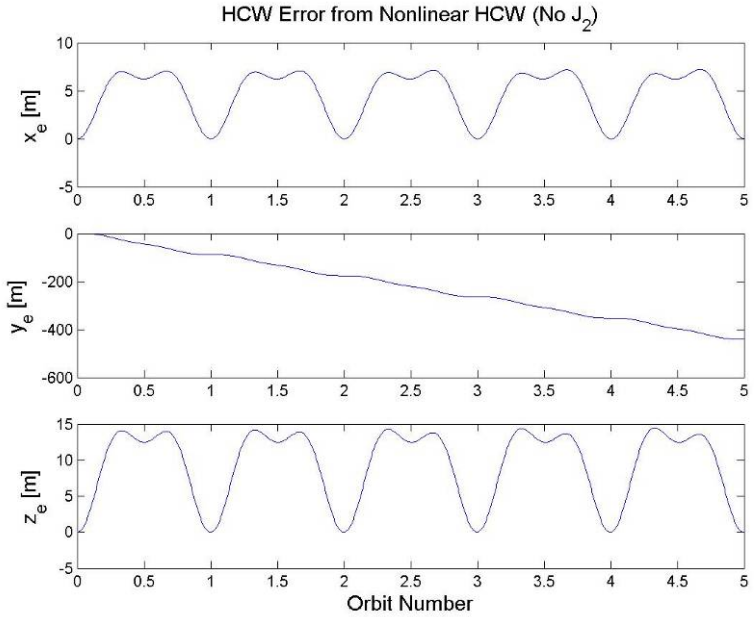

Fig. 4.1 *HCW* model (4.15) position errors from the nonlinear *HCW* Eqns. (4.4-5) for deputy satellite 1

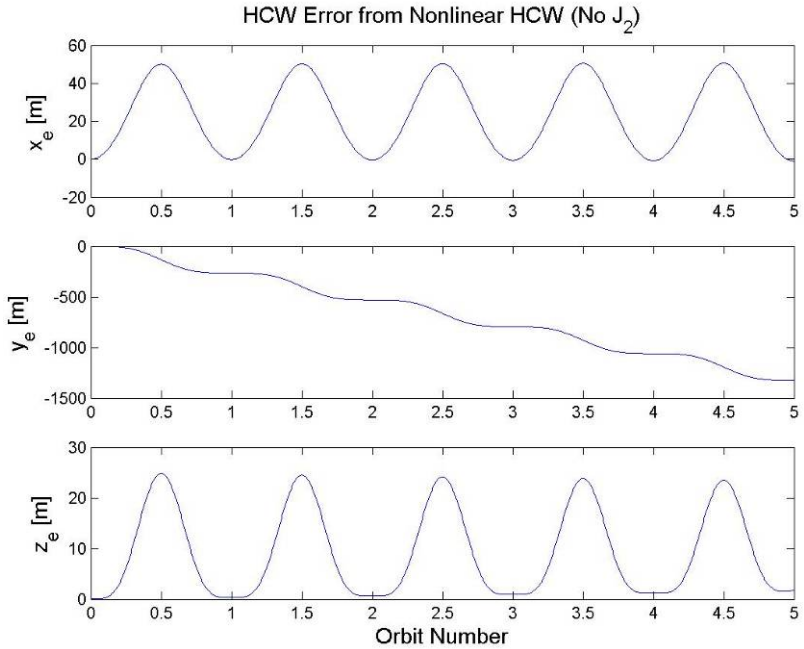

Fig. 4.2 *HCW* model (4.15) position errors from the nonlinear *HCW* Eqns. (4.4-5) for deputy satellite 2

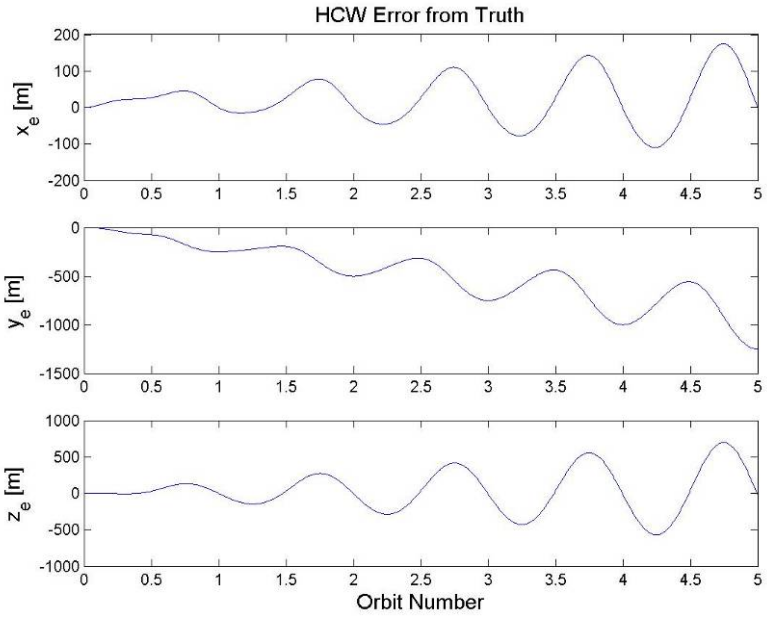

Fig. 4.3 *HCW* model (4.15) position errors from truth (3.27-33) for deputy satellite 1

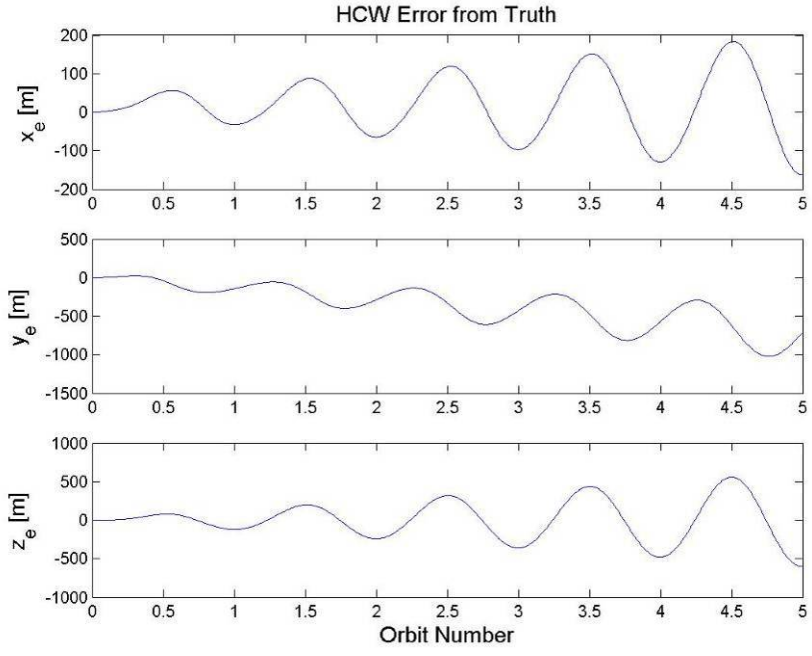

Fig. 4.4 *HCW* model (4.15) position errors from truth (3.27-33) for deputy satellite 2

As seen in Fig. 4.3 and 4.4, the *HCW* solutions also fail to capture the true relative motion, as the linear dynamics do not capture any perturbations due to the oblateness of the Earth. This set of linearized constant coefficient differential equations is valid only under the following assumptions: a circular chief orbit governed by the dynamics from Eqn. (4.5), linearized differential gravity field, and a spherical central body of uniform density. As such, these equations breakdown when these assumptions are violated. The next sections will work on improving this model to yield higher fidelity linear analytical solutions to the *HCW* equations.

4.4 Adding Nonlinear Differential Gravity

We now wish to add the effects of the second-order nonlinear differential gravity terms to the *HCW* equations in order to remove growth associated with higher order differential gravity terms.

$$\begin{bmatrix} \ddot{x} - 2n\dot{y} - 3n^2 x \\ \ddot{y} + 2n\dot{x} \\ \ddot{z} + n^2 z \end{bmatrix} = \nabla U_{d_{HOT}} \tag{4.16}$$

The higher order terms due to differential gravity were ignored in the previous section. These higher order terms may be expressed by the same perturbing potential

$$U_{d_{HOT}} = -\frac{\mu}{r}\sum_{\ell=3}^{\infty}(-1)^n \left(\frac{\rho}{r}\right)^n P_n\left(x/\rho\right) \tag{4.17}$$

The gradient of the perturbing potential was given in Eqn. (4.12) as

$$\frac{\partial U_{d_{HOT}}}{\partial \vec{\rho}} = \frac{\mu}{r_c^3}\sum_{n=3}^{\infty}(-1)^n \left(\frac{\rho}{r_c}\right)^{n-2} \frac{n}{y^2+z^2}\left[\rho^2 P_n\left(x/\rho\right)\hat{i}_1 + \rho P_{n-1}\left(x/\rho\right)\hat{i}_2\right] \tag{4.18}$$

If we retain only the quadratic terms, which correspond to $n=3$, then the perturbation due to second-order nonlinear differential gravity is

$$\begin{aligned}
\frac{\partial U_{d_{HOT}}}{\partial x} &= \frac{3\mu}{2r_c^4}\left[y^2+z^2-2x^2\right] \\
\frac{\partial U_{d_{HOT}}}{\partial y} &= \frac{3\mu}{2r_c^4}2xy \\
\frac{\partial U_{d_{HOT}}}{\partial z} &= \frac{3\mu}{2r_c^4}2xz
\end{aligned} \tag{4.19}$$

Eqn. (4.19) may be substituted into Eqn. (4.16) to yield the second-order nonlinear *HCW* equations:

$$\begin{aligned}
\ddot{x}-2n\dot{y}-3n^2x &= \frac{3\mu}{2r_c^4}\left[y^2+z^2-2x^2\right] \\
\ddot{y}+2n\dot{x} &= \frac{3\mu}{2r_c^4}2xy \\
\ddot{z}+n^2z &= \frac{3\mu}{2r_c^4}2xz
\end{aligned} \tag{4.20}$$

How does this approximation compare to the full nonlinear *HCW* solution from Eqns. (4.4-5)? This second-order approximation of the differential gravity field is a fairly reasonable approximation. Fig. 4.5 and 4.6 shows the deviation of the nonlinear *HCW* in the absence of J_2 from the desired *HCW* bounded orbit. Notice the drift in each position component is no more than about 2 *m* after 5 orbits in the along-track direction.

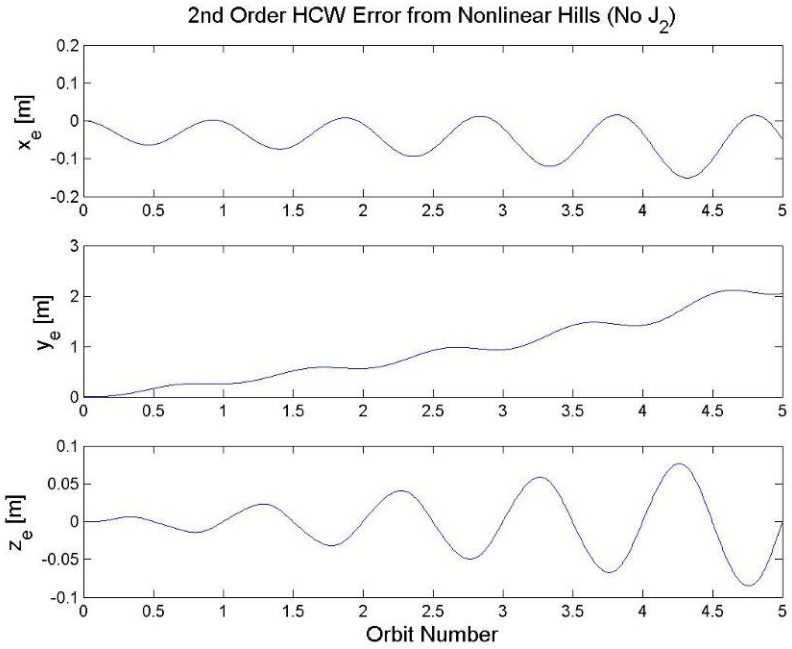

Fig. 4.5 Second-order nonlinear HCW (4.20) error from full nonlinear *HCW* solution (4.4-5) for deputy satellite 1

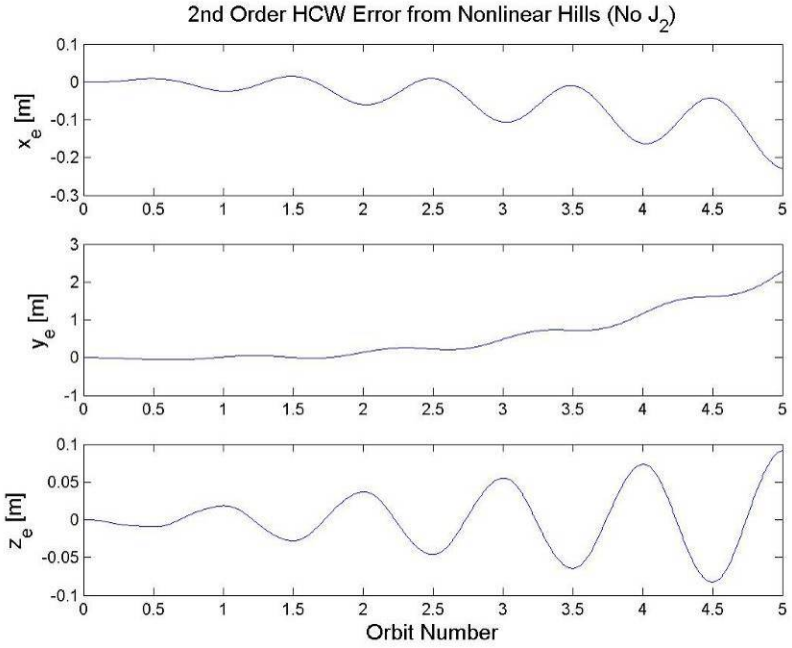

Fig. 4.6 Second-order nonlinear HCW (4.20) error from full nonlinear HCW solution (4.4-5) for deputy satellite 2

4.5 Method of Perturbations

The following derivations are adapted from Ref. 9, and add the effects of second-order differential gravity to the *HCW* equations. We use the method of perturbations, assuming that Eqns. (4.20) have solutions of the following form:

$$\begin{aligned} x &= x_h + \varepsilon x_p \qquad \dot{x} = \dot{x}_h + \varepsilon \dot{x}_p \qquad \ddot{x} = \ddot{x}_h + \varepsilon \ddot{x}_p \\ y &= y_h + \varepsilon y_p \qquad \dot{y} = \dot{y}_h + \varepsilon \dot{y}_p \qquad \ddot{y} = \ddot{y}_h + \varepsilon \ddot{y}_p \\ z &= z_h + \varepsilon z_p \qquad \dot{z} = \dot{z}_h + \varepsilon \dot{z}_p \qquad \ddot{z} = \ddot{z}_h + \varepsilon \ddot{z}_p \end{aligned} \tag{4.21}$$

The subscript *h* refers to the solutions of the *HCW* equations and in this context will be termed the homogeneous solution; the subscript *p* refers to the correction due to the nonlinear gravitational terms added to Eqns. (4.20) and will be termed the perturbation solution. We now define our perturbation parameter as

$$\varepsilon \equiv \frac{3}{2}\frac{\mu}{r_c^4} \tag{4.22}$$

It is noted that this perturbation parameter is not dimensionless. This is done intentionally, in order to compare results obtained from Ref. 9. The new nonlinear equations of motion are now

$$\begin{aligned} \ddot{x} - 2n\dot{y} - 3n^2 x &= \varepsilon\left(y^2 + z^2 - 2x^2\right) \\ \ddot{y} + 2n\dot{x} &= 2\varepsilon xy \\ \ddot{z} + n^2 z &= 2\varepsilon xz \end{aligned} \tag{4.23}$$

Substituting Eqns. (4.21) into (4.23) we obtain

$$\begin{aligned} &\ddot{x}_h - 2n\dot{y}_h - 3n^2 x_h + \varepsilon\left(\ddot{x}_p - 2n\dot{y}_p - 3n^2 x_p\right) = \varepsilon\left[\left(y_h + \varepsilon y_p\right)^2 + \left(z_h + \varepsilon z_p\right)^2 - 2\left(x_h + \varepsilon x_p\right)^2\right] \\ &\ddot{y}_h + 2n\dot{x}_h + \varepsilon\left(\ddot{y}_p + 2n\dot{x}_p\right) = 2\varepsilon\left(x_h + \varepsilon x_p\right)\left(y_h + \varepsilon y_p\right) \\ &\ddot{z}_h + n^2 z_h + \varepsilon\left(\ddot{z}_p + n^2 z_p\right) = 2\varepsilon\left(x_h + \varepsilon x_p\right)\left(z_h + \varepsilon z_p\right) \end{aligned} \tag{4.24}$$

As $\varepsilon \ll 1$, we can expand and drop the higher order terms of ε to obtain the following equations of motion for the second-order gravitational perturbation.

$$\begin{aligned} &\ddot{x}_p - 2n\dot{y}_p - 3n^2 x_p = \varepsilon\left(y_h^2 + z_h^2 - 2x_h^2\right) \\ &\ddot{y}_p + 2n\dot{x}_p = 2\varepsilon x_h y_h \\ &\ddot{z}_p + n^2 z_p = 2\varepsilon x_h z_h \end{aligned} \tag{4.25}$$

4.6 Perturbed HCW Solution

The perturbation due to second-order differential gravity has the form of a linear system with a forcing function added to it. As such, the solution of the perturbation may be written using the state transition matrix of the homogenous solution to Eqn. (4.25). We make note of the fact that the homogeneous solution to Eqn. (4.25) is equivalent to the *HCW* solution. A more detailed proof is provided in Appendix B (also see Ref. 11). We define our perturbation state vector as the relative perturbed position and velocity vectors.

$$\bar{x}_p = \begin{bmatrix} x_p & y_p & z_p & \dot{x}_p & \dot{y}_p & \dot{z}_p \end{bmatrix}^T \tag{4.26}$$

We may then write Eqn. (4.24) in state-space form as,

$$\dot{\bar{x}}_p = \mathbf{A}_h(t)\bar{x}_p + \mathbf{B}(t)\bar{u}_h(t) \tag{4.27}$$

The first term yields the homogeneous solution when integrated, and the second term is the forcing function. $\mathbf{A}_h$ is the system matrix, and is constant, $\bar{u}_h(t)$ is the perturbation term (RHS of Eqns. (4.25)), and the matrix $\boldsymbol{B}$ is the compatibility matrix. The general solution to Eqn. (4.27) may be written as

$$\vec{x}_p(t) = \mathbf{\Phi}_h(t,t_0)\vec{x}_p(t_0) + \int_{t_0}^{t} \mathbf{\Phi}_h(t,\tau)\mathbf{B}\vec{u}_h(\tau)d\tau \tag{4.28}$$

Where the system matrices are defined as[23]

$$\mathbf{A}_h = \begin{bmatrix} 0 & 0 & 0 & 1 & 0 & 0 \\ 0 & 0 & 0 & 0 & 1 & 0 \\ 0 & 0 & 0 & 0 & 0 & 1 \\ 3n^2 & 0 & 0 & 0 & 2n & 0 \\ 0 & 0 & 0 & -2n & 0 & 0 \\ 0 & 0 & -n^2 & 0 & 0 & 0 \end{bmatrix} \qquad \mathbf{B} = \begin{bmatrix} 0 & 0 & 0 \\ 0 & 0 & 0 \\ 0 & 0 & 0 \\ 1 & 0 & 0 \\ 0 & 1 & 0 \\ 0 & 0 & 1 \end{bmatrix} \qquad \vec{u}_h = \begin{bmatrix} y_h^2 + z_h^2 - 2x_h^2 \\ 2x_h y_h \\ 2x_h z_h \end{bmatrix}$$

$$\mathbf{\Phi}_h = \begin{bmatrix} 4-3\cos nt & 0 & 0 & \frac{\sin nt}{n} & \frac{2}{n}(1-\cos nt) & 0 \\ 6(\sin nt - nt) & 1 & 0 & -\frac{2}{n}(1-\cos nt) & \frac{4\sin nt - 3nt}{n} & 0 \\ 0 & 0 & \cos nt & 0 & 0 & \frac{\sin nt}{n} \\ 3n\sin nt & 0 & 0 & \cos nt & 2\sin nt & 0 \\ -6n(1-\cos nt) & 0 & 0 & -2\sin nt & 4\cos nt - 3 & 0 \\ 0 & 0 & -n\sin nt & 0 & 0 & \cos nt \end{bmatrix}$$

The homogeneous solutions are substituted into x_h, y_h, z_h, respectively. We have thus effectively approximated the solution to the second-order differential gravity perturbation to the *HCW* equations.

Equation. (4.28) yields direct solutions for the relative position and velocity of the nonlinear differential gravity perturbation. The perturbation positions as a function of time are written below, where $r_{rel} \equiv 2A$.

$$x_p(t) = [4 - 3\cos nt]\, x_{p,0} + \frac{\sin nt}{n}\dot{x}_{p,0} + 2\frac{1-\cos nt}{n}\dot{y}_{p,0} + \frac{1}{48}\left(\frac{r_{rel}}{n}\right)^2 (18 + 12\cos 2\alpha') + \frac{1}{48}\left(\frac{r_{rel}}{n}\right)^2 [2\cos(2nt + 2\alpha') - 5\cos(nt - 2\alpha') - 9\cos(nt + 2\alpha') - 18\cos nt] \tag{4.29}$$

$$y_p(t) = [6\sin nt - 6nt]\, x_{p,0} + y_{p,0} - 2\frac{1-\cos nt}{n}\dot{x}_{p,0} + \frac{4\sin nt - 3nt}{n}\dot{y}_{p,0} - \frac{nt}{48}\left(\frac{r_{rel}}{n}\right)^2 (36 + 18\cos 2\alpha') - \frac{1}{48}\left(\frac{r_{rel}}{n}\right)^2 [5\sin(2nt + 2\alpha') + 3\sin 2\alpha' - 18\sin(nt + 2\alpha') - 10\sin(nt - 2\alpha') - 36\sin nt] \tag{4.30}$$

$$z_p(t) = z_{p,0}\cos nt + \frac{\sin nt}{n}\dot{z}_{p,0} + \frac{1}{24}\left(\frac{r_{rel}}{n}\right)^2 [2\cos(2nt + 2\alpha') - 6\cos nt + \cos(nt - 2\alpha') - 3\cos(nt + 2\alpha')] \tag{4.31}$$

The initial formation angle α' is defined in terms of the integral constant α as

$$\alpha' \equiv \alpha + \pi/2$$

This is due to the 90^o phase difference in defining our formation with the formation in Ref. 9 (see Fig. 4.7).

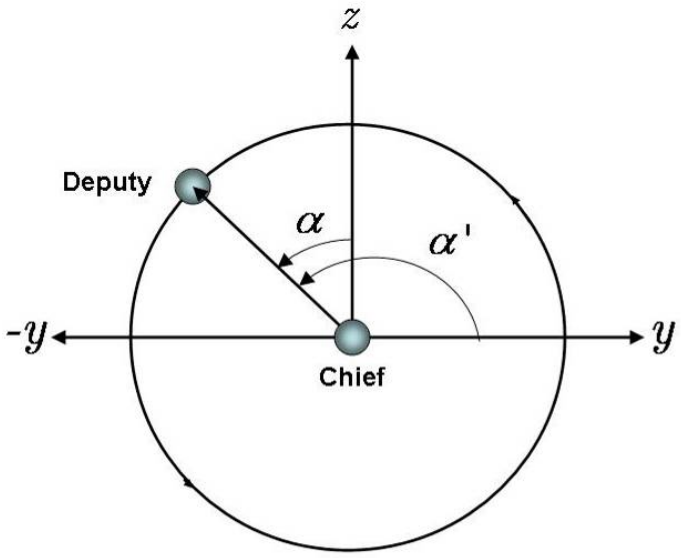

Fig. 4.7 Deputy satellite location in the *y*-z plane

Now that the homogenous solutions are known from Eqns. (4.15) and the perturbed solutions are given in Eqns. (4.29-31), they may be substituted into Eqns. (4.21) to obtain the full solution.

Example 4. Perturbed HCW Simulation Error from HCW Solution

We define the initial homogeneous conditions for the perturbed *HCW* solution as those evaluated at $t = t_0$ for the *HCW* position and velocity equations; i.e. they have the same initial relative position and velocities as the *HCW* solutions. The homogeneous initial conditions for both deputy satellites are then

$$\vec{x}_{d1,h}(0) = \begin{bmatrix} 5 & 0 & 10 \end{bmatrix}^T \; km$$
$$\dot{\vec{x}}_{d1,h}(0) = \begin{bmatrix} 0 & -8.8233665\times10^{-3} & 0 \end{bmatrix}^T \; km/sec$$

$$\vec{x}_{d2,h}(0) = \begin{bmatrix} 0 & -10 & 0 \end{bmatrix}^T \; km$$
$$\dot{\vec{x}}_{d2,h}(0) = \begin{bmatrix} -4.4116833\times10^{-3} & 0 & -8.8233665\times10^{-3} \end{bmatrix}^T \; km/sec$$

The perturbed initial conditions are calculated by utilizing a weak criterion for zero secular growth in the along track direction. By inspecting Eqn. (4.29), this is accomplished when the secular terms are set to zero:

$$-6nx_{p,0} - 3\dot{y}_{p,0} - \frac{n}{48}\left(\frac{\rho}{n}\right)^2 (36 + 18\cos 2\alpha') = 0 \tag{4.31}$$

The more specific solution to Eqn. (4.31) used in the simulations is

$$\begin{aligned} x_p(0) &= 0 \\ \dot{y}_p(0) &= -\left(\frac{\rho^2}{48n}\right)(12 + 6\cos 2\alpha') \end{aligned} \tag{4.32}$$

The perturbed initial conditions for the two deputy satellites are set to zero for all components except the along-track velocity.

Comparing the nonlinear simulation using the corrected initial conditions defined above and Eqns. (4.4-5), to the desired *HCW* bounded relative orbit (4.15), we see that the added correction based on the model which contains second-order differential gravity yields favorable results (see Fig. 4.8 and 4.9). The secular growth in the along-track direction has almost vanished, yielding a solution that is almost bounded, but only when the effects of J_2 are ignored.

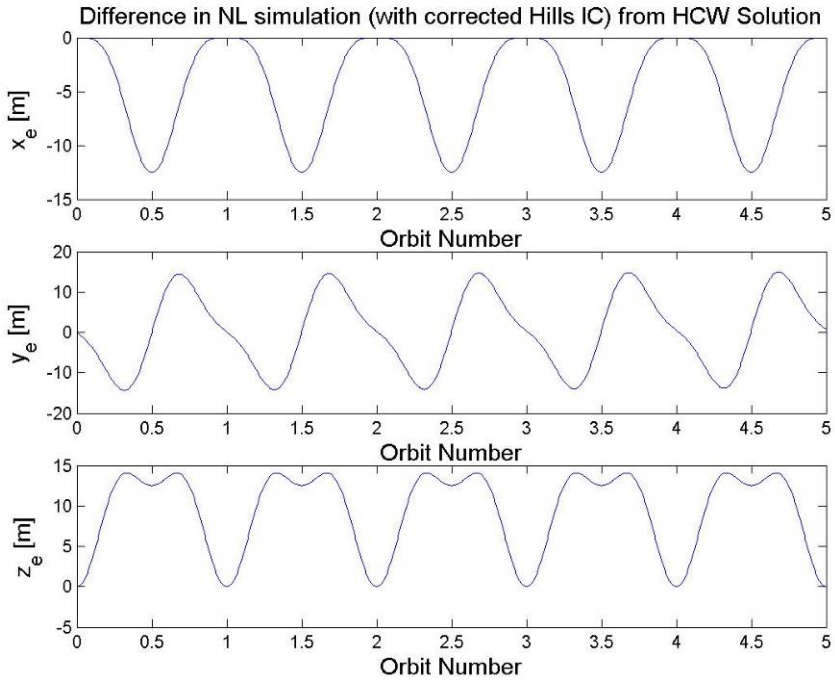

Fig. 4.8 Errors of nonlinear *HCW* simulation (4.4-5) with corrected ICs from *HCW* solution (4.15) for deputy satellite 1

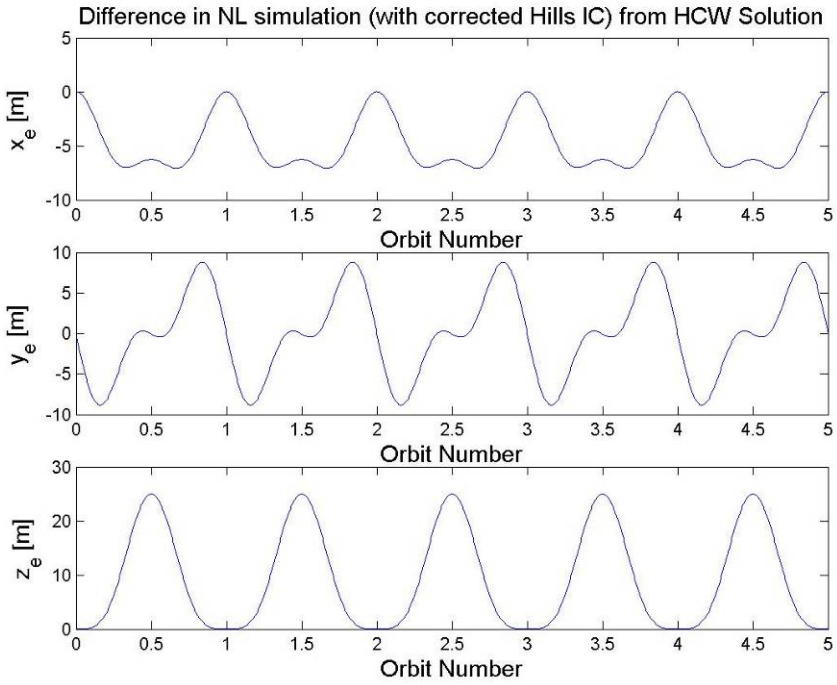

Fig. 4.9 Errors of nonlinear *HCW* simulation (4.4-5) with corrected ICs from *HCW* solution (4.15) for deputy satellite 2

This set of differential equations is valid only under the following assumptions: a circular chief orbit governed by the dynamics from Eqn. (4.5), second-order differential gravity field, and a spherical central body of uniform density. As such, these equations yield results that drift when these assumptions are violated. Neither the *HCW* equations nor the perturbed *HCW* equations presented in this chapter have included the effects of J_2. The next chapter will work on improving this model to yield higher fidelity linear analytical solutions to the *HCW* equations by obtaining analytical solutions including the linearized approximation of J_2.

CHAPTER 5

LINEARIZED J_2 MODELS

5.1 J_2-Modified Hill-Clohessy-Wiltshire Equations

It is possible to obtain an analytical solution of the relative motion that includes the time-averaged, linearized effects of the J_2 perturbation.[7,8] Beginning with the regular two-body equation, the J_2 acceleration is added resulting in the following dynamics in the inertial frame

$$\ddot{\vec{r}} = \vec{g}\left(\vec{r}\right) + \vec{J}_2\left(\vec{r}\right) \tag{5.1}$$

where $\vec{g}\left(\vec{r}\right)$ is the gravitational acceleration and $\vec{J}_2\left(\vec{r}\right)$ is the acceleration due to second-order zonal harmonics. Both accelerations are expressed in the $\left(\hat{r} \quad \hat{\theta} \quad \hat{i}\right)$ coordinate frame as

$$\vec{g}\left(\vec{r}\right) = -\frac{\mu}{r^2}\hat{r} \tag{5.2}$$

and

$$\vec{J}_2\left(\vec{r}\right) = -\frac{3}{2}\frac{\mu J_2 R_\oplus^2}{r^4}\begin{bmatrix} \left(1-3\sin^2 i\right) \\ \left(2\sin^2 i \sin\theta\cos\theta\right) \\ \left(2\sin i\cos i\sin\theta\right) \end{bmatrix} \tag{5.3}$$

where J_2 is the oblateness perturbation, $R_\oplus$ is the equatorial radius of the Earth, i is the orbit

inclination, which in the remainder of the text will be the chief orbit inclination, and θ is the argument of latitude of the satellite.

5.1.1 Linearizing J_2

Obtaining the relative equations of motion follows a similar procedure to that of the Hill's equations. We begin with a two-body Keplerian chief (reference) orbit, modeled the same as in the Hill's equations.

$$\ddot{\vec{r}}_c = \vec{g}\left(\vec{r}_c\right) \tag{5.4}$$

Linearizing Eqn. (5.1) for the deputy satellite with respect to the chief orbit results in

$$\ddot{\vec{r}}_d = \vec{g}\left(\vec{r}_c\right) + \nabla\left(\vec{g}\left(\vec{r}_c\right)\right)\cdot\vec{\rho} + \bar{J}_2\left(\vec{r}_c\right) + \nabla\left(\bar{J}_2\left(\vec{r}_c\right)\right)d\theta\cdot\vec{\rho} \tag{5.5}$$

It is noted due to this linearization, all angles and angular velocities expressed below are associated with the chief satellite.

The gradient of the gravitational force is calculated in the $\left(\hat{r} \quad \hat{\theta} \quad \hat{i}\right)$ coordinate system, and the gradient of the J_2 perturbation is given in the $\left(\hat{R} \quad \hat{T} \quad \hat{N}\right)$ coordinate system as defined in Ref. 23; which correlates with the $\left(\hat{r} \quad \hat{\theta} \quad \hat{i}\right)$ system. The resulting gradients are

$$\nabla\vec{g}\left(\vec{r}\right) = \begin{bmatrix} 2\dfrac{\mu}{r^3} & 0 & 0 \\ 0 & -\dfrac{\mu}{r^3} & 0 \\ 0 & 0 & -\dfrac{\mu}{r^3} \end{bmatrix} \tag{5.6}$$

and

$$\nabla \vec{J}_2 = \frac{6\mu J_2 R_\oplus^2}{r_c^5}\begin{bmatrix} \left(1-3\sin^2 i\sin^2\theta\right) & \sin^2 i\sin 2\theta & \sin 2i\sin\theta \\ \sin^2 i\sin 2\theta & -\frac{1}{2}-\sin^2 i\left(\frac{1}{2}-\frac{7}{4}\sin^2\theta\right) & -\frac{\sin 2i\cos\theta}{4} \\ \sin 2i\sin\theta & -\frac{\sin 2i\cos\theta}{4} & -\frac{3}{4}+\sin^2 i\left(\frac{1}{2}+\frac{5}{4}\sin^2\theta\right) \end{bmatrix} \quad (5.7)$$

The relative distance between the chief and deputy is the same as with the derivation of the *HCW* equations. We will drop the subscript *d* denoting the deputy satellite.

$$\vec{\rho} = \vec{r} - \vec{r}_c \quad (5.8)$$

Because the chief orbit is rotating, the relative motion dynamics are still calculated through the use of the *transport theorem*.

$$\ddot{\vec{\rho}} + 2\vec{\omega}\times\dot{\vec{\rho}} + \dot{\vec{\omega}}\times\vec{\rho} + \vec{\omega}\times\left(\vec{\omega}\times\vec{\rho}\right) = \ddot{\vec{r}} - \ddot{\vec{r}}_c \quad (5.9)$$

The rotation rate of the chief orbit $\vec{\omega}$ is the angular velocity vector of the chief orbit as previously stated. For a circular orbit with no other external forces this is

$$\vec{\omega} = \dot{\theta} = \sqrt{\frac{\mu}{r_c^3}}\hat{z} = n\hat{z} \quad (5.10)$$

We now substitute Eqn. (5.5) into Eqn. (5.9) to yield

$$\ddot{\vec{\rho}} + 2\vec{\omega}\times\dot{\vec{\rho}} + \dot{\vec{\omega}}\times\vec{\rho} + \vec{\omega}\times\left(\vec{\omega}\times\vec{\rho}\right) = \vec{g}\left(\vec{r}_c\right) + \nabla\left(\vec{g}\left(\vec{r}_c\right)\right)\cdot\vec{\rho} + \vec{J}_2\left(\vec{r}_c\right) + \nabla\left(\vec{J}_2\left(\vec{r}_c\right)\right)\cdot\vec{\rho} - \ddot{\vec{r}}_c \quad (5.11)$$

5.1.2 Time-Averaging J_2

The J_2 gradient term yields problems in obtaining a closed-form solution, as it is only constant for the equatorial orbit case. However, since it is periodic, we are able

to obtain an approximate solution by taking the average value of this gradient over one orbit. The resulting term for the gradient is now

$$\frac{1}{2\pi}\int_0^{2\pi}\nabla\left(\vec{J}_2\left(\vec{r}_c\right)\right)d\theta=\frac{\mu}{r^3}\begin{bmatrix}4s & 0 & 0\\ 0 & -s & 0\\ 0 & 0 & -3s\end{bmatrix} \tag{5.12}$$

where

$$s\equiv\frac{3J_2R_\oplus^2}{8r^2}\left(1+3\cos 2i\right) \tag{5.13}$$

and the inclination angle i of the chief orbit is constant.

5.1.3 Adjusting the Period of the Chief Orbit

The inclusion of the J_2 perturbation alters the orbital period and the crossing of the equatorial plane of the satellite. This means the angular velocity vector expressed in Eqn. (5.10) is no longer valid when J_2 acceleration is present. We can fix this discrepancy by adjusting the period of the reference orbit, which will yield a new mean angular velocity vector. We start by modifying the equation of motion for the chief orbit, which was first assumed to be Keplerian with the following forcing term

$$\frac{1}{2\pi}\int_0^{2\pi}\vec{J}_2\left(\vec{r}_c\right)d\theta \tag{5.14}$$

The new averaged J_2 forcing term is simply

$$\frac{1}{2\pi}\int\vec{J}_2\left(\vec{r}_c\right)d\theta=-n^2rs\hat{x} \tag{5.15}$$

It is noted that there is still drift associated with the longitude of ascending node. In order to alleviate this drift, the normal component of the J_2 disturbance is added to the chief orbit equations of motion, as this is the only J_2 component that causes the separation of longitude of ascending node. This condition matches the drift in the longitude of ascending node of both the chief and deputy satellite with respect to the mean osculating elements. The additional forcing term is

$$\vec{J}_2\left(\vec{r}_c\right)\cdot\hat{N} \tag{5.16}$$

The angular velocity vector of the rotating coordinate system is updated using the following relation

$$\vec{\omega}\times\left(\vec{\omega}\times\vec{r}_c\right)=\frac{\mu}{r_c^3}\hat{r}+\frac{1}{2\pi}\int_0^{2\pi}\vec{J}_2\left(\vec{r}_c\right)d\theta+\vec{J}_2\left(\vec{r}_c\right)\cdot\hat{N} \tag{5.17}$$

which yields the new time-averaged angular velocity

$$\vec{\omega}=\dot{\theta}\hat{z}=nc\hat{z} \tag{5.18}$$

$$c=\sqrt{1+s} \tag{5.19}$$

We stress the fact that the angular velocity vector we will use for this solution is a time-averaged angular velocity vector, and that the chief reference orbit normal is assumed to always point in the same direction relative to the ECI frame. In doing so, we neglect the fact that the orbit normal (direction of angular momentum), and therefore the angular velocity, actually wobbles about the Z-axis when the inclination is not equal to 0^o. It is possible to alleviate this wobble in the analytical solution, but it does increase the number of differential equations and is not presented here.

5.1.4 Modified HCW Solution

The relative equations of motion now become

$$\ddot{\vec{\rho}} + 2\vec{\omega}\times\dot{\vec{\rho}} + \dot{\vec{\omega}}\times\vec{\rho} + \vec{\omega}\times\left(\vec{\omega}\times\vec{\rho}\right) = \nabla\left(\vec{g}\left(\vec{r}_c\right)\right)\cdot\vec{\rho} + \vec{J}_2\left(\vec{r}_c\right) + \frac{1}{2\pi}\int_0^{2\pi}\nabla\left(\vec{J}_2\left(\vec{r}_c\right)\right)d\theta\cdot\vec{\rho} - \frac{1}{2\pi}\int_0^{2\pi}\nabla\left(\vec{J}_2\left(\vec{r}_c\right)\right)d\theta - \vec{J}_2\left(\vec{r}_c\right)\cdot\vec{N} \tag{5.20}$$

With the appropriate substitutions, we can express the equations of motion in terms of the $\vec{\rho} = \begin{pmatrix} x & y & z \end{pmatrix}^T$ relative coordinate frame,

$$\begin{aligned} \ddot{x} - 2nc\dot{y} - (5c^2 - 2)n^2 x &= -3n^2 J_2 \frac{R_\oplus^2}{r_c}\left(\frac{1}{2} - \frac{3}{2}\sin^2 i \sin^2 kt - \frac{1+3\cos 2i}{8}\right) \\ \ddot{y} + 2nc\dot{x} &= -\frac{3}{2}n^2 J_2 \frac{R_\oplus^2}{r_c}\sin^2 i \sin 2kt \\ \ddot{z} + (3c^2 - 2)n^2 z &= 0 \end{aligned} \tag{5.21}$$

$$k = nc + \frac{3\sqrt{\mu}J_2 R_\oplus^2}{2r_c^{7/2}}\cos^2 i \tag{5.22}$$

where k is the modified argument of latitude due to the J_2 perturbation. The homogeneous solution to this system is similar to that of the *HCW* equations, but with changes in the gain and gyroscopic coefficients imposed by adding the effects of J_2 The z equation is still a simple harmonic oscillator, and the in-plane motion is still coupled. The particular solution to the RHS may be integrated directly, so the total solution is straightforward by the use of the method of variation of parameters for the coupled in-plane equations.

The relative positions as a function of time given appropriate initial conditions are found to be

$$x(t)=\left[\frac{5s+3}{s-1}x_{h0}+\frac{2\sqrt{1+s}}{n(s-1)}\dot{y}_{h0}+\frac{1}{4}\frac{A_{J2}\left(3k-2n\sqrt{1+s}\right)\sin^2 i}{k\left(-n^2+n^2s+4k^2\right)}\right]\cos\left(n\sqrt{1-s}t\right)$$
$$-\frac{1}{4}\frac{A_{J2}\left(3k-2n\sqrt{1+s}\right)\sin^2 i}{k\left(-n^2+n^2s+4k^2\right)}\cos 2kt+\frac{\dot{x}_{h0}}{n\sqrt{1-s}}\sin\left(n\sqrt{1-s}t\right)-\frac{4(1+s)}{s-1}x_{h0}-\frac{2\sqrt{1+s}}{n(s-1)}\dot{y}_{h0} \tag{5.23}$$

$$y(t)=\left[\frac{2(5s+3)\sqrt{1+s}}{(1-s)^{3/2}}x_{h0}+\frac{4(1+s)}{n(1-s)^{3/2}}\dot{y}_{h0}+\frac{1}{2}\frac{A_{J2}\left(2ns-3k\sqrt{1+s}+2n\right)\sin^2 i}{k\sqrt{1-s}\left(-n^2+n^2s+4k^2\right)}\right]\sin\left(n\sqrt{1-s}t\right)$$
$$-\frac{1}{8}\frac{A_{J2}\left(5n^2s+4k^2+3n^2-6nk\sqrt{1+s}\right)\sin^2 i}{k^2\left(-n^2+n^2s+4k^2\right)}\sin 2kt-\frac{2\sqrt{1+s}}{n(s-1)}\dot{x}_{h0}\cos\left(n\sqrt{1-s}t\right) \tag{5.24}$$
$$+\left[\frac{2n(5s+3)\sqrt{1+s}}{(s-1)}\dot{x}_{h0}+\frac{5s+3}{s-1}\dot{y}_{h0}+\frac{A_{J2}\sin^2 i}{4k}\right]t+\frac{2\sqrt{1+s}}{n(s-1)}\dot{x}_{h0}+y_{h0}$$

$$z(t)=z_{h0}\cos\left(n\sqrt{1+3s}t\right)+\frac{\dot{z}_{h0}}{n\sqrt{1+3s}}\sin\left(n\sqrt{1+3s}t\right) \tag{5.25}$$

$$A_{J2}\equiv -3n^2J_2\frac{R_\oplus^2}{r_c}$$

Equations (5.21) will be referred to as the J_2-*Modified-Hill-Clohessy-Wiltshire* (MHCW) equations that have the general solutions presented in Eqns. (5.23-25). The velocities are simply the time derivatives of the position.

Example 5. Error of Nonlinear Simulation from J_2-Modified HCW Simulation

We define the initial conditions for the *MHCW* solution in a similar manner as *Example 3*. The relative initial positions are those evaluated at $t=t_0$ for the *HCW* position equations, i.e. they have the same initial relative positions as the *HCW* solutions. The initial cross-track velocity is also the same as the *HCW* initial condition. However the initial velocities in the radial and along-track directions are calculated in

order to remove the secular and drift terms associated with equations 5.23-25. The new velocity initial conditions are calculated as

$$\dot{x}_{h0} = y_{h0} n \left(\frac{1-s}{2\sqrt{1+s}} \right)$$

$$\dot{y}_{h0} = -2n\sqrt{1+s}\, x_{h0} + \frac{3nJ_2 R_{\oplus}^2}{8kr_c}\left(1-\cos 2i\right)$$

Fig. 5.1 and 5.2 shows the error of the desired bounded J_2-*Modified HCW* model from the full nonlinear model governed by Eqns. (3.27-28, 31) for both satellites. As can be seen, the drift in the along-track direction has not disappeared, but the growth in the cross-track direction has been reduced, when compared to the *HCW* model.

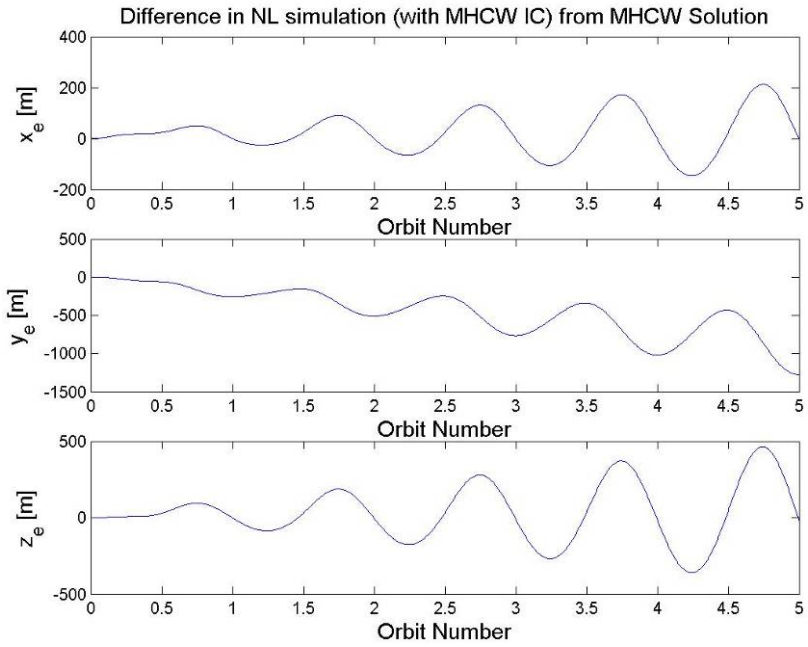

Fig. 5.1 *MHCW* model (5.23-25) position errors from full nonlinear simulation (3.27-28, 31) for deputy satellite 1

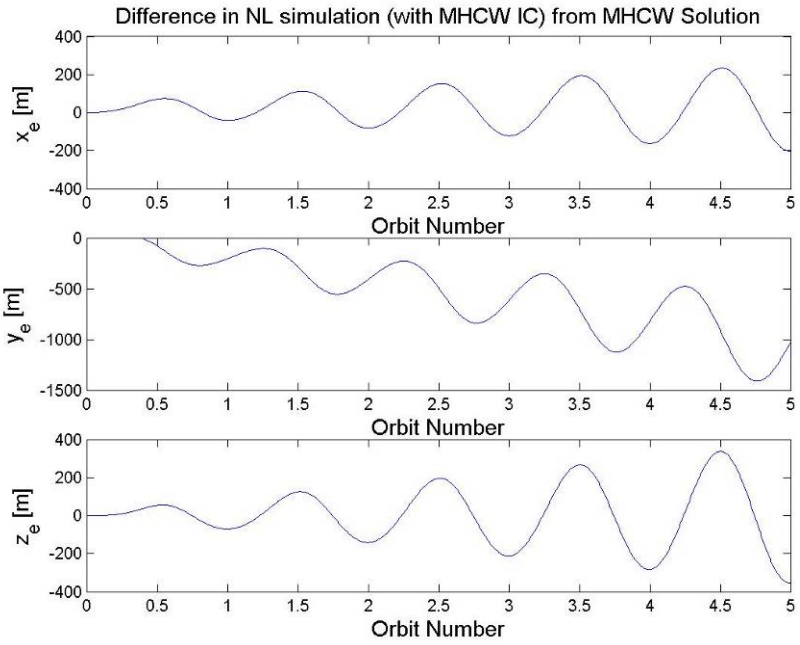

Fig. 5.2 *MHCW* model (5.23-25) position errors from full nonlinear simulation (3.27-28, 31) for deputy satellite 2

If we instead implement the MHCW initial conditions to the nonlinear equations defined to include only the linearized effects of J_2 and up to second order differential gravity, as defined by Eqn. (5.27) in the next section, we obtain similar results to the simulation from *Example 3* (Fig. 4.1 and 4.2). Eqn. (5.27) is in effect, the J_2-*Modified* version of Eqn. (4.4). Fig. 5.3 and 5.4 below show the difference of this nonlinear simulation with the *MHCW* initial conditions from the desired bounded orbit defined by Eqns. (5.23-5.25), subject to the zero secular growth and zero offset terms as defined in this example. Notice the radial and cross-track motion differences of this linearized J_2 model are now bounded, however the along-track difference still displays a large secular growth. This also comes from the fact that the initial conditions are defined from the Eqns. (5.23-25), which do not take into account second-order differential

gravity effects. This drift may be alleviated by adding the effects of second-order differential gravity, as was done for the *HCW* equations in Chapter 4.

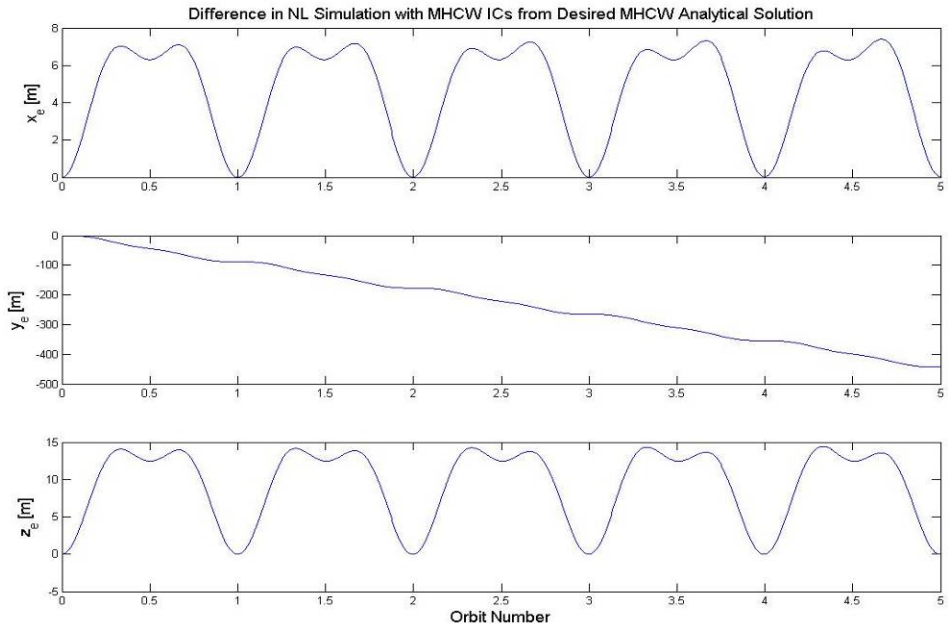

Fig. 5.3 *MHCW* model (5.23-25) position errors from nonlinear simulation (5.27) for deputy satellite 1

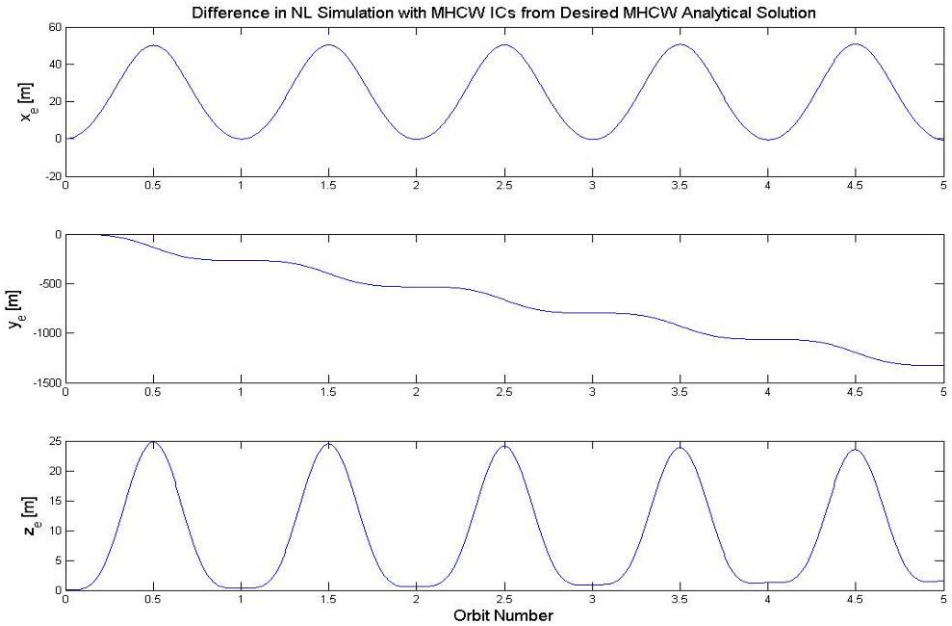

Fig. 5.4 *MHCW* model (5.23-25) position errors from full nonlinear simulation (5.27) for deputy satellite 2

5.2 The Perturbed J2-Modified Hill-Clohessy-Wiltshire Equations

5.2.1 Describing Dynamics

This section follows §4.5 exactly, except now we will assume that the solutions to the *MHCW* equations are the "homogeneous" solution to the following nonlinear system (J_2 terms included).

$$\left\{\begin{array}{l}\ddot{x}-2nc\dot{y}-\left(5c^2-2\right)n^2x\\ \ddot{y}+2nc\dot{x}\\ \ddot{z}+\left(3c^2-2\right)z\end{array}\right\}=\vec{J}_2\left(\vec{r}_c\right)-\frac{1}{2\pi}\int_0^{2\pi}\vec{J}_2\left(\vec{r}_c\right)d\theta+\vec{J}_2\left(\vec{r}_c\right)\cdot\hat{N}+O\left(\bar{g}\left(\bar{\rho},\vec{r}_c\right)^2\right) \quad (5.26)$$

The second-order terms due to differential gravity were added to the *HCW* equations in the previous section. These higher order terms will be added to the *MHCW* equations in the same manner. The new nonlinear equations of motion are now

$$\begin{aligned}\ddot{x}-2nc\dot{y}-(5c^2-2)n^2x&=-3n^2J_2\frac{R_\oplus^2}{r_c}\left(\frac{1}{2}-\frac{3}{2}\sin^2 i\sin^2 kt-\frac{1+3\cos 2i}{8}\right)+\varepsilon\left[y^2+z^2-2x^2\right]\\ \ddot{y}+2nc\dot{x}&=-\frac{3}{2}n^2J_2\frac{R_\oplus^2}{r_c}\sin^2 i\sin 2kt+\varepsilon 2xy\\ \ddot{z}+(3c^2-2)n^2z&=\varepsilon 2xz\end{aligned} \quad (5.27)$$

Equations (5.27) will be referred to as the nonlinear *Perturbed* J_2*-MHCW* equations (the perturbation being second-order differential gravity).

We now assume that Eqn. (5.26) have solutions of the following form:

$$\begin{array}{lll}x=x_h+\varepsilon x_p & \dot{x}=\dot{x}_h+\varepsilon\dot{x}_p & \ddot{x}=\ddot{x}_h+\varepsilon\ddot{x}_p\\ y=y_h+\varepsilon y_p & \dot{y}=\dot{y}_h+\varepsilon\dot{y}_p & \ddot{y}=\ddot{y}_h+\varepsilon\ddot{y}_p\\ z=z_h+\varepsilon z_p & \dot{z}=\dot{z}_h+\varepsilon\dot{z}_p & \ddot{z}=\ddot{z}_h+\varepsilon\ddot{z}_p\end{array} \quad (5.28)$$

The subscript *h* refers to the solutions of the *MHCW* equations and the subscript *p* refers to the correction due to the second-order nonlinear differential gravity terms added to Eqn. (5.27). The perturbation parameter is defined from the perturbation itself. Therefore it is the same as Eqn. (4.22)

$$\varepsilon \equiv \frac{3}{2}\frac{\mu}{r_c^4} \tag{5.29}$$

We note the following defined coefficients and lump the J_2 terms on the RHS together as J_{2x}, J_{2y}, and J_{2z} (J_{2z} is 0 in this describing model).

$$\begin{aligned} n_0 &\equiv nc \\ \alpha^2 &\equiv \frac{5c^2-2}{c^2} \\ \beta^2 &\equiv \frac{3c^2-2}{c^2} \end{aligned} \tag{5.30}$$

Substituting Eqns. (5.28-30) into (5.27) we obtain

$$\begin{aligned} \cancel{\ddot{x}_h - 2n_0\dot{y}_h - \alpha^2 n_0^2 x_h - J_{2x}} + \varepsilon\left(\ddot{x}_p - 2n_0\dot{y}_p - \alpha^2 n_0^2 x_p\right) &= \varepsilon\left[\left(y_h+\varepsilon y_p\right)^2 + \left(z_h+\varepsilon z_p\right)^2 - 2\left(x_h+\varepsilon x_p\right)^2\right] \\ \cancel{\ddot{y}_h + 2n_0\dot{x}_h - J_{2y}} + \varepsilon\left(\ddot{y}_p + 2n_0\dot{x}_p\right) &= 2\varepsilon\left(x_h+\varepsilon x_p\right)\left(y_h+\varepsilon y_p\right) \\ \cancel{\ddot{z}_h + \beta^2 n_0^2 z_h - J_{2z}} + \varepsilon\left(\ddot{z}_p + \beta^2 n_0^2 z_p\right) &= 2\varepsilon\left(x_h+\varepsilon x_p\right)\left(z_h+\varepsilon z_p\right) \end{aligned} \tag{5.31}$$

Since $\varepsilon \ll 1$, we may once again expand and drop the nonlinear terms of ε to obtain the following equations of motion for the second-order gravitational perturbation.

$$\begin{aligned} \ddot{x}_p - 2n_0\dot{y}_p - \alpha^2 n_0^2 x_p &= y_h^2 + z_h^2 - 2x_h^2 \\ \ddot{y}_p + 2n_0\dot{x}_p &= 2x_h y_h \\ \ddot{z}_p + \beta^2 n_0^2 z_p &= 2x_h z_h \end{aligned} \tag{5.32}$$

5.2.2 Perturbed MHCW Solution

The homogeneous solution proves to be the same homogeneous solution as the *MHCW* equations. As such, the state transition matrix for the homogeneous solution to Eqn. (5.32) is the same as the state transition matrix for the *MHCW* equations. We define our perturbation state vector as

$$\vec{x}_p = \begin{bmatrix} x_p & y_p & z_p & \dot{x}_p & \dot{y}_p & \dot{z}_p \end{bmatrix}^T \tag{5.33}$$

We may then write Eqn. (5.32) in state-space form as,

$$\dot{\vec{x}}_p = \mathbf{A}_h(t)\vec{x}_p + \mathbf{B}(t)\vec{u}_h(t) \tag{5.34}$$

The general solution to Eqn. (5.34) (see Appendix B) is

$$\vec{x}_p(t) = \mathbf{\Phi}_h(t,t_0)\vec{x}_p(t_0) + \int_{t_0}^{t} \mathbf{\Phi}_h(t,\tau)\mathbf{B}\vec{u}_h(\tau)d\tau \tag{5.35}$$

where the system matrices are defined in Appendix C.

The perturbation positions as a function of time are written in a simplified form below. The coefficients are constant and in terms of the homogeneous and perturbed initial conditions. Their defined values may be found in Appendix D. The general solution follows the same procedure as discussed in §4.5.

$$\begin{aligned} x_p(t) = {} & \left[X_{p,cnc2k}\cos(2kt) + X_{p,cns2k}\sin(2kt) + X_{p,cn0} \right]\cos\left(n\sqrt{1-s}t\right) \\ & + \left[X_{p,snc2k}\cos(2kt) + X_{p,sns2k}\sin(2kt) + X_{p,sn0} \right]\sin\left(n\sqrt{1-s}t\right) \\ & + X_{p,c2n}\cos\left(2n\sqrt{1-s}t\right) + X_{p,s2n}\sin\left(2n\sqrt{1-s}t\right) \\ & + X_{p,c2n3s}\cos\left(2n\sqrt{1+3s}t\right) + X_{p,s2n3s}\sin\left(2n\sqrt{1+3s}t\right) \\ & + X_{p,c4k}\cos(4kt) + X_{p,c2k}\cos(2kt) + X_{p,s2k}\sin(2kt) + X_{p,0} \end{aligned} \tag{5.36}$$

$$
\begin{aligned}
y_p(t) = &\left[Y_{p,cnc2k} \cos(2kt) + Y_{p,cns2k} \sin(2kt) + Y_{p,cn0} \right] \cos\left(n\sqrt{1-st} \right) \\
&+ \left[Y_{p,snc2k} \cos(2kt) + Y_{p,sns2k} \sin(2kt) + Y_{p,sn0} \right] \sin\left(n\sqrt{1-st} \right) \\
&+ Y_{p,c2n} \cos\left(2n\sqrt{1-st} \right) + Y_{p,s2n} \sin\left(2n\sqrt{1-st} \right) \\
&+ Y_{p,c2n3} \cos\left(2n\sqrt{1+3st} \right) + Y_{p,s2n3} \sin\left(2n\sqrt{1+3st} \right) \\
&+ Y_{p,skc3k} \sin(kt) \cos(3kt) + Y_{p,s2k} \sin(2kt) + Y_{p,t} t + Y_{p0}
\end{aligned}
\tag{5.37}
$$

$$
\begin{aligned}
z_p(t) = &\begin{bmatrix} Z_{p,c3scn} \cos\left(n\sqrt{1-st} \right) + Z_{p,c3ssn} \sin\left(n\sqrt{1-st} \right) \\ + Z_{p,c3sc2k} \cos(2kt) + Z_{p,c3ss2k} \sin(2kt) + Z_{p,c3s0} \end{bmatrix} \cos\left(n\sqrt{1+3st} \right) \\
&+ \begin{bmatrix} Z_{p,s3scn} \cos\left(n\sqrt{1-st} \right) + Z_{p,s3ssn} \sin\left(n\sqrt{1-st} \right) \\ + Z_{p,s3sc2k} \cos(2kt) + Z_{p,s3ss2k} \sin(2kt) + Z_{p,s3s0} \end{bmatrix} \sin\left(n\sqrt{1+3st} \right)
\end{aligned}
\tag{5.38}
$$

Example 6. Nonlinear Simulation Error with Corrected MHCW ICs from Desired MHCW Model

The homogeneous initial conditions for the nonlinear simulation in this example are the same as defined in *Example 5*

$$
\begin{aligned}
\vec{x}_{d1,h}(0) &= \begin{bmatrix} 5 & 0 & 10 \end{bmatrix}^T \; km \\
\dot{\vec{x}}_{d1,h}(0) &= \begin{bmatrix} 0 & -8.8233665 \times 10^{-3} & 0 \end{bmatrix}^T \; km/sec
\end{aligned}
$$

$$
\begin{aligned}
\vec{x}_{d2,h}(0) &= \begin{bmatrix} 0 & -10 & 0 \end{bmatrix}^T \; km \\
\dot{\vec{x}}_{d2,h}(0) &= \begin{bmatrix} -4.4116833 \times 10^{-3} & 0 & -8.8233665 \times 10^{-3} \end{bmatrix}^T \; km/sec
\end{aligned}
$$

The perturbed initial conditions are also set to zero except the along-track velocities, which are subject to satisfying

$$Y_{p,t} = 0$$

The general solution to this equation is

$$\dot{y}_{p0} = -2n\sqrt{1+s}\,x_{p0} + \frac{\alpha_2^2\sqrt{1+s}}{n(5s+3)(4k^2-n^2+n^2s)}\left(12k^2+9n^2+23n^2s\right) - \frac{\sqrt{1+s}\beta_2^2}{n(5s+3)} - \frac{4\alpha_2\beta_2\left(-12k^2-n^2+n^2s\right)}{4k\left(4k^2-n^2+n^2s\right)}$$
$$+\frac{\sqrt{1+s}x_{h0}^2}{n(5s+3)} - \frac{\alpha_2\sqrt{1+s}}{n(5s+3)(4k^2-n^2+n^2s)}\left(8k^2+10n^2+11n^2s\right)x_{h0}$$
$$-\frac{4\beta_2 k x_{h0}}{4k^2-n^2+n^2s} - \frac{(11s+5)y_{h0}^2}{4n\sqrt{1+s}(5s+3)} - \frac{\sqrt{1+s}z_{h0}^2}{n(5s+3)} - \frac{\sqrt{1+s}\dot{z}_{h0}^2}{n^3(5s+3)(3s+1)}$$

When compared to the desired bounded *MHCW* solution, the addition of nonlinear differential gravity to this set of linearized equations of motion does not alleviate the drift of the model, but does correct it (see Fig. 5.5 and 5.6). These remaining drifts may be physically explained, as will be done in the next chapter.

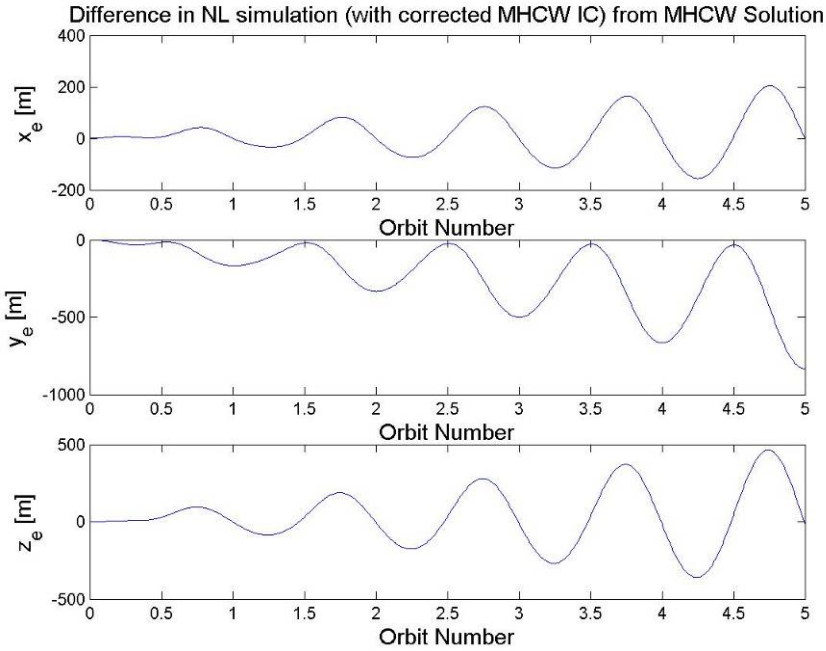

Fig. 5.5 Position errors of full nonlinear simulation (3.27-28, 31) with corrected *MHCW* initial conditions from desired *MHCW* model (5.23-25) for deputy satellite 1

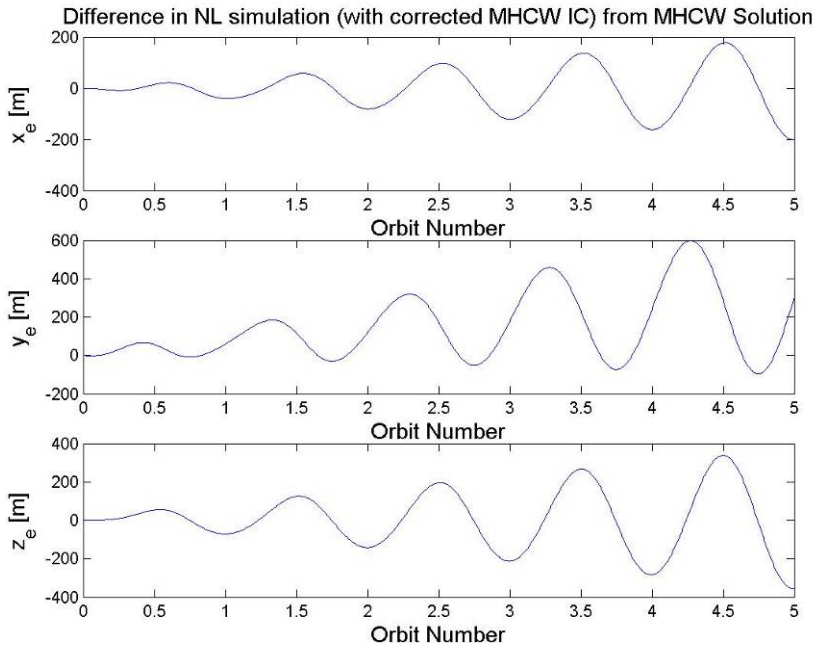

Fig. 5.6 Position errors of full nonlinear simulation (3.27-28, 31) with corrected *MHCW* initial conditions from desired *MHCW* model (5.23-25) for deputy satellite 1

However, when we apply the MHCW initial conditions corrected to include second-order differential gravity to the approximated nonlinear equations defined by (5.27), we obtain similar results to the simulation from *Example 4* (Fig. 4.8 and 4.9). Fig. 5.7 and 5.8 below shows the difference of this nonlinear simulation with the corrected *MHCW* initial conditions from the desired bounded orbit defined by Eqns. (5.23-25), which are also subject to the zero secular growth and zero offset terms as defined in *Example 5*. Notice the radial and cross-track motion differences of this linearized J_2 model are now bounded in the along-track direction, showing the corrected *MHCW* initial conditions have effectively removed the secular drift seen in Fig. 5.3 and 5.4.

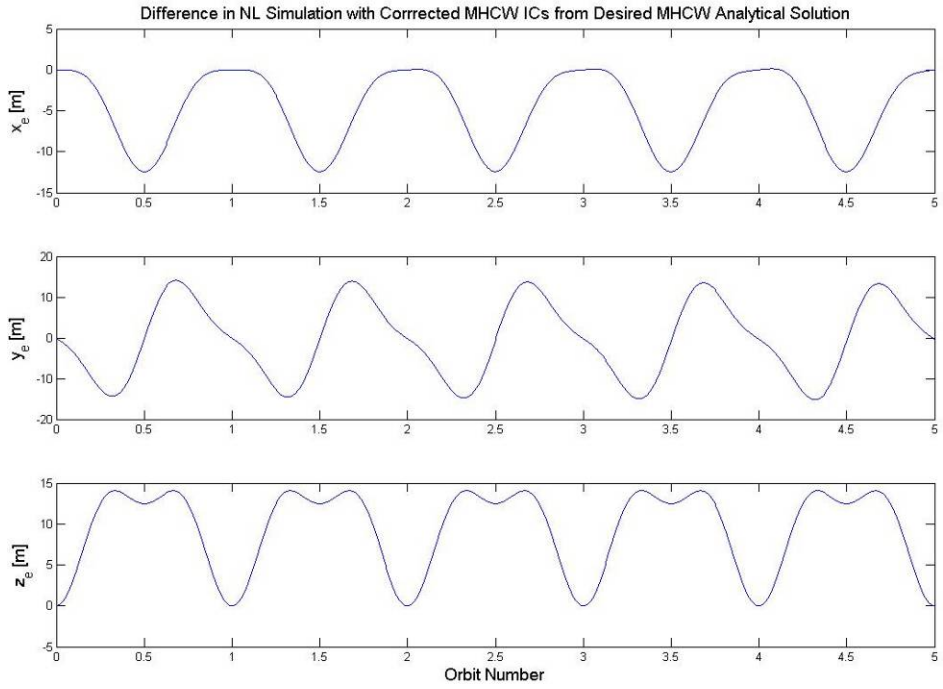

Fig. 5.7 Position errors of nonlinear simulation (5.27) with corrected *MHCW* initial conditions from desired *MHCW* model (5.23-25) for deputy satellite 1

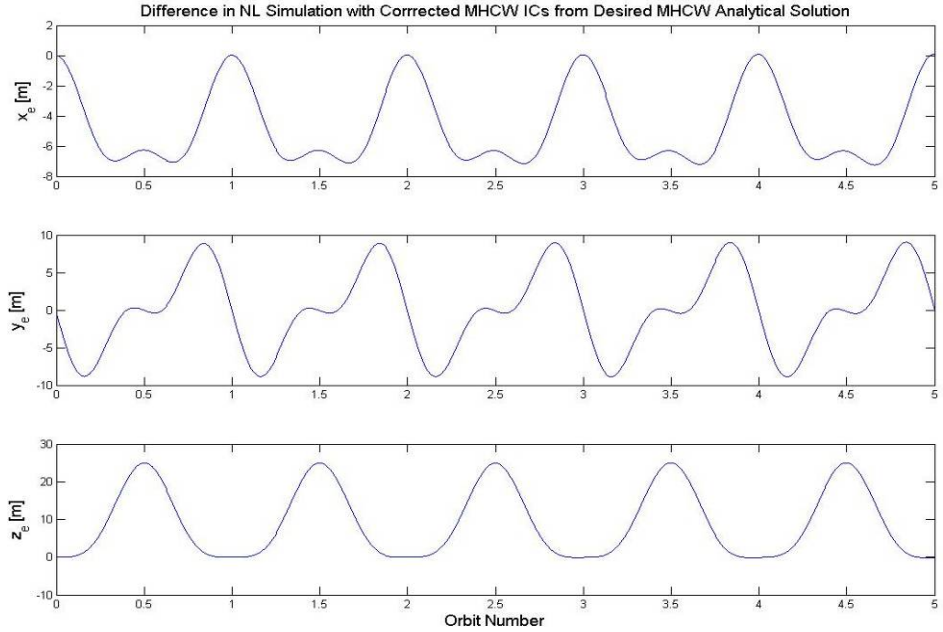

Fig. 5.8 Position errors of nonlinear simulation (5.27) with corrected *MHCW* initial conditions from desired *MHCW* model (5.23-25) for deputy satellite 2

CHAPTER 6

ANALYSIS OF RESULTS

6.1 Validation of the J2 Models

In this section we will discuss the validity of the solutions by mathematical comparison and simulated results. The *HCW* equations need no validation as they are proven to be a valid linearization of the relative motion dynamical system. Many references are available for describing the *HCW* equations.[6,12,23]

We begin by comparing the J_2 -*Modified HCW* equations to the *HCW* equations. We may do so in a variety of different ways. The simplest form is comparison of the state transition matrices of the two models. Since both models are linear equations of motion, their states at any time *t* may be calculated explicitly from the state transition matrix for the *HCW* equations. We refer to Appendix B for describing linear systems in terms of the state transition matrix. In the absence of J_2 perturbations, the state transition matrix for the J_2-*Modified HCW* equations should revert to the state transition matrix defined for the *HCW* solution.

The state transition matrix of the *HCW* solution is defined as[23]

$$\boldsymbol{\Phi}_h = \begin{bmatrix} 4-3\cos nt & 0 & 0 & \frac{\sin nt}{n} & \frac{2}{n}(1-\cos nt) & 0 \\ 6(\sin nt - nt) & 1 & 0 & -\frac{2}{n}(1-\cos nt) & \frac{4\sin nt - 3nt}{n} & 0 \\ 0 & 0 & \cos nt & 0 & 0 & \frac{\sin nt}{n} \\ 3n\sin nt & 0 & 0 & \cos nt & 2\sin nt & 0 \\ -6n(1-\cos nt) & 0 & 0 & -2\sin nt & 4\cos nt - 3 & 0 \\ 0 & 0 & -n\sin nt & 0 & 0 & \cos nt \end{bmatrix}$$

The nonzero terms for the state transition matrix for the *MHCW* equations are calculated as shown in Appendix C. For brevity, only the nonzero terms in the first and second states (*x* and *y*) are shown below. It is also noted that both matrices satisfy the *symplectic* property that transition matrices display.

$$\mathbf{\Phi}_{1,1} = \frac{(5s+3)\cos\left(n\sqrt{1-s}t\right) - 4\left(1+s\right)}{s-1}$$

$$\mathbf{\Phi}_{1,4} = \frac{\sin\left(n\sqrt{1-s}t\right)}{n\sqrt{1-s}}$$

$$\mathbf{\Phi}_{1,5} = \frac{2\sqrt{1+s}\left(\cos\left(n\sqrt{1-s}t\right)-1\right)}{n\left(s-1\right)}$$

$$\mathbf{\Phi}_{2,1} = -\frac{2\left(5s+3\right)\sqrt{1+s}\left(n\sqrt{1-s}t - \sin\left(n\sqrt{1-s}t\right)\right)}{\left(1-s\right)^{3/2}}$$

$$\mathbf{\Phi}_{2,2} = 1$$

$$\mathbf{\Phi}_{2,4} = -\frac{2\sqrt{1+s}\left(\cos\left(n\sqrt{1-s}t\right)-1\right)}{n\left(s-1\right)}$$

$$\mathbf{\Phi}_{2,5} = -\frac{(5s+3)\sqrt{1-s}t - 4(s+1)\sin\left(n\sqrt{1-s}t\right)}{n\left(s-1\right)^{3/2}}$$

Ignoring the effects of J_2 perturbations is equivalent to setting the constant s to zero. Substituting this value in to the *MHCW* state transition matrix and comparing to the *HCW*, the two matrices, and therefore their solutions, are equivalent.

$$\mathbf{\Phi}_{1,1} = \frac{(\cancel{5}s+3)\cos\left(n\sqrt{1-\cancel{s}}t\right) - 4\left(1+\cancel{s}\right)}{\cancel{s}-1} = 4 - 3\cos\left(nt\right)$$

$$\mathbf{\Phi}_{2,1} = -\frac{2\left(\cancel{5}s+3\right)\sqrt{1+\cancel{s}}\left(n\sqrt{1-\cancel{s}}t - \sin\left(n\sqrt{1-\cancel{s}}t\right)\right)}{\left(1-\cancel{s}\right)^{3/2}} = 6\left(\sin\left(nt\right) - nt\right)$$

This may also be proven via simulation of the two analytical solutions, when the J_2 perturbation is set to zero. In this case, both the *MHCW* and *HCW* solutions should both yield the same solution. Fig. 6.1 and 6.2 shows the solutions for the *MHCW* case

and the relative error between the two model simulations for both deputy satellites. Notice that the *MHCW* solutions match the *HCW* solutions from *Example 3* as expected. These show that the errors are computationally zero so the models indeed match when J_2 is ignored.

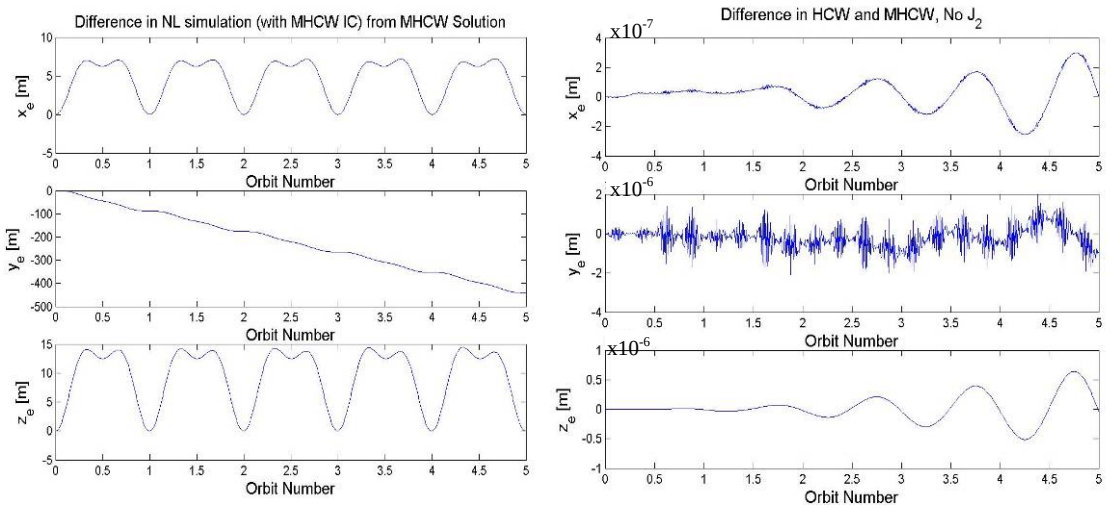

Fig. 6.1 *MHCW* and *HCW* solutions and error between in the absence of J_2 for deputy satellite 1

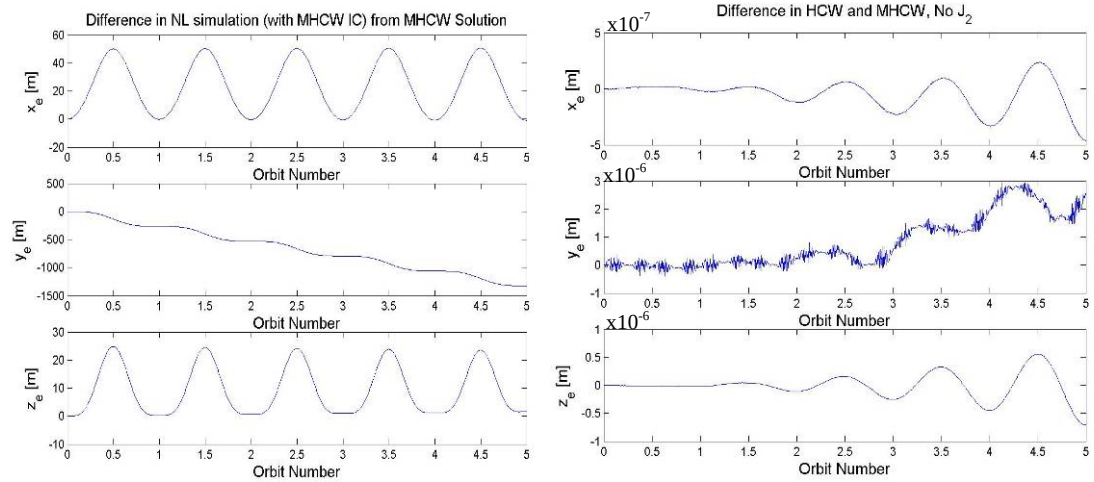

Fig. 6.2 *MHCW* and *HCW* solutions and error between in the absence of J_2 for deputy satellite 2

The two perturbed solutions may be proven in a similar manner. Following the review of linear systems in Appendix B, the two perturbed solutions are inherently proven to be equivalent in the absence of J_2 based on the previous validation. The two perturbed solutions are solved explicitly using the state transition matrix. Since the state transition matrices were proven to be equivalent when J_2 is ignored, the homogeneous solutions to the two systems are equivalent. Furthermore, as the forcing terms are equivalent when J_2 is ignored, the convoluted terms are equivalent as well.

The way the solutions are written, the solution of the perturbed *MHCW* equations contain terms which are divided by zero when J_2 is ignored. A simple alleviation in simulating the solution is to set J_2 itself to an infinitesimal value ($\sim 10^{-16}$) but not exactly zero.

The solution itself may still be fixed for simulation purposes. This may be alleviated by evaluating the limit as $J_2 \to 0$ for all the terms with zero denominators, and setting them to their limit when $J_2 \to 0$. These denominators may also be algebraically manipulated to ensure the denominators do not contain zeros when J_2 effects are ignored. The difference in the nonlinear simulation with corrected *MHCW* initial conditions from the bounded *MHCW* solution in the absence of J_2 are shown in Fig. 6.3 and 6.4. Note that these do indeed match Fig. 4.8 and 4.9 for the respective deputy satellite.

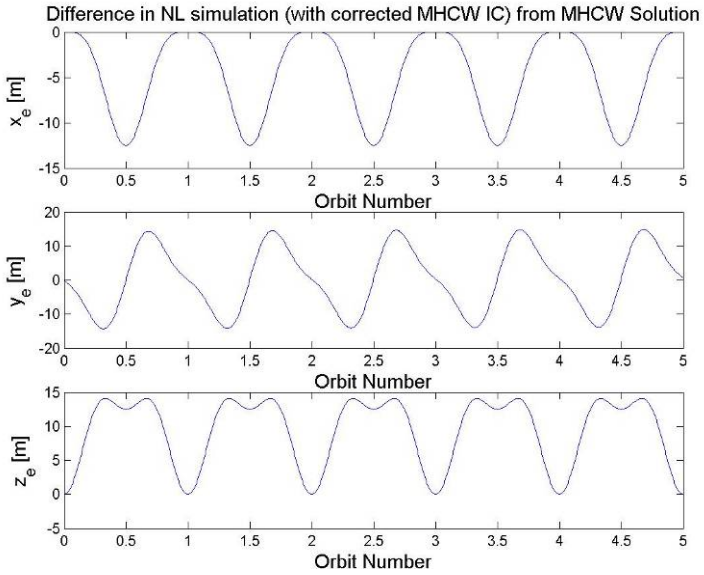

Fig. 6.3 Perturbed *MHCW* solutions in the absence of J_2 for deputy satellite 1

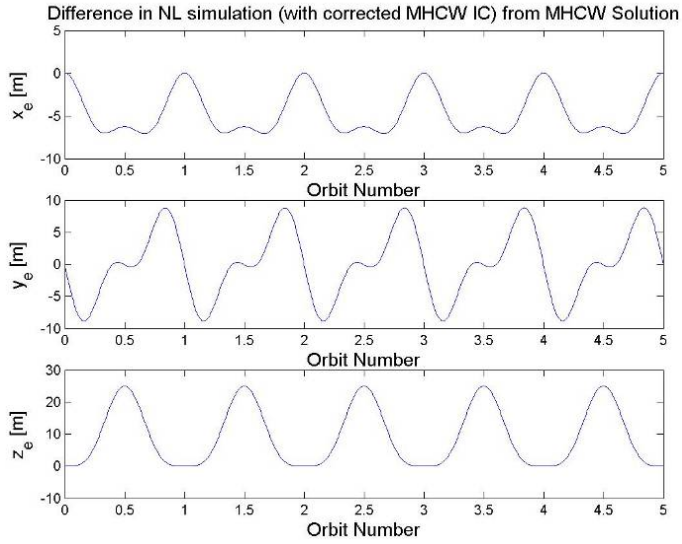

Fig. 6.4 Perturbed *MHCW* solutions in the absence of J_2 for deputy satellite 2

6.2 Relative Truth Errors

Fig. 6.5 and 6.6 below show the errors of the two J_2-*Modified HCW* nonlinear simulations (3.27-33) in Chapter 5 (*Ex. 5 and 6*), from the desired bounded relative orbit solution given by Eqns. (5.23-25), which was subject to the initial conditions given in *Example 5*. We will first discuss the comparative results for each direction, and then conclude with an overall performance of each model with respect to the truth model.

In the radial component direction, the two nonlinear simulations display similar deviations from the *MHCW* solution. They both have amplitude growth associated with trigonometric terms, but this still allows the errors at each passing of the ascending node to be zero. Therefore all the errors are bounded over one period. However, the growth in the radial direction is less for the simulation with the corrected *MHCW* initial conditions.

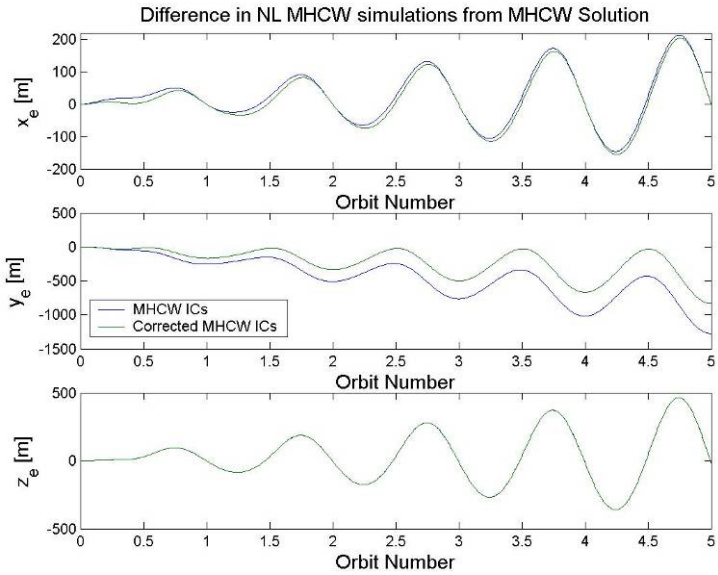

Fig. 6.5 Nonlinear simulation (3.27-28, 31) errors from desired trajectory for the MHCW models (5.23-25) subject to the first deputy satellite ICs

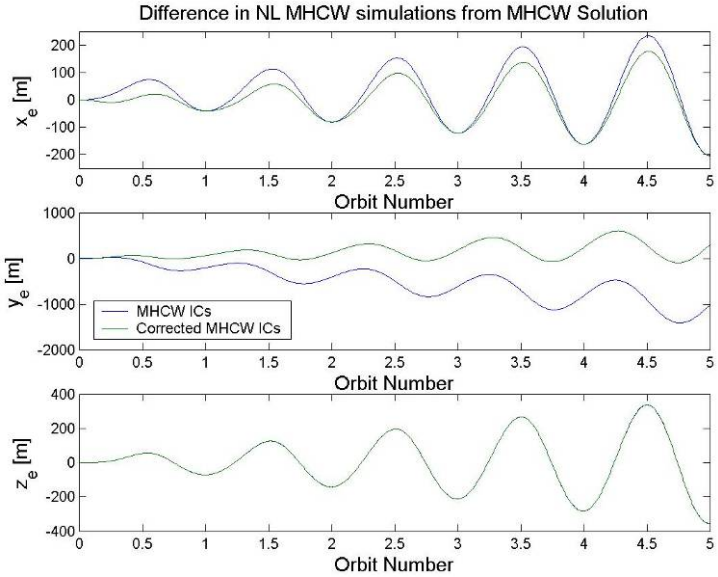

Fig. 6.6 Nonlinear simulation (3.27-33) errors from desired trajectory for the MHCW models (5.23-25) subject to the second deputy satellite ICs

In the along-track direction, there is secular growth for both cases, as well as unbounded amplitude growths, but the nonlinear simulation with corrected *MHCW* initial conditions shows improvement in the growth from the *MHCW* initial condition simulation. The cross-track direction shows the most significant improvements of the addition of J_2 perturbations to the models. Both the J_2-modified solutions have the same motion in the cross-track direction and both the *HCW* solutions have the same motion in the cross-track direction, which may be seen from Fig. 6.7, noting the *MHCW* solution is indeed better than the *HCW* in the cross-track direction and matches well with the perturbed *MHCW* results for both deputy satellites.

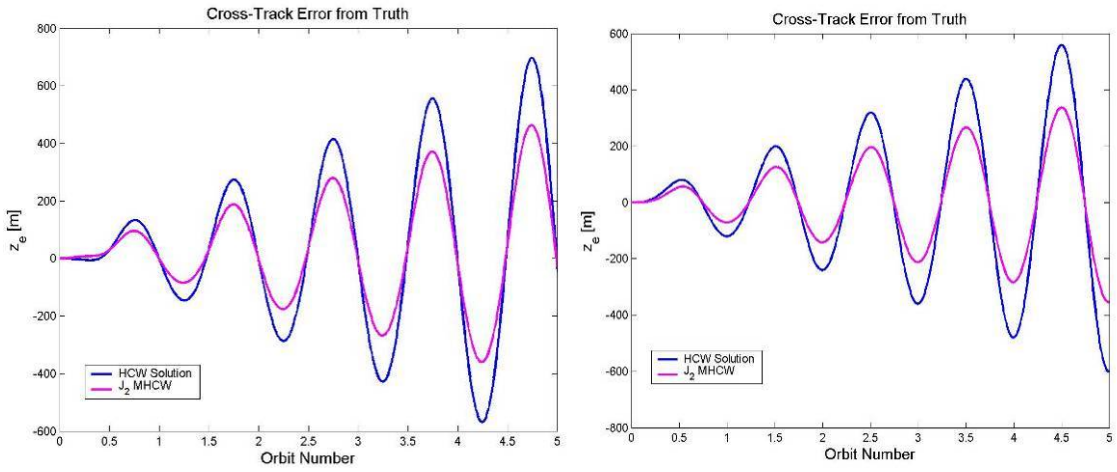

(a) (b)

Fig. 6.7 Cross-track errors from truth model for the *HCW* and *MHCW* solutions for (a) deputy satellite 1 and (b) deputy satellite 2. It is noted that these plots show analytical model errors from the same truth model which includes J_2 perturbations.

6.2.1 Result Comparison of the HCW Solutions to the MHCW Solutions

Most of the example problems expressed the results of the solutions by applying the initial conditions found from the various analytical solutions to a nonlinear model,

and comparing these results from one of two desired bounded relative orbits. The first being the *HCW* solution, which only includes the effects of linearized differential gravity, and the second is the J_2-*MHCW* solution, which includes the effects of linearized differential gravity, and linearized, time-averaged J_2. In this section, the *HCW* and *MHCW* solutions are compared to each other to determine the effect of adding linearized J_2 to the analytical model.

We begin by using the nonlinear system defined by Eqn. (5.27), and applying the four sets of initial conditions for numerical integration: The bounded *HCW* initial conditions, the corrected *HCW* initial conditions, the bounded *MHCW* initial conditions, and the corrected *MHCW* initial conditions. These simulations are first compared to their respective desired bounded relative orbit, defined from Eqns. (4.15) for the *HCW* equations and (5.23-25) for the *MHCW* equations. Fig. 6.8 and 6.9 below display the comparison of differences of the simulations with the *HCW* and *MHCW* initial conditions. As can be seen from these two figures, under the presence of J_2 and nonlinear differential gravity, the *HCW* equations do not admit a desirable bounded relative orbit. The simulation with the *HCW* initial conditions, when compared to the *HCW* analytical solution, displays growth in all three component directions.

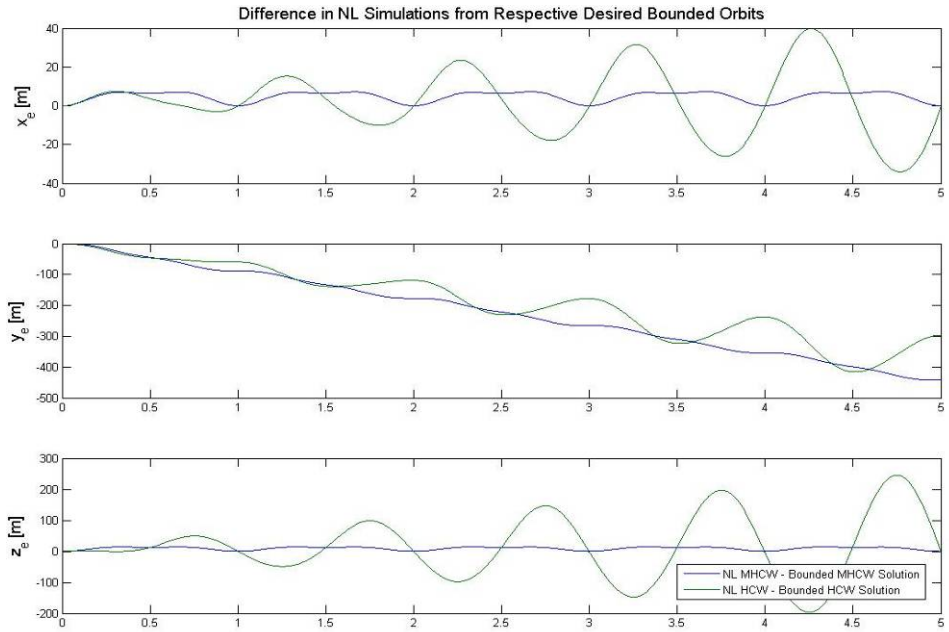

Fig. 6.8 Nonlinear simulation (5.27) errors from desired trajectory subject to the first deputy satellite ICs

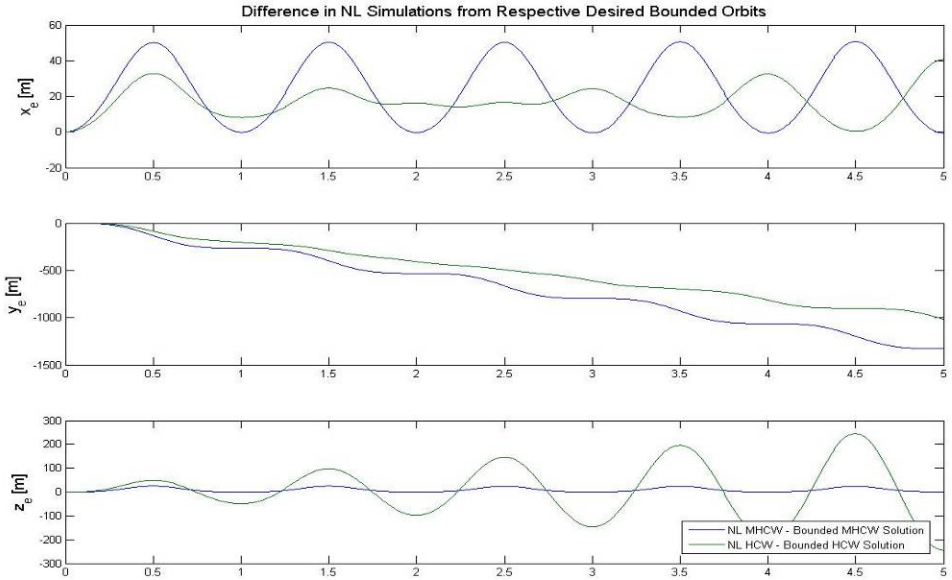

Fig. 6.9 Nonlinear simulation (5.27) errors from desired trajectory subject to the second deputy satellite ICs

However, when the effects of second order differential gravity perturbations are added to the initial conditions for the nonlinear simulations, the *HCW* orbit appears to

still be a desirable relative orbit. Fig. 6.10 and 6.11 displays the comparison of differences of the simulations with the corrected *HCW* and *MHCW* initial conditions. It is noticed that the effect of linearized J_2 is small when compared to the effect of differential gravity, as seen from the ability of the nonlinear simulation with corrected *HCW* initial conditions to obtain a bounded error from the analytical *HCW* solution, which contains no J_2 perturbations. There is slight secular growth in the along-track direction that is also coupled with a small frequency divergence, both of which are due to the absence of J_2 in the *HCW* analytical solution governed by Eqn. (4.15).

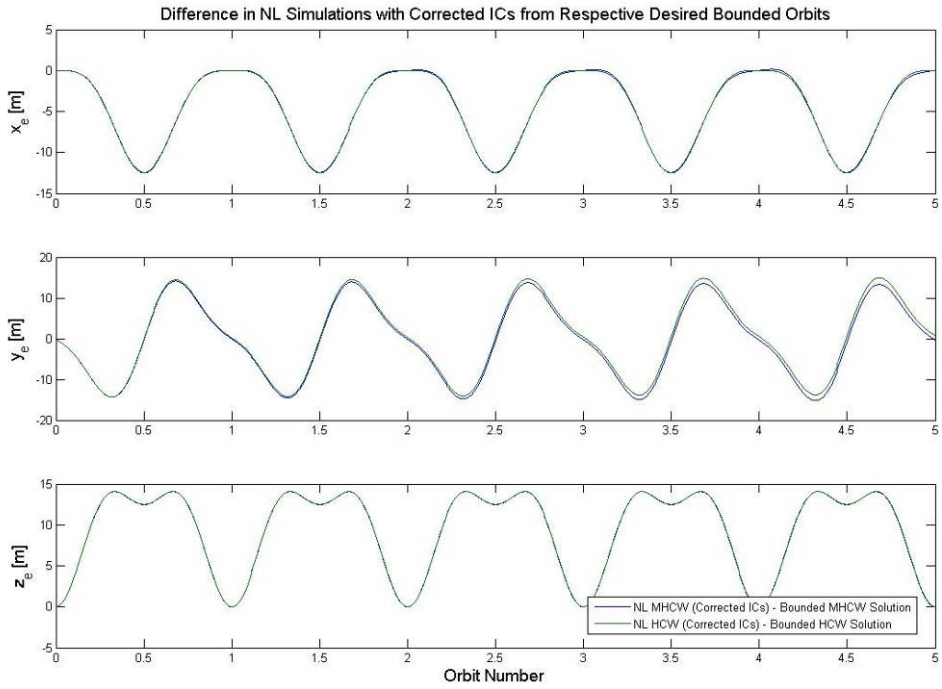

Fig. 6.10 Nonlinear simulation (5.27) errors with corrected ICs from desired trajectory for deputy satellite 1

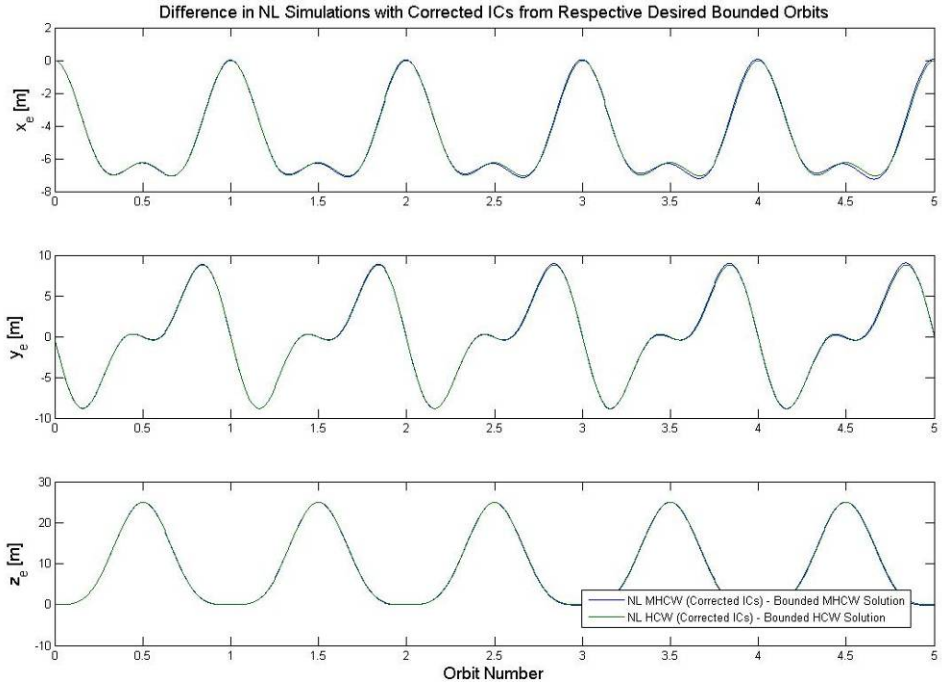

Fig. 6.11 Nonlinear simulation (5.27) errors with corrected ICs from desired trajectory for deputy satellite 2

We now compare the four nonlinear simulations from above to the same desired bounded relative orbit. The *MHCW* equations provide bounded motion based on a higher fidelity model, and is used for this evaluation. Fig. 6.12 and 6.13 display the differences of the nonlinear simulations with the *HCW* and *MHCW* initial conditions, and 6.14 and 6.15 present the differences of the nonlinear simulations with corrected initial conditions. As can be seen from Fig. 6.12 and 6.13, the differences for the nonlinear simulation with the *HCW* initial conditions match more closely the desired orbit. However, there is still secular growth associated with second order differential gravity.

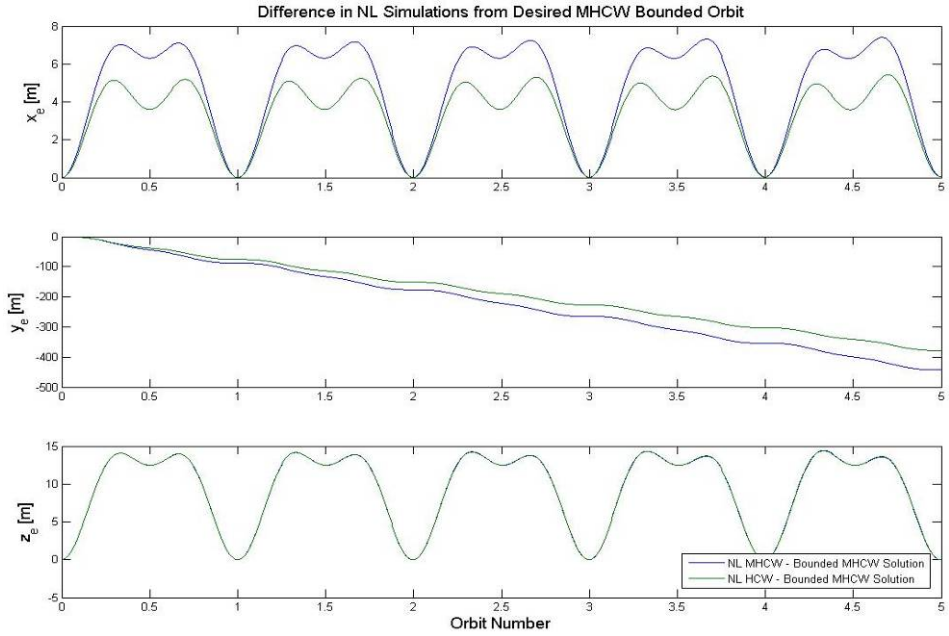

Fig. 6.12 Nonlinear simulation (5.27) errors from desired *MHCW* trajectory subject to the first deputy satellite ICs

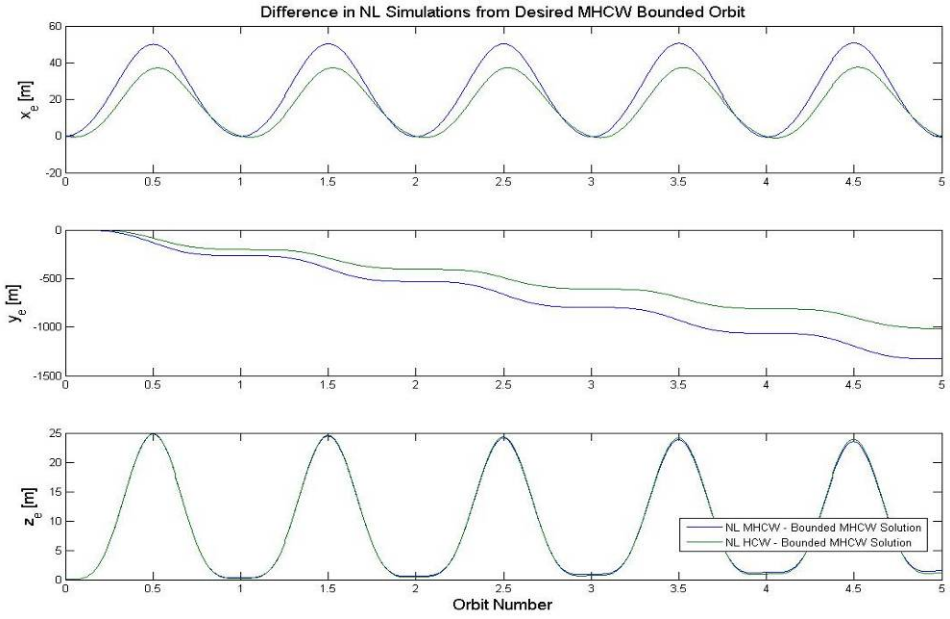

Fig. 6.13 Nonlinear simulation (5.27) errors from desired *MHCW* trajectory subject to the second deputy satellite ICs

When the initial condition corrections for added second order differential gravity are imposed on the nonlinear simulations, the *MHCW* simulation displays a bounded error from the desired orbit, whereas the *HCW* simulation still shows a secular growth in the along-track direction, although the corrected initial conditions have reduced this growth significantly. The differences between the *HCW* models and the *MHCW* models are small over a short time span, but over longer periods the deviation from the desired motion constitutes a larger velocity correction, meaning more fuel consumption if the dynamics were derived neglecting the effects of J_2.

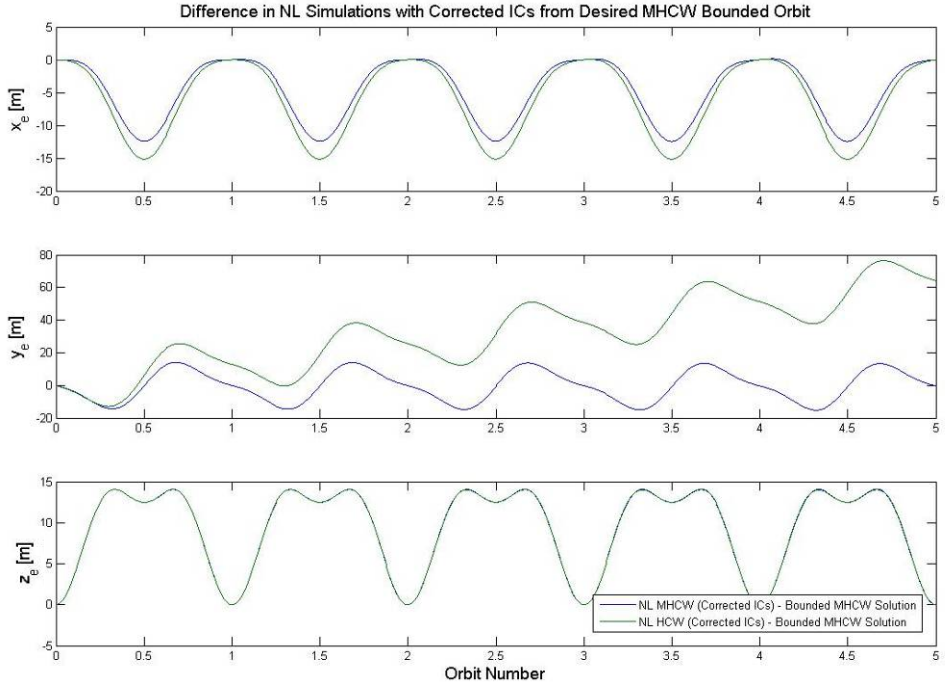

Fig. 6.14 Nonlinear simulation (5.27) errors with corrected ICs from desired *MHCW* trajectory for deputy satellite 1

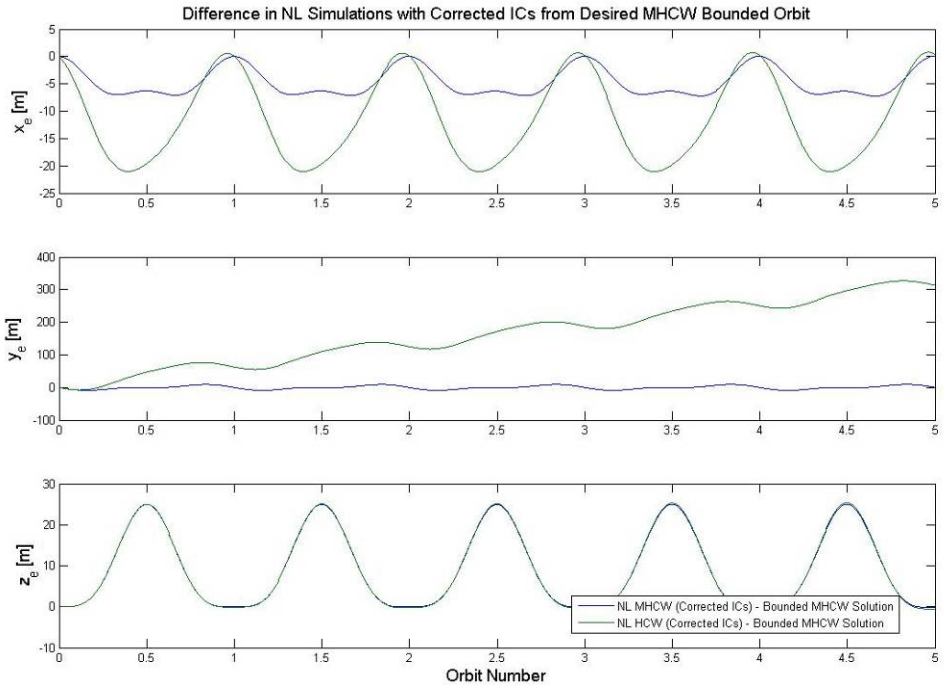

Fig. 6.15 Nonlinear simulation (5.27) errors with corrected ICs from desired *MHCW* trajectory for deputy satellite 2

6.3 Errors in the J2 Models

The errors from the desired model that take J_2 into account still have unbounded growth in all three directions as seen from the nonlinear simulations in Fig. 6.5 and 6.6. Why do the J_2-modified solutions, which improve the errors from the truth model when compared to the *HCW* solutions, not provide more significant improvements to the desired trajectory? We refer back to §5.1 when we discussed the calculation of the angular velocity vector.

An important phenomenon which affects a satellite's orbit when it rotates about an oblate sphere is that the orbit tends to wobble about the Z-axis in the ECI frame. This wobble is due to the nodal regression, and occurs because of the change in

direction only, of the angular-momentum vector, which precesses about the Z-axis, which is the axis of symmetry.

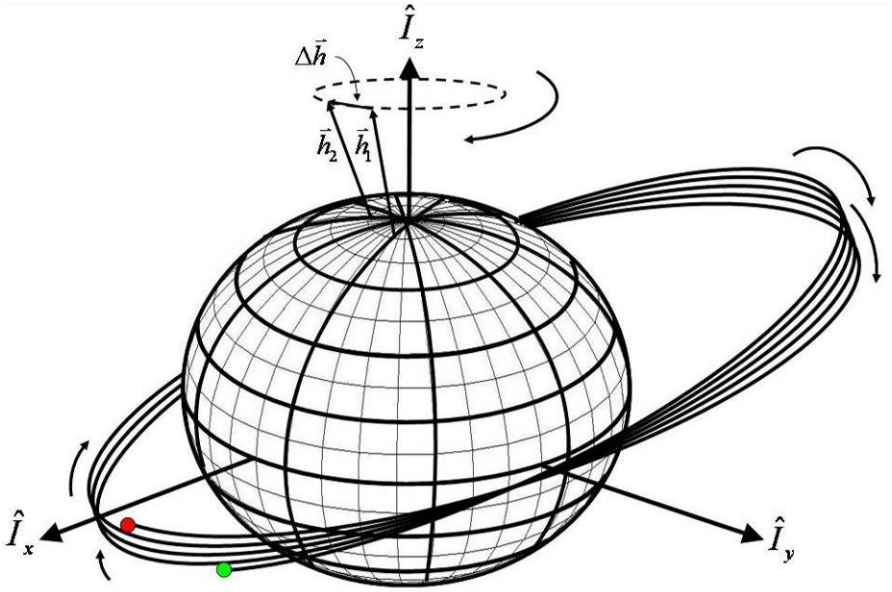

Fig. 6.16 Amplified Effect of nodal regression for a satellite in an inclined orbit. The green dot represents the start of the orbit, and the red dot represents the end of the last orbit.

Precession of the angular momentum implies nodal regression, and vice versa. The effects of nodal regression are eliminated if both chief and deputy orbits are in equatorial (oblateness effects vanish completely) or polar orbits (apsidal rotation still occurs in eccentric orbits). Since we assume a time-averaged angular velocity, in which the angular momentum vector does not precess, the linearized describing dynamics presented here drift from the true relative motion of the two satellites.

This effect may still be incorporated into the linearized equations of motion.[8] This is accomplished by solving for a new time-varying period and amplitude in the cross-track direction. Looking at only the *MHCW* equations with no perturbation due to

second-order differential gravity, the changing direction of the angular momentum vector only affects the cross-track direction, and would only show more reduction in the unbounded amplitude in the cross-track direction. However, the perturbed *MHCW* equations allow for the effects of this precession to appear in the radial, and the along-track direction via coupling of the homogeneous solutions, which should effectively reduce the drift of the linearized model from the truth in these two directions as well.

The inclusion of the angular momentum precession to the equations of motion adds more calculations to the solution. However these are also linearized approximations of the exact solutions, and therefore still analytically solvable.

CHAPTER 7

CONCLUSIONS

The research proposed in this thesis has combined two solutions to account for the two main perturbations which cause the *HCW* equations to deviate from the true nonlinear equations of motion. The new model consists of an unforced linear system which takes on a similar form to the *HCW* equations, with modified coefficients due to the J_2 perturbation

HCW Equations	Homogeneous MHCW Equations
$\ddot{x} - 2n\dot{y} - 3n^2 x = 0$	$\ddot{x} - 2n_0\dot{y} - \alpha^2 n_0^2 x = 0$
$\ddot{y} + 2n\dot{x} = 0$	$\ddot{y} + 2n_0\dot{x} = 0$
$\ddot{z} + n^2 z = 0$	$\ddot{z} + \beta^2 n_0^2 z = 0$

The particular solution to the HCW equations may be solved for by direct integration yielding an analytical model. The effects of second-order differential gravity may be added to the J_2-*Modified HCW* equations using the method of perturbations

$$\vec{x} = \vec{x}_h + \varepsilon\vec{x}_p$$

where the homogeneous solution is the exact solution obtained from the J_2-*Modified HCW* equations, and the perturbed solution is solved by the following linear, constant-coefficient, differential equations:

$$\ddot{x}_p - 2n_0\dot{y}_p - \alpha^2 n_0^2 x_p = y_h^2 + z_h^2 - 2x_h^2$$
$$\ddot{y}_p + 2n_0\dot{x}_p = 2x_h y_h$$
$$\ddot{z}_p + \beta^2 n_0^2 z_p = 2x_h z_h$$

These equations may be directly integrated to obtain the closed-form solution of the perturbation. When compared to the two different solutions that only take one of the disturbances into account, it is seen that this new combined solution yields better results when compared to the truth model, providing for periodically bounded solutions in all relative component directions. It was expected that the addition of the J_2 perturbation to the *HCW* equations would be to reduce the growth in the cross-track direction, and the new solution does (about 250 *m* maximum difference over 5 orbits). It was also expected that adding the perturbation associated with second-order differential gravity would improve upon the in-plane motion of the new solution, and is done so by bounding the errors from truth in the along-track direction.

The fidelity of this new perturbed J_2-*Modified HCW* model may be improved upon to eliminate the unbounded growths in amplitude in the radial and cross-track direction, by taking into account the precession of the angular velocity vector. It is also believed that further analysis by adding this influence will provide for a stronger criterion for eliminating the secular growth in the along-track direction.

APPENDIX A

DERIVATION OF THE ASPHERICAL POTENTIAL

The following derivation follows from Refs. 11 and 24.

A.1. Describing Geometry of the Aspherical-Potential Function

For completion, the geometry associated with deriving the aspherical potential is re-described here from §3.4. In order to determine the gravitational potential at point *P*, each point in the Earth, m_Q must be taken into account. The angles ϕ are the respective co-latitudes, λ_Q and θ_{sat} are the longitudinal arguments, and Λ is the angle between the vectors $\vec{r}_Q$ and $\vec{r}_{sat}$, also known as the ground range or total range angle. All the above angle measurements are geocentric. See Fig. A.1 for describing geometry.

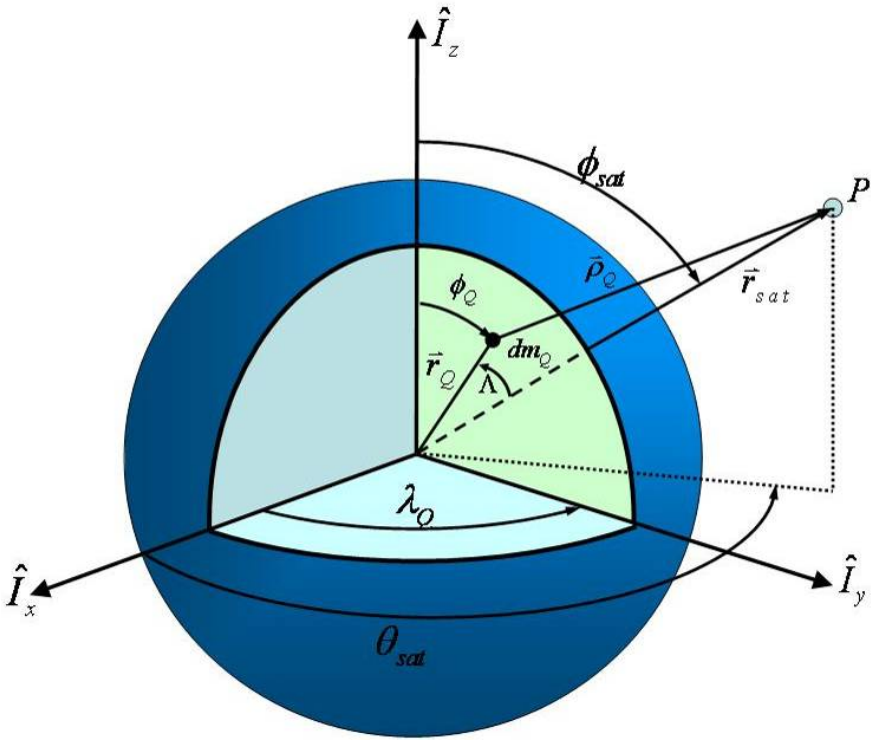

Fig. A.1 Geometry used to derive the gravitational potential

A.2 Aspherical-Potential Function

The gravitational potential at the point *P* defined by $\vec{r}_{sat}$ is defined as

$$U = G\sum_{Q=1}^{\infty}\frac{m_Q}{\rho_Q} \tag{A.1}$$

where ρ_Q is the distance between the point *P* and the point mass element m_Q, defined by their respective coordinates:

$$\begin{aligned}\vec{r}_{sat} &= (x, y, z)^T \\ \vec{r}_Q &= (\xi, \eta, \zeta)^T\end{aligned} \tag{A.2}$$

The change in potential due to an infinitesimal mass $dm_\oplus$, is

$$dU = G\frac{dm_\oplus}{\rho_Q} \tag{A.3}$$

The summation of each mass approaches an integral, giving the total gravitational potential at *P* to be

$$U = G\int_{body}\frac{1}{\rho_Q}dm_\oplus = G\int_{body}\frac{1}{\left[\left(x-\xi\right)^2+\left(x-\eta\right)^2+\left(x-\zeta\right)^2\right]^{1/2}}dm_\oplus \tag{A.4}$$

A more useful form may be introduced using the law of cosines

$$U = G\int_{body}\frac{1}{\left[r_{sat}^2+r_Q^2-2r_{sat}r_Q\cos\Lambda\right]^{1/2}}dm_\oplus \tag{A.5}$$

By making note that the rational term inside the integral is the generating function used to describe a series of *Legendre polynomials*:[25]

$$\left(1-2\alpha\gamma+\alpha^2\right)^{-1/2}=\sum_{\ell=0}^{\infty}\alpha^{\ell}P_{\ell}\left[\gamma\right] \tag{A.6}$$

We define the argument γ

$$\gamma=\cos\left(\Lambda\right)=\frac{\vec{r}_{sat}\cdot\vec{r}_{Q}}{r_{sat}r_{Q}}=\frac{x\xi+y\eta+z\zeta}{r_{sat}r_{Q}} \tag{A.7}$$

and α may be found by factoring out r_{sat}

$$\rho_{Q}^{2}=r_{sat}\sqrt{1-2\frac{r_{Q}}{r_{sat}}\cos\left(\Lambda\right)+\left(\frac{r_{Q}}{r_{sat}}\right)^{2}}=r\sqrt{1-2\alpha\gamma+\alpha^{2}} \tag{A.8}$$

$$\alpha=\frac{r_{Q}}{r_{sat}} \tag{A.9}$$

The potential is then written as:

$$U=\frac{G}{r_{sat}}\sum_{\ell=0}^{\infty}\alpha^{\ell}P_{\ell}\left[\gamma\right]dm_{\oplus} \tag{A.10}$$

and the *conventional* Legendre polynomials may be defined using the *Rodrigues' formula*[25]

$$\begin{aligned}P_{\ell}\left[\gamma\right]&=\frac{1}{2^{\ell}\ell!}\frac{d^{\ell}\left(\gamma^{2}-1\right)^{\ell}}{d\gamma^{\ell}}\\&=\frac{1}{2^{\ell}}\sum_{j=0}^{\ell}\frac{\left(-1\right)^{j}\left(2\ell-2j\right)!}{j!\left(\ell-j\right)!\left(\ell-2j\right)!}\gamma^{\ell-2j}\end{aligned} \tag{A.11}$$

Addition Theorem for Legendre polynomials

Using the cosine law of spherical trigonometry, the range angle Λ may be described as

$$\cos\left(\Lambda\right)=\cos\left(\phi_{gc_{Q}}\right)\cos\left(\phi_{gc_{sat}}\right)+\sin\left(\phi_{gc_{Q}}\right)\sin\left(\phi_{gc_{sat}}\right)\cos\left(\theta_{sat}-\lambda_{Q}\right) \tag{A.12}$$

We rewrite the Legendre polynomials utilizing the *addition theorem for Legendre polynomials*

$$P_{\ell,m}\left[\gamma\right]=\left(1-\gamma^2\right)^{m/2}\frac{d^m}{d\gamma^\ell}P_\ell\left[\gamma\right] \tag{A.13}$$

This form is known as the *associated Legendre functions of the first kind of degree m and order* ℓ. The Legendre polynomial may then be written in terms of the spherical coordinates by substituting (A.13) into (A.12)

$$\begin{aligned}P_\ell\left[\cos(\Lambda)\right]&=P_\ell\left[\cos\left(\phi_Q\right)\right]P_\ell\left[\cos\left(\phi_{sat}\right)\right]\\&\quad+2\sum_{m=\ell}^{\ell}\frac{(\ell-m)!}{(\ell+m)!}P_{\ell,m}\left[\cos\left(\phi_{sat}\right)\right]P_{\ell,m}\left[\cos\left(\phi_Q\right)\right]\cos\left(m\left(\theta_{sat}-\lambda_Q\right)\right)\end{aligned} \tag{A.14}$$

The gravitational potential due to an aspherical central body is written as

$$U=\frac{\mu}{r}\left[\begin{aligned}&1-\sum_{\ell=2}^{\infty}J_\ell\left(\frac{R_\oplus}{r}\right)^\ell P_\ell\left[\cos\left(\phi_{gc_{sat}}\right)\right]\\&+\sum_{\ell=2}^{\infty}\sum_{m=\ell}^{\ell}\left(\frac{R_\oplus}{r}\right)^\ell P_{\ell,m}\left[\cos\left(\phi_{gc_{sat}}\right)\right]\left\{C_{\ell,m}\cos\left(m\lambda_{sat}\right)+S_{\ell,m}\sin\left(m\lambda_{sat}\right)\right\}\end{aligned}\right] \tag{A.15}$$

where $J_\ell=-C_{\ell,0}, C_{\ell,m}, C_{\ell,m}$ are the associated gravitational coefficients which are determined empirically by satellite observations.

APPENDIX B

REVIEW OF LINEAR SYSTEMS

B.1 Linear System Theory

The following derivation is adapted from Refs. 11 and 24.

B.1.1 Homogeneous Linear Systems

Homogeneous linear time-varying equations of motion may be written in the form

$$\frac{d\vec{x}}{dt} = \mathbf{A}(t)\vec{x} \tag{B.1}$$

where $\vec{x}$ is the state vector defined in our case as the states to the three-dimensional, second-order differential equations of motion

$$\vec{x} = \begin{bmatrix} x & y & z & \dot{x} & \dot{y} & \dot{z} \end{bmatrix}^T \tag{B.2}$$

$\mathbf{A}(t)$ is the state matrix which defines the overall stability of the system. Eqn. (B.1) for our system admits six linearly independent solutions. We may describe these solutions as the columns of a square matrix $\mathbf{\Phi}$ whose dimensions are equal to the number of states (6 in this case). Furthermore, if the initial conditions are defined such that the n^{th} state has all the column components of the n^{th} row of $\mathbf{\Phi}$ to be zero except the n^{th} diagonal component, and the n^{th} component is 1, then the matrix $\mathbf{\Phi}$ will be a function of both t and t_0, which satisfies the matrix differential equation

$$\frac{d}{dt}\mathbf{\Phi}(t,t_0) = \mathbf{A}(t)\mathbf{\Phi}(t,t_0) \tag{B.3}$$

subject to

$$\mathbf{\Phi}(t_0,t_0) = \mathbf{I} \tag{B.4}$$

$\mathbf{\Phi}$ is known as the state transition matrix, which represents the partial derivatives of the state at time t to the initial states at t_0. If the initial states are known, then the states at any time t are obtained from the initial states as

$$\vec{x}(t) = \mathbf{\Phi}(t, t_0)\vec{x}(t_0) \tag{B.5}$$

We now define an important property of the state transition matrix using Eqn. (B.5). By interchanging t and t_0 in Eqn. (B.5)

$$\vec{x}(t_0) = \mathbf{\Phi}(t_0, t)\vec{x}(t)$$

Therefore,

$$\mathbf{\Phi}^{-1}(t, t_0) = \mathbf{\Phi}(t_0, t) \tag{B.6}$$

Equation (B.6) implies that the state transition matrix is *symplectic*.

A square matrix is *symplectic* if

$$\mathbf{\Phi}^T \mathbf{J} \mathbf{\Phi} = \mathbf{J} \tag{B.7}$$

Where $\mathbf{J}$ is analogous to the pure imaginary number in complex algebra:

$$\mathbf{J} = \begin{bmatrix} \mathbf{0} & \mathbf{I} \\ \mathbf{-I} & \mathbf{0} \end{bmatrix} \qquad \mathbf{J}^2 = \mathbf{-I} \tag{B.8}$$

In order to determine if the state transition matrix is indeed *symplectic*, we begin with the initial state. From Eqns. (B.4) and (B.6),

$$\mathbf{\Phi}(t_0, t_0) = \mathbf{I} \quad \& \quad \mathbf{\Phi}^{-1}(t_0, t_0) = \mathbf{\Phi}(t_0, t_0)$$

$$\therefore \mathbf{\Phi}^T(t_0, t_0)\mathbf{J}\mathbf{\Phi}(t_0, t_0) = \mathbf{J}$$

Therefore, in order for the state transition matrix to be symplectic for all time t, it must satisfy

$$\frac{d}{dt}\left[\boldsymbol{\Phi}^T\left(t,t_0\right)\mathbf{J}\boldsymbol{\Phi}\left(t,t_0\right)\right]=\mathbf{0} \tag{B.9}$$

Substituting Eqn. (B.3) into (B.9), the *symplectic* condition in terms of the system matrix becomes

$$\boldsymbol{\Phi}^T\left(t,t_0\right)\left[\mathbf{A}^T\left(t\right)\mathbf{J}+\mathbf{J}\mathbf{A}\left(t\right)\right]\boldsymbol{\Phi}\left(t,t_0\right)=\mathbf{0}$$

B 1.2 Forced Linear Dynamical Systems

Any linear system subject to outside disturbances may be written in terms of the homogeneous portion and the forcing function

$$\frac{d\vec{x}}{dt}=\mathbf{A}\left(t\right)\vec{x}+\mathbf{B}\vec{u}\left(t\right) \tag{B.10}$$

where $\mathbf{B}$ is known as the compatibility matrix. For the systems defined in this thesis,

$$\mathbf{B}=\begin{bmatrix}\mathbf{0}_{3\times3}\\ \mathbf{I}_{3\times3}\end{bmatrix}$$

The non-homogeneous solution to Eqn. (B.10) may be written using the state transition matrix of the homogeneous system, via Lagrange's method of variation of parameters, so that the solution to (B.10) becomes

$$\vec{x}\left(t\right)=\boldsymbol{\Phi}\left(t,t_0\right)\vec{g}\left(t\right),\quad \vec{g}\left(t_0\right)=\vec{x}\left(t_0\right) \tag{B.11}$$

where $\vec{g}\left(t\right)$ is an $n\times1$ vector to be determined. Differentiating (B.11) and substituting Eqn. (B.3) for $\dot{\boldsymbol{\Phi}}$ yields

$$\dot{\vec{x}}\left(t\right)=\boldsymbol{\Phi}\left(t,t_0\right)\dot{\vec{g}}\left(t\right)+\mathbf{A}\left(t\right)\boldsymbol{\Phi}\left(t,t_0\right)\vec{g}\left(t\right) \tag{B.12}$$

By substituting Eqns. (B.11) and (B.12) into (B.10), we obtain

$$\mathbf{\Phi}(t,t_0)\dot{\bar{g}}(t) + \cancel{\mathbf{A}(t)\mathbf{\Phi}(t,t_0)\bar{g}(t)} = \cancel{\mathbf{A}(t)\mathbf{\Phi}(t,t_0)\bar{g}(t)} + \mathbf{B}\bar{u}(t)$$

Solving for $\dot{\bar{g}}(t)$ yields

$$\dot{\bar{g}}(t) = \mathbf{\Phi}^{-1}(t,t_0)\mathbf{B}(t)\bar{u}(t) \tag{B.13}$$

We integrate (B.13) to obtain

$$\bar{g}(t) = \bar{x}(t_0) + \int_{t_0}^{t} \mathbf{\Phi}^{-1}(\tau,t_0)\mathbf{B}\bar{u}(\tau)d\tau \tag{B.14}$$

Substituting Eqn. (B.14) into (B.10) yields

$$\bar{x}(t) = \mathbf{\Phi}(t,t_0)\bar{x}(0) + \mathbf{\Phi}(t,t_0)\int_{t_0}^{t} \mathbf{\Phi}^{-1}(\tau,t_0)\mathbf{B}\bar{u}(\tau)d\tau \tag{B.15}$$

Using the symplectic nature of the state transition matrix it is easily shown that

$$\mathbf{\Phi}^{-1}(\tau,t_0) = \mathbf{\Phi}^{-1}(t,t_0)\mathbf{\Phi}(t,\tau) \tag{B.16}$$

The solution of the inhomogeneous system is then found to be

$$\bar{x}(t) = \mathbf{\Phi}(t,t_0)\bar{x}(0) + \int_{t_0}^{t} \mathbf{\Phi}(t,\tau)\mathbf{B}\bar{u}(\tau)d\tau \tag{B.17}$$

APPENDIX C

J_2-MODIFIED HCW SYSTEM MATRICES

C.1 State Matrix

$$\mathbf{A}_h = \begin{bmatrix} 0 & 0 & 0 & 1 & 0 & 0 \\ 0 & 0 & 0 & 0 & 1 & 0 \\ 0 & 0 & 0 & 0 & 0 & 1 \\ \alpha^2 n_0^2 & 0 & 0 & 0 & 2n_0 & 0 \\ 0 & 0 & 0 & -2n_0 & 0 & 0 \\ 0 & 0 & \beta^2 n_0^2 & 0 & 0 & 0 \end{bmatrix}$$

C.2 Compatibility Matrix

$$\mathbf{B} = \begin{bmatrix} 0 & 0 & 0 \\ 0 & 0 & 0 \\ 0 & 0 & 0 \\ 1 & 0 & 0 \\ 0 & 1 & 0 \\ 0 & 0 & 1 \end{bmatrix}$$

C.3 Forcing Functions Due to 2nd Order Nonlinear Differential Gravity

$$\bar{u}_h = \begin{bmatrix} y_h^2 + z_h^2 - 2x_h^2 \\ 2x_h y_h \\ 2x_h z_h \end{bmatrix}$$

C.4 Nonzero Terms of the State Transition Matrix

$$\mathbf{\Phi}_{1,1} = \frac{(5s+3)\cos\left(n\sqrt{1-st}\right) - 4(1+s)}{s-1}$$

$$\mathbf{\Phi}_{1,4} = \frac{\sin\left(n\sqrt{1-st}\right)}{n\sqrt{1-s}}$$

$$\mathbf{\Phi}_{1,5} = \frac{2\sqrt{1+s}\left(\cos\left(n\sqrt{1-st}\right)-1\right)}{n(s-1)}$$

$$\mathbf{\Phi}_{2,1} = -\frac{2(5s+3)\sqrt{1+s}\left(n\sqrt{1-st} - \sin\left(n\sqrt{1-st}\right)\right)}{(1-s)^{3/2}}$$

$$\mathbf{\Phi}_{2,2} = 1$$

$$\mathbf{\Phi}_{2,4} = -\frac{2\sqrt{1+s}\left(\cos\left(n\sqrt{1-st}\right)-1\right)}{n(s-1)}$$

$$\mathbf{\Phi}_{2,5} = -\frac{(5s+3)\sqrt{1-st} - 4(s+1)\sin\left(n\sqrt{1-st}\right)}{n(s-1)^{3/2}}$$

$$\mathbf{\Phi}_{3,3} = \cos\left(n\sqrt{1+3st}\right)$$

$$\mathbf{\Phi}_{3,6} = \frac{\sin\left(n\sqrt{1+3st}\right)}{n\sqrt{1+3s}}$$

$$\mathbf{\Phi}_{4,1} = \frac{n(3+5s)\sin\left(n\sqrt{1-st}\right)}{\sqrt{1-s}}$$

$$\mathbf{\Phi}_{4,4} = \cos\left(n\sqrt{1-st}\right)$$

$$\mathbf{\Phi}_{4,5} = \frac{2\sqrt{1+s}\sin\left(n\sqrt{1-st}\right)}{\sqrt{1-s}}$$

$$.\mathbf{\Phi}_{5,1} = -\frac{2n(5s+3)\sqrt{1+s}\left(\cos\left(n\sqrt{1-st}\right)-1\right)}{s-1}$$

$$\mathbf{\Phi}_{5,4} = -\frac{2\sqrt{1+s}\sin\left(n\sqrt{1-st}\right)}{\sqrt{1-s}}$$

$$\mathbf{\Phi}_{5,5} = -\frac{4\cos\left(n\sqrt{1-st}\right)(s+1) - (5s+3)}{s-1}$$

$$\mathbf{\Phi}_{6,3} = -n\sqrt{1+3s}\sin\left(n\sqrt{1+3st}\right)$$

$$\mathbf{\Phi}_{6,6} = \cos\left(n\sqrt{1+3st}\right)$$

APPENDIX D

PERTURBATION SOLUTIONS TO THE J_2-MODIFIED HCW EQUATIONS

D.1 Perturbed Solutions

$$
\begin{aligned}
x_p(t) = &\left[X_{p,cnc2k} \cos(2kt) + X_{p,cns2k} \sin(2kt) + X_{p,cn0} \right] \cos\left(n\sqrt{1-s}t\right) \\
&+ \left[X_{p,snc2k} \cos(2kt) + X_{p,sns2k} \sin(2kt) + X_{p,sn0} \right] \sin\left(n\sqrt{1-s}t\right) \\
&+ X_{p,c2n} \cos\left(2n\sqrt{1-s}t\right) + X_{p,s2n} \sin\left(2n\sqrt{1-s}t\right) \\
&+ X_{p,c2n3s} \cos\left(2n\sqrt{1+3s}t\right) + X_{p,s2n3s} \sin\left(2n\sqrt{1+3s}t\right) \\
&+ X_{p,c4k} \cos(4kt) + X_{p,c2k} \cos(2kt) + X_{p,s2k} \sin(2kt) + X_{p,0}
\end{aligned}
$$

$$
\begin{aligned}
y_p(t) = &\left[Y_{p,cnc2k} \cos(2kt) + Y_{p,cns2k} \sin(2kt) + Y_{p,cn0} \right] \cos\left(n\sqrt{1-s}t\right) \\
&+ \left[Y_{p,snc2k} \cos(2kt) + Y_{p,sns2k} \sin(2kt) + Y_{p,sn0} \right] \sin\left(n\sqrt{1-s}t\right) \\
&+ Y_{p,c2n} \cos\left(2n\sqrt{1-s}t\right) + Y_{p,s2n} \sin\left(2n\sqrt{1-s}t\right) \\
&+ Y_{p,c2n3} \cos\left(2n\sqrt{1+3s}t\right) + Y_{p,s2n3} \sin\left(2n\sqrt{1+3s}t\right) \\
&+ Y_{p,skc3k} \sin(kt)\cos(3kt) + Y_{p,s2k} \sin(2kt) + Y_{p,t}t + Y_{p0}
\end{aligned}
$$

$$
\begin{aligned}
z_p(t) = &\begin{bmatrix} Z_{p,c3scn} \cos\left(n\sqrt{1-s}t\right) + Z_{p,c3ssn} \sin\left(n\sqrt{1-s}t\right) \\ + Z_{p,c3sc2k} \cos(2kt) + Z_{p,c3ss2k} \sin(2kt) + Z_{p,c3s0} \end{bmatrix} \cos\left(n\sqrt{1+3s}t\right) \\
&+ \begin{bmatrix} Z_{p,s3scn} \cos\left(n\sqrt{1-s}t\right) + Z_{p,s3ssn} \sin\left(n\sqrt{1-s}t\right) \\ + Z_{p,s3sc2k} \cos(2kt) + Z_{p,s3ss2k} \sin(2kt) + Z_{p,s3s0} \end{bmatrix} \sin\left(n\sqrt{1+3s}t\right)
\end{aligned}
$$

D.2 *x* Perturbed Coefficients

$$X_{p,cn0} = -\frac{2x_{h0}^2}{3n^2(s-1)} + \frac{2k\beta_2\sqrt{1+s}x_{h0} + 2/3\alpha_2\left(4k^2+5n^2+7n^2s\right)x_{h0}/n}{n(s-1)\left(k^2-n^2+n^2s\right)}$$
$$\frac{2(2s+1)y_{h0}^2}{3n^2(1+s)(1-s)} + \frac{(7s+1)z_{h0}^2 + 2\dot{z}_{h0}^2/n^2}{n^2(3+13s)(s-1)} + \frac{(5s+3)x_{p0}}{s-1} + \frac{2\sqrt{1+s}\dot{y}_{p0}}{s-1}$$
$$-\frac{\left[n^4(11s+1)(s-1)+8k^2\left(10k^2+7n^2+17n^2s\right)\right]\alpha_2^2}{3n^2(s-1)\left(k^2-n^2+n^2s\right)\left(16k^2-n^2+n^2s\right)} + \frac{8k^2\beta_2^2}{n^2(s-1)\left(16k^2-n^2+n^2s\right)}$$
$$+\frac{6k\sqrt{1+s}\left(n^2s-4k^2-n^2\right)\beta_2\alpha_2}{n(s-1)\left(k^2-n^2+n^2s\right)\left(16k^2-n^2+n^2s\right)} \quad \text{(D.1)}$$

$$X_{p,cnc2k} = \frac{\left[\left(4k^2+5n^2+7n^2s\right)\alpha_2 + 6kn\sqrt{1+s}\beta_2\right]}{\left(k^2-n^2+n^2s\right)\left(4k^2-n^2+n^2s\right)}\left(x_{h0}-\alpha_2\right) \quad \text{(D.2)}$$

$$X_{p,cns2k} = \frac{\alpha_2 n\left(3s^2n^2-2n^2s-8k^2-n^2\right)y_{h0}}{2k\sqrt{1+s}\left(k^2-n^2+n^2s\right)\left(4k^2-n^2+n^2s\right)} + \frac{\beta_2\left(n^2s-2k^2-n^2\right)}{\left(k^2-n^2+n^2s\right)\left(4k^2-n^2+n^2s\right)} \quad \text{(D.3)}$$

$$X_{p,sn0} = -\frac{2y_{h0}x_{h0}}{3n^2\sqrt{1-s}\sqrt{1+s}} + \frac{\dot{x}_{p0}}{n\sqrt{1-s}} + \frac{2z_{h0}\dot{z}_{h0}}{n^3\sqrt{1-s}(3+13s)} + \frac{2\beta_2 k y_{h0}}{n\sqrt{1-s}\left(k^2-n^2+n^2s\right)}$$
$$\frac{\alpha_2\left(4k^2+5n^2+7n^2s\right)y_{h0}}{6n^2\sqrt{1-s}\sqrt{1+s}\left(k^2-n^2+n^2s\right)} \quad \text{(D.4)}$$

$$X_{p,snc2k} = -\frac{\alpha_2(s-1)\left(4k^2+5n^2+7n^2s\right)y_{h0}}{2\sqrt{1-s}\sqrt{1+s}\left(4k^2-n^2+n^2s\right)\left(k^2-n^2+n^2s\right)} + \frac{3\beta_2 kn\sqrt{1-s}y_{h0}}{\left(4k^2-n^2+n^2s\right)\left(k^2-n^2+n^2s\right)} \quad \text{(D.5)}$$

$$X_{p,sns2k} = -\frac{2\sqrt{1+s}\left(n^2s-2k^2-n^2\right)\left(\alpha_2-x_{h0}\right)}{\sqrt{1-s}\left(4k^2-n^2+n^2s\right)\left(k^2-n^2+n^2s\right)} + \frac{\alpha_2 n\left(3n^2s^2-2n^2s-8k^2-n^2\right)\left(\alpha_2-x_{h0}\right)}{k\sqrt{1-s}\left(4k^2-n^2+n^2s\right)\left(k^2-n^2+n^2s\right)} \quad \text{(D.6)}$$

$$X_{p,c2n3s} = \frac{-n^2\left(1+3s\right)z_{h0}^2 + \dot{z}_{h0}^2}{2n^4\left(1+3s\right)\left(3+13s\right)} \tag{D.7}$$

$$X_{p,c2n} = -\frac{4\left(1+s\right)\left(x_{h0}-\alpha_2\right)^2 + \left(s-1\right)y_{h0}^2}{12n^2\left(s-1\right)\left(1+s\right)} \tag{D.8}$$

$$X_{p,c4k} = \frac{k\left(2\alpha_2^2+\beta_2^2\right) + 2n\alpha_2\beta_2\sqrt{1+s}}{2k\left(16k^2-n^2+n^2s\right)} \tag{D.9}$$

$$X_{p,s2n3s} = -\frac{z_{h0}\dot{z}_{h0}}{n^3\sqrt{1+3s}\left(3+13s\right)} \tag{D.10}$$

$$X_{p,s2n} = \frac{y_{h0}\left(x_{h0}-\alpha_2\right)}{3n^2\sqrt{1-s}\sqrt{1+s}} \tag{D.11}$$

$$\begin{aligned} X_{p,0} = {} & \frac{x_{h0}^2}{n^2\left(s-1\right)} - \frac{2\left[\alpha_2\left(4k^2+3n^2+5n^2s\right)+4\beta_2 nk\sqrt{1+s}\right]x_{h0}}{n^2\left(s-1\right)\left(4k^2-n^2+n^2s\right)} - \frac{\left(5s+3\right)y_{h0}^2}{4n^2\left(s-1\right)\left(s+1\right)} \\ & - \frac{\dot{z}_{h0}^2}{2n^4\left(s-1\right)\left(1+3s\right)} - \frac{z_{h0}^2}{2n^2\left(s-1\right)} - \frac{2\sqrt{1+s}\,\dot{y}_{p0}}{n\left(s-1\right)} - \frac{4\left(s+1\right)x_{p0}}{s-1} \\ & + \frac{2\left[\left(2s-1\right)\left(4k^2+3n^2s\right)-3n^2\right]\alpha_2^2}{n^2\left(s-1\right)^2\left(4k^2-n^2+n^2s\right)} - \frac{2s\alpha_2^2}{n^2\left(s-1\right)^2} - \frac{\beta_2^2}{2n^2\left(s-1\right)^2} \\ & - \frac{\alpha_2\beta_2\sqrt{1+s}\left(n^2s-12k^2-n^2\right)}{2nk\left(s-1\right)\left(4k^2-n^2+n^2s\right)} \end{aligned} \tag{D.12}$$

D.3 *y* Perturbed Coefficients

$$Y_{p,cnc2k} = \frac{2\beta_2 nk\left[n^2(s-1)(7s+3)-2k^2(s+3)\right]y_{h0}}{\sqrt{1+s}\left(k^2-n^2+n^2s\right)\left(4k^2-n^2+n^2s\right)^2} + \frac{\alpha_2\left(2k^2+n^2+3n^2s\right)\left(-4k^2-5n^2+5n^2s\right)y_{h0}}{\left(k^2-n^2+n^2s\right)\left(4k^2-n^2+n^2s\right)^2} \tag{D.13}$$

$$Y_{p,cns2k} = \frac{2\alpha_2 n\sqrt{1+s}\left(2k^2+n^2+3n^2s\right)\left(-8k^2-n^2+n^2s\right)}{k\left(k^2-n^2+n^2s\right)\left(4k^2-n^2+n^2s\right)^2}\left(x_{h0}-\alpha_2\right) + \frac{2\beta_2\left[n^4(s-1)(1+3s)-k^2\left(n^2(19s+13)+4k^2\right)\right]}{\left(k^2-n^2+n^2s\right)\left(4k^2-n^2+n^2s\right)^2}\left(x_{h0}-\alpha_2\right) \tag{D.14}$$

$$Y_{p,cn0} = \frac{4x_{h0}y_{h0}}{3n^2(s-1)} - \frac{2\beta_2 k\sqrt{1+s}\,y_{h0}}{n(s-1)\left(k^2-n^2+n^2s\right)} - \frac{2\alpha_2\left(4k^2+5n^2+7n^2s\right)y_{h0}}{3n^2(s-1)\left(k^2-n^2+n^2s\right)} - \frac{2\sqrt{1+s}\left[n^2(13s+3)\dot{x}_{p0}+2z_{h0}\dot{z}_{h0}\right]}{n^3(s-1)(13s+3)} \tag{D.15}$$

$$Y_{p,snc2k} = \frac{4\beta_2 nk\left[n^2(s-1)(7s+3)-2k^2(s+3)\right]}{\sqrt{1-s}\left(k^2-n^2+n^2s\right)\left(4k^2-n^2+n^2s\right)^2}\left(\alpha_2-x_{h0}\right) \frac{2\alpha_2\sqrt{1+s}\left(2k^2+n^2+3n^2s\right)\left(-4k^2-5n^2+5n^2s\right)}{\sqrt{1-s}\left(k^2-n^2+n^2s\right)\left(4k^2-n^2+n^2s\right)^2}\left(x_{h0}-\alpha_2\right) \tag{D.16}$$

$$Y_{p,sns2k} = -\frac{\alpha_2 n(s-1)\left(2k^2+n^2+3n^2s\right)\left(-8k^2-n^2+n^2s\right)}{k\sqrt{1-s}\left(k^2-n^2+n^2s\right)\left(4k^2-n^2+n^2s\right)^2}y_{h0} - \frac{\beta_2(s-1)\left[n^4(s-1)(1+3s)-k^2\left(n^2(19s+13)+4k^2\right)\right]}{\sqrt{1-s}\sqrt{1+s}\left(k^2-n^2+n^2s\right)\left(4k^2-n^2+n^2s\right)^2}y_{h0} \tag{D.17}$$

$$
\begin{aligned}
Y_{p,sn0} = &-\frac{4\sqrt{1+s}\,x_{h0}^2}{3n^2(1-s)^{3/2}} + \frac{4(1+2s)y_{h0}^2}{3n^2\sqrt{1+s}(1-s)^{3/2}} + \frac{2\sqrt{1+s}(7s+1)z_{h0}^2}{n^2(1-s)^{3/2}(13s+3)} \\
&+ \frac{4\beta_2 k(1+s)x_{h0}}{n(1-s)^{3/2}\left(k^2-n^2+n^2s\right)} + \frac{2\alpha_2\sqrt{1+s}\left(4k^2+5n^2+7n^2s\right)x_{h0}}{3n^2(1-s)^{3/2}\left(k^2-n^2+n^2s\right)} \\
&+ \frac{4\sqrt{1+s}\,\dot{z}_{h0}^2}{n^4(1-s)^{3/2}(13s+3)} + \frac{4(1+s)\dot{y}_{p0}}{n(1-s)^{3/2}} + \frac{2\sqrt{1+s}(3+5s)x_{p0}}{(1-s)^{3/2}} \\
&- \frac{2\alpha_2^2\sqrt{1+s}\left[n^4(11s+1)(s-1)+8k^2\left(n^2(17s+7)+10k^2\right)\right]}{3n^2(1-s)^{3/2}\left(k^2-n^2+n^2s\right)\left(16k^2-n^2+n^2s\right)} \\
&+ \frac{12\alpha_2\beta_2 k(1+s)\left(-4k^2-n^2+n^2s\right)}{n(1-s)^{3/2}\left(k^2-n^2+n^2s\right)\left(16k^2-n^2+n^2s\right)} + \frac{16\beta_2^2k^2\sqrt{1+s}}{n^2(1-s)^{3/2}\left(16k^2-n^2+n^2s\right)}
\end{aligned}
\tag{D.18}
$$

$$
Y_{p,c2n} = \frac{(x_{h0}-\alpha_2)y_{h0}}{6n^2(s-1)} \tag{D.19}
$$

$$
Y_{p,s2n} = \frac{4(1+s)\left(x_{h0}^2-2\alpha_2 x_{h0}+\alpha_2^2\right)+(s-1)y_{h0}^2}{24n^2(1-s)^{3/2}\sqrt{1+s}} \tag{D.20}
$$

$$
Y_{p,c2n3s} = -\frac{\sqrt{1+s}\,z_{h0}\dot{z}_{h0}}{n^3(1+3s)(3+13s)} \tag{D.21}
$$

$$
Y_{p,s2n3s} = \frac{\sqrt{1+s}\left[n^2(1+3s)z_{h0}^2-\dot{z}_{h0}^2\right]}{2n^4(1+3s)^{3/2}(3+13s)} \tag{D.22}
$$

$$
Y_{p,c3ksk} = -\frac{4kn(1+s)\left(2\alpha_2^2+\beta_2^2\right)+\alpha_2\beta_2\sqrt{1+s}\left(16k^2+3n^2+5n^2s\right)}{8k^2\sqrt{1+s}\left(16k^2-n^2+n^2s\right)} \tag{D.23}
$$

$$Y_{p,s2k} = -\frac{4kn(1+s)\left(2\alpha_2^2+\beta_2^2\right)+\alpha_2\beta_2\sqrt{1+s}\left(16k^2+3n^2+5n^2s\right)}{16k^2\sqrt{1+s}\left(16k^2-n^2+n^2s\right)} \tag{D.24}$$

$$\begin{aligned} Y_{p,t} = &-\frac{\sqrt{1+s}x_{h0}^2}{n(s-1)}+\frac{(5+11s)y_{h0}^2}{4n\sqrt{1+s}(s-1)}+\frac{\sqrt{1+s}z_{h0}^2}{n(s-1)}+\frac{\sqrt{1+s}\dot{z}_{h0}^2}{n^3(s-1)(1+3s)}+\frac{\beta_2^2\sqrt{1+s}}{n(s-1)} \\ &+\frac{4\beta_2 k(3+5s)x_{h0}}{(s-1)\left(4k^2-n^2+n^2s\right)}+\frac{2\alpha_2\sqrt{1+s}\left(4k^2+5n^2+11n^2s\right)x_{h0}}{n(s-1)\left(4k^2-n^2+n^2s\right)} \\ &+\frac{\alpha_2\beta_2(3+5s)\left(-12k^2-n^2+n^2s\right)}{4k(s-1)\left(4k^2-n^2+n^2s\right)}+\frac{2n\sqrt{1+s}(3+5s)x_{p0}}{s-1} \\ &+\frac{3+5s}{s-1}\dot{y}_{p0}-\frac{\alpha_2^2\sqrt{1+s}\left(12k^2+9n^2+23n^2s\right)}{n(s-1)\left(4k^2-n^2+n^2s\right)} \end{aligned} \tag{D.25}$$

$$\begin{aligned} Y_{p,0} = &\, y_{p0}+\frac{2\sqrt{1+s}\dot{x}_{p0}}{n(s-1)}+\frac{\sqrt{1+s}z_{h0}\dot{z}_{h0}}{n^3(s-1)(1+3s)}-\frac{3y_{h0}x_{h0}}{2n^2(s-1)} \\ &-\frac{\alpha_2\left[n^4(25s+7)(s-1)-8k^2\left(n^2\left(7+9s+6k^2\right)\right)\right]y_{h0}}{2n^2(s-1)\left(4k^2-n^2+sn^2\right)} \\ &-\frac{4\beta_2 k\left[n^2(3s+1)(s-1)-8k^2(1+s)\right]y_{h0}}{n\sqrt{1+s}(s-1)\left(4k^2-n^2+sn^2\right)} \end{aligned} \tag{D.26}$$

D.4 *z* Perturbed Coefficients

$$Z_{p,c3sc2k} = \frac{\alpha_2 z_{h0}}{2\left(-k^2+n^2+3n^2s\right)} \tag{D.27}$$

$$Z_{p,c3ss2k} = -\frac{\alpha_2\dot{z}_{h0}}{2k\left(-k^2+n^2+3n^2s\right)} \tag{D.28}$$

$$Z_{p,c3scn} = \frac{2n\sqrt{1+s}\left(x_{h0}-\alpha_2\right)z_{h0} + y_{h0}\dot{z}_{h0}}{n^3\sqrt{1+s}\left(3+13s\right)} \tag{D.29}$$

$$Z_{p,c3ssn} = -\frac{4\sqrt{1+s}\left(x_{h0}-\alpha_2\right)\dot{z}_{h0} + ny_{h0}z_{h0}}{n^3\sqrt{1+s}\sqrt{1-s}\left(3+13s\right)} \tag{D.30}$$

$$Z_{p,c3s0} = z_{p0} - \frac{2y_{h0}\dot{z}_{h0}}{n^3\sqrt{1+s}\left(3+13s\right)} - \frac{2x_{h0}z_{h0}}{n^2\left(3+13s\right)} - \frac{\alpha_2\left(4k^2-n^2+n^2s\right)}{n^2\left(3+13s\right)\left(-k^2+n^2+3n^2s\right)} \tag{D.31}$$

$$Z_{p,s3sc2k} = \frac{\alpha_2\dot{z}_{h0}}{2n\sqrt{1+3s}\left(-k^2+n^2+3n^2s\right)} \tag{D.32}$$

$$Z_{p,s3ss2k} = -\frac{\alpha_2 n\sqrt{1+3s}z_{h0}}{2k\left(-k^2+n^2+3n^2s\right)} \tag{D.33}$$

$$Z_{p,s3ssn} = -\frac{4\alpha_2\sqrt{1+3s}z_{h0}}{n^2\sqrt{1-s}\left(3+13s\right)} + \frac{4\sqrt{1+3s}x_{h0}z_{h0}}{n^2\sqrt{1-s}\left(3+13s\right)} + \frac{\sqrt{1-s}y_{h0}\dot{z}_{h0}}{n^3\sqrt{1+3s}\sqrt{1+s}\left(3+13s\right)} \tag{D.34}$$

$$Z_{p,s3scn} = -\frac{2\left[\sqrt{1+s}\left(x_{h0}-\alpha_2\right)\dot{z}_{h0} - n\left(1+3s\right)y_{h0}z_{h0}\right]}{n^3\sqrt{1+3s}\sqrt{1+s}\left(3+13s\right)} \tag{D.35}$$

$$\begin{aligned} Z_{p,s3s0} = {} & \frac{\dot{z}_{p0}}{n\sqrt{1+3s}} + \frac{\alpha_2\left(4k^2-n^2+n^2s\right)\dot{z}_{h0}}{2n^3\sqrt{1+3s}\left(3+13s\right)\left(-k^2+n^2+3n^2s\right)} \\ & + \frac{2x_{h0}\dot{z}_{h0}}{n^3\sqrt{1+3s}\left(3+13s\right)} + \frac{\left(7s+1\right)y_{h0}z_{h0}}{n^2\sqrt{1+s}\sqrt{1+3s}\left(3+13s\right)} \end{aligned} \tag{D.36}$$

REFERENCES

[1]Das, A., Cobb, R and Stallard, M., “Techsat 21 - A Revolutionary Concept in Distributed Space Based Sensing,” AIAA Defense and Civil Space Programs Conference and Exhibit, Huntsville, AL, Oct. 28-30, 1998.

[2]Yeh, H-H, Sparks, A., “Geometry and control of satellite formations,” American Control Conference, Chicago, IL, June 28-30, 2000. pp. 384-388.

[3]NASA Report, “EO-1 Brochure,”

http://eo1.gsfc.nasa.gov/overview/Brochure_Final_08-02.pdf.

[4]Bauer F., et al, “Satellite formation flying using an innovative autonomous control system (AutoCon) environment,” AIAA Guidance, Navigation, and Control Conference, New Orleans, LA, Aug. 11-13, 1997.

[5]Naasz, B. J., “Classical Element Feedback Control for Spacecraft Orbital Maneuvers,” M.S. thesis, Virginia Polytechnic Institute and State University May 28, 2002 Blacksburg, Virginia.

[6]Schaub, H., and Junkins, J.L., *Analytical Mechanics of Space Systems*, AIAA Educational Series, AIAA, Reston, VA, 2003, pp. 11-15, 593-673.

[7]Schweighart, S. A., and Sedwick, R. J., "Development and Analysis of a High Fidelity Linearized J_2 Model for Satellite Formation Flying,” AIAA Space 2001 - Conference and Exposition, Albuquerque, NM, Aug. 28-30,2001.

[8]Schweighart, S. A., “Development and Analysis of a High Fidelity Linearized J2 Model for Satellite Formation Flying,” M.S. thesis, Massachusetts Institute of Technology, June 2001.

[9]Vaddi, S.S., Vadali, S.R., and Alfriend, K.T., “Formation Flying: Accommodating Nonlinearity and Eccentricity Perturbations,” *Journal of Guidance, Control, and Dynamics*, Vol. 26, No. 2, 2003, pp. 214-223.

[10]Wang, P. K. C., and Hadaegh, F. Y., "Optimal formation-reconfiguration for multiple spacecraft,” AIAA Guidance, Navigation, and Control Conference and Exhibit, Boston, MA, Aug. 10-12, 1998. pp. 686-696.

[11]Battin, R.H., *An Introduction to the Mathematics and Methods of Astrodynamics, Revised Edition*, AIAA Educational Series, AIAA, Reston, VA, 1999.

[12]Vallado, D. A., *Fundamentals of Astrodynamics and its Applications*, 2nd ed., The Space Technology Library and Microcosm Press, El Segundo, Calif., 2001.

[13]Kechichian, J. A., “The Analysis of the Relative Motion in General Elliptic Orbit with Respect to a Dragging and Precessing Coordinate Frame,” *Proceedings of the AAS/AIAA Astrodynamics Specialist Conference*, No. AAS 97-733, AAS Publications, San Diego, CA, Aug., 1997.

[14]Vadali, et al., “Control of Satellite Formations,” AIAA Guidance, Navigation, and Control Conference and Exhibit Aug. 6-9, 2001 Montreal, Canada.

[15]Schaub, H. and Alfriend, K. T., “ J_2 Invariant Relative Orbits for Formation Flying," International Journal of Celestial Mechanics and Dynamical Astronomy, Vol. 79, 2001, pp. 77-95.

[16]Vadali, S. R., “An Analytical Solution for Relative Motion of Satellites," Proceedings of the DCSSS Conference, Cranfield University, Cranfield, UK, July 2002.

[17]Sengupta, P., “Satellite Relative Motion Propagation and Control in the Presence of J_2 Perturbations,” M.S. thesis, Texas A&M University, December, 2003.

[18]Efroimsky, M, “Equations for the Keplerian Elements: Hidden Symmetry,” *Preprint #1844 of the Institute of Mathematics and its Applications, University of Minnesota*, Feb. 2002.

[19]Efroimsky, M, and Goldreich, P, “Gauge Freedom in the N-body problem of Celestial Mechanics,” *Astronomy and Astrophysics*, Vol. 415, 2004, pp. 1187-1199.

[20]Gurfil, P, “Analysis of J2-Perturbed Motion Using Mean Non-Osculating Orbital Elements,” *Celestial Mechanics and Dynamical Astronomy*, Vol. 90, 2004, pp. 289-306.

[21]Gurfil, P, “Relative Motion Between Elliptic Orbits: Generalized Boundedness Conditions and Optimal Formation Keeping,” *Journal of Guidance, Control, and Dynamics*, Vol. 28, No. 4, 2005, pp. 761-767.

[22]Sengupta, P., et al, “Periodic Motion Near a General Keplerian Orbit with Nonlinear Differential Gravity,” Department of Aerospace Engineering, Texas A&M University, College Station, TX, 77840, June, 2005.

[23]Prussing, J. E., and Conway, B. A., *Orbital Mechanics*, Oxford University Press, New York, 1993, pp. 139-167.

[24]Crassidis, J. L., and Junkins, J. L., *Optimal Estimation of Dynamical Systems*, Chapman and Hall, Boca Raton, FL, 2004, pp. 119-131.

[25]Zwillinger, D., *CRC Standard Mathematical Tables and Formulae*, Chapman and Hall, Boca Raton, FL, 2003.

BIOGRAPHICAL INFORMATION

Jeffery S. Ginn was born in Norfolk, Virginia to parents Jeffery T. Ginn and Annette M. Ginn. Jeffery grew up in Virginia Beach, Virginia and Enterprise, Alabama, where he graduated from High School in May, 2000. Jeffery then attended The Ohio State University, where he earned his Bachelor of Science in Aeronautical and Astronautical Engineering in June, 2004. Jeffery continued his studies at The University of Texas at Arlington, where he completed his Master of Science in Aerospace Engineering with a concentration in orbital mechanics in August, 2006. He plans to pursue a career in dynamics and control.